A METHOD FOR PROCESSING DATA FROM A REGIONAL CONTINUOUS CRUSTAL DEFORMATION GPS MONITORING NETWORK

CHUNLIN SHEN

February 2004

TECHNICAL REPORT NO. 221

A METHOD FOR PROCESSING DATA FROM A REGIONAL CONTINUOUS CRUSTAL DEFORMATION GPS MONITORING NETWORK

Chunlin Shen

Department of Geodesy and Geomatics Engineering
University of New Brunswick
P.O. Box 4400
Fredericton, N.B.
Canada
E3B 5A3

February 2004

© Chunlin Shen 2004

PREFACE

This technical report is an unedited reproduction of a thesis submitted in partial fulfillment of the requirements for the degree of Master of Science in Engineering in the Department of Geodesy and Geomatics Engineering, February 2004. The research was supervised by Dr. Richard B. Langley, and funding was provided by NSERC, the Natural Sciences and Engineering Research Council of Canada, with additional support from GEOIDE, the Geomatics for Informed Decisions Network of Centres of Excellence.

As with any copyrighted material, permission to reprint or quote extensively from this report must be received from the author. The citation to this work should appear as follows:

Shen, C. (2004). *A Method for Processing Data from a Regional Continuous Crustal Deformation GPS Monitoring Network.* M.Sc.E. thesis, Department of Geodesy and Geomatics Engineering Technical Report No. 221, University of New Brunswick, Fredericton, New Brunswick, Canada, 125 pp.

Abstract

This thesis focuses on improvement of methods for processing GPS data to detect regional crustal deformation signals of centimetre or even millimetre level, based on the DIfferential POsitioning Program (DIPOP) GPS software package.

The experimental field is the Western Canada Deformation Array (WCDA), a regional continuous GPS tracker network for monitoring crustal deformation in western Canada. As part of the Canadian National Earthquake Hazards Program, WCDA was established by the Geological Survey Canada, Natural Resources Canada primarily for the study of the seismic hazard in this region.

DIPOP is a development of the Department of Geodesy and Geomatics Engineering, University of New Brunswick. Since the birth of DIPOP 1.0 in 1985, DIPOP has been continuously upgraded with the advance of GPS and computer techniques, and is still under development.

Since error correction models directly affect the quality of processing results, the models of the tide and residual atmospheric delay corrections have been tested with the longest baseline of the WCDA network. Also, a weeklong GPS data set from 7 WCDA baselines was processed to evaluate the performance of DIPOP. The solutions for both the height component and baseline length show daily repeatability better than 1 cm for baselines ranging from 254 to 672 km. Differences between the weekly solutions from DIPOP and the ITRF2000 solutions published by International Earth Rotation Service

(IERS) are of the order of a few centimetres in the components of latitude, longitude, and height.

In order to test the capability of DIPOP to extract deformation signals, a continuous 52-week data set from 3 selected WCDA baselines was processed. Annual movement rates for the components of latitude, longitude, and height were estimated by weighted least squares linear fitting and assessed by values of the coefficient of determination and the F-test. The daily time series of the position solutions at the 3 remote sites show movement rates of 0.4 - 1.4 cm per year and -7.8 - 2.6 mm per year in the horizontal and vertical components, respectively.

By analyzing the processed results, potential error sources affecting the accuracy of the DIPOP solutions were assessed. It is suggested that the methods for estimating residual tropospheric delay and correcting receiver antenna phase center variation need to be improved; and reduction of multipath interference needs to be taken into consideration in data processing for high-precision positioning.

Improvement of the technique for detecting and fixing cycle slips was also studied. A method of automatically detecting cycle slips was developed and implemented in the preprocessor PREDD of DIPOP. The new method shows better efficiency for data processing with DIPOP.

Acknowledgements

I am very pleased to take this opportunity to express my deepest gratitude to everyone who has helped, supported and inspired me during my graduate career.

First, I would like to thank my supervisor, Professor Richard B. Langley for providing me with the opportunity to study in the area of GPS applications, for his expert guidance and advice, for his encouragement and support. His confidence, extensive knowledge, and rigorous attitude of working gave a strong impression to me. I especially appreciate his patience with correcting my thesis from sentences to words, punctuation and more.

My thanks also go to Professor Peter Dare and Professor Marcelo C. Santos for all their supervision and support. During my stay on campus, I obtained a lot of useful ideas from the GPS group meeting every Friday afternoon. Here I would like to give my thanks to the members of our GPS group, Dr. Kim Dong Hyun, Mr. Sunil Bisnath, Mr. Tomas Beran, and Mr. Hyunho Rho.

In addition, I would like to thank Mrs. Linda O'Brien and all the members of GGE, UNB for a great time I had during my campus life at UNB; and my thanks go to all my friends for their help.

Finally, I would like to thank my husband Jianliang Huang for his understanding and support; and I would like to thank my son Kaiwen for his love. They gave me strength and confidence. My progress could not be made without their help.

Contents

Abstract ii

Acknowledgements iv

Table of Contents v

List of Tables ix

List of Figures xii

List of Abbreviations xv

1 Introduction **1**

1.1 Research Background 1

1.2 GPS Applications in Monitoring Regional Crustal Deformation 2

1.3 Objectives of the Thesis 5

1.4 Outline of the Thesis 6

2 Western Canada Deformation Array **8**

2.1 Earthquakes in Western Canada Region 8

2.1.1 Earthquakes and Plate Tectonics 10

2.1.2 Plate Tectonics Setting in Western Canada Region 12

2.2 The WCDA Network…… 13

2.2.1 Configuration of the WCDA Network 14

2.2.2 Equipment and Data Acquisition of WCDA 16

3 DIPOP Software Package 18

3.1 Review of DIPOP Software Package Development 18

3.2 DIPOP Software Package 21

3.2.1 Principles of Adjustment in DIPOP 23

3.2.2 Preprocessors: PREGO and PREDD 24

3.2.3 Main Processor and Postprocessor: MPROC and PPROC 26

3.2.3.1 Tide Corrections 27

3.2.3.2 Atmospheric Delays: ionospheric delay and tropospheric delay 32

3.2.3.3 Measurement Weighting 37

3.2.3.4 Linear Combinations of Carrier Phase Observables 38

3.2.3.5 Least-squares Adjustment 40

3.2.3.6 Cycle Slip Editing 41

3.2.3.7 Postprocessor: PPROC 42

3.3 Summary 43

4 A Test of Data Processing with DIPOP 44

4.1 Some Considerations 44

4.2 Estimation of Residual Tropospheric Zenith Delay 46

4.2.1 Prediction Models of Tropospheric Zenith Delay and Mapping Functions 46

4.2.2 Parameter Estimation of Residual Tropospheric Zenith Delay 49
4.2.3 Modeling Residual Tropospheric Zenith Delay within a Sequential Interval 51
4.2.4 Sequential Intervals for the Estimation of Residual Tropospheric Zenith Delay 54
4.3 Tide Corrections 56
4.4 Experience with WCDA Data 58
4.4.1 Data Processing Strategy 58
4.4.2 Summary of Results 61
4.4.3 Comparisons of Results 68
4.4.4 The Error Budget 72
4.4.4.1 Multipath Effects 72
4.4.4.2 Tropospheric Delay 73
4.4.4.3 Phase Center Corrections 74
4.5 Summary 76
5 Cycle Slip Detection 77
5.1 Cycle Slips 77
5.2 Algorithm of Cycle Slip Detection in PREDD 82
5.3 Method of Automatically Detecting Cycle Slips 84
5.3.1 Examination of Noise Level 85
5.3.2 Setting Threshold Values 89
5.3.3 Ruling out the Probability of Falsely Detecting Cycle Slips 90

5.4 Summary 96

6 Velocity Estimations 98

6.1 Introduction 98

6.1.1 GPS Data Sets 98

6.1.2 Method of Velocity Estimations 99

6.1.2.1 Weighted Least Squares Fitting 100

6.1.2.2 Assessments of Linear Fitting 102

6.2 Time Series and Velocity Estimations 105

7 Conclusions and Recommendations 111

7.1 Conclusions 111

7.2 Recommendations 113

References 116

Appendix A DIPOP References 123

Vita

List of Tables

2.1 WCDA network sites 15

3.1 The main tidal harmonics 31

3.2 The models of tropospheric zenith delay and the mapping functions in DIPOP 36

3.3 The linear combinations of carrier phase observables 40

4.1 Options of estimating residual tropospheric zenith delay in DIPOP 49

4.2 Statistics of the baseline DAHL over 7 days for different residual tropospheric zenith estimation 51

4.3 Statistics of the baseline DAHL during 7 days for fitting residual zenith delay within a sequential interval 52

4.4 Statistics of the solutions at different sequential intervals for the baseline DAHL over 7 days 55

4.5 Averaged height and length differences of the solutions with tide corrections minus without tide corrections over 7 days (DAHL) 56

4.6 Averaged mean and RMS of the double difference residuals with tide corrections and without tide corrections over 7 days (DAHL) 57

4.7 Tested data sets 59

4.8 The position and velocities of DRAO at epoch 1997.0 in ITRF97

converted from ITRF2000 solutions of IERS at epoch 1997.0 61

4.9 Statistics of daily relative height variation referring to the mean of 7 daily solutions and standard deviation of the daily variations in three components of baseline 65

4.10 Statistics of daily baseline length variation referring to the mean of 7 daily length solutions and standard deviation of the relative variations 66

4.11 Averaged pseudorange multipath plus noise over 7 days at 8 WCDA stations 66

4.12 The positions at epoch 1997.0 in ITRF97 converted from ITRF2000 solutions of IERS 69

4.13 The velocities in ITRF97 converted from ITRF2000 solutions of IERS 69

4.14 Accuracy of ITRF2000 solutions at epoch 1997.0 from IERS 70

4.15 The weekly position solutions from DIPOP at epoch 1997.0 in ITRF97 70

4.16 Comparison of absolute position solutions at epoch 1997.0 in ITRF97 (DIPOP minus IERS) 71

4.17 Comparison of baseline length solutions at epoch 1997.0 in ITRF97 referring to DRAO (DIPOP minus IERS) 71

5.1 Effects of small cycle slips on phase ambiguity 79

5.2 Multiple choices of observations for detecting cycle slips in PREDD 83

5.3 Linear combination characteristics 84

5.4 Selected values from the normal distribution 88

6.1 Daily data sets for estimation of movement velocity 99

6.2 Variations in latitude (+North) 107

6.3 Variations in longitude (+East) 107

6.4 Variations in height (+Up) 107

6.5 Variations in baseline length 107

List of Figures

2.1 Earthquakes in western Canada between 1996 and 2001 9

2.2 The major plates of the Earth..... 10

2.3 Locations of earthquakes around the globe between 1965 and 1995 11

2.4 Plate tectonic setting of western Canada 12

2.5 Configuration of the WCDA network (PGC1 is a site used for receiver and antenna testing. NEAH is a site operated by the University of Washington)..... 15

3.1 General program structure 19

3.2 The flowchart of DIPOP 22

4.1 Residuals plots of double difference in estimating tropospheric zenith delay..... 50

4.2 Tropospheric zenith delays at the two stations, DRAO and HOLB 53

4.3 Residuals of double difference for modeling residual tropospheric zenith delay in sequential intervals..... 53

4.4 Residuals of the double differences for different intervals..... 55

4.5 Daily variations of length and relative height solutions for baseline DAAB (Referring to the mean of the 7 daily solutions)..... 62

4.6 Daily variations of length and relative height solutions for baseline DAHL (Referring to the mean of the 7 daily solutions)..... 62

4.7 Daily variations of length and relative height solutions for baseline DANA (Referring to the mean of the 7 daily solutions)..... 63
4.8 Daily variations of length and relative height solutions for baseline DANN (Referring to the mean of the 7 daily solutions)..... 63
4.9 Daily variations of length and relative height solutions for baseline DAUL (Referring to the mean of the 7 daily solutions)..... 64
4.10 Daily variations of length and relative height solutions for baseline DAWL (Referring to the mean of the 7 daily solutions)..... 64
4.11 Daily variations of length and relative height solutions for baseline DAWS (Referring to the mean of the 7 daily solutions)..... 65
4.12 Multipath plus noise at site NANO (205-211/2000)..... 67
4.13 Multipath plus noise at site HOLB (205-211/2000) 67
5.1 Carrier phase observations (L1) on 205/2001 ((a), (b), (c), and (d)) and the Double Differences (e) and Triple Differences (f)..... 78
5.2 Change rate of double difference observations..... 80
5.3 Double difference observations 81
5.4 Time difference series of double differences..... 86
5.5 The moving average and mean of the time series..... 87
5.6 Occurrences of a cycle slip and a noise peak in the double difference series and time difference series 89
5.7 Principle of distinguishing a cycle slip and a noise spike..... 91
5.8 Time difference series of the four combinations with different sensitivities to cycle slips..... 93

5.9 Double differences of the four combinations with different sensitivities to cycle slips 93
5.10 Time difference series of the four combinations with a large noise spike 94
5.11 Double differences of the four combinations with a large noise spike 94
5.12 Time difference series of the four combinations with a detected cycle slip 95
5.13 Double differences of the four combinations with a cycle slip 95
6.1 The computation of r^2 103
6.2 r^2 and linear regression fitting 103
6.3 Time series of variations at ALBH with respect to DRAO in latitude (+N), longitude (+E) and height (+up) and of the baseline DAAB length 108
6.4 Time series of variations at HOLB with respect to DRAO in latitude (+N), longitude (+E) and height (+up) and of the baseline DAHL length 109
6.5 Time series of variations at UCLU with respect to DRAO in latitude (+N), longitude (+E) and height (+up) and of the baseline DAUL length 110

List of Abbreviations

ALBH	Albert Head, Victoria, B.C. Canada
CACS	Canadian Active Control System
C/N0	Carrier-to-noise power density ratio
DAAB	Baseline formed by reference site DRAO and remote site ALBH
DAHL	Baseline formed by reference site DRAO and remote site HOLB
DANA	Baseline formed by reference site DRAO and remote site NEAH
DANN	Baseline formed by reference site DRAO and remote site NANO
DAUL	Baseline formed by reference site DRAO and remote site UCLU
DAWL	Baseline formed by reference site DRAO and remote site WILL
DAWS	Baseline formed by reference site DRAO and remote site WSLR
DD	Double Difference
DIPOP	DIfferential POsitioning Program
DRAO	Dominion Radio Astrophysical Observatory, Penticton, B.C., Canada
GEOIDE	Geomatics for Informed Decisions
GPS	Global Positioning System
GSC	Geological Survey of Canada
HOLB	Holberg, B.C., Canada
IERS	International Earth Rotation Service

IGS	International GPS Service
ITRF	International Terrestrial Reference Frame
L1	L1 carrier
L2	L2 carrier
NA	North American (NA)
NANO	Nanoos Bay, B.C. Canada
NCE	Networks of Centres of Excellence
NEAH	Neah Bay, Washington, U.S.A.
NRCan	Natural Resources Canada
PANGA	Pacific Northwest Geodetic Array
PCV	Phase Center Variation
PPM	Parts Per Million
RMS	Root Mean Square
SD	Standard Deviation
SLR	Satellite Laser Ranging
SV	Space Vehicle
TD	Triple Difference
UCLU	Ucluelet, B.C., Canada
UNB	University of New Brunswick
VLBI	Very Long Baseline Interferometry
WCDA	Western Canada Deformation Array
WILL	Williams Lake, B.C., Canada
WSLR	Whistler, B.C., Canada

WVR Water Vapor Radiometer

Chapter 1

Introduction

While the Global Positioning System (GPS) is widely applied by the military, civilian, industrial and scientific communities due to its capability of providing 24-hour, all-weather global positioning, improving the accuracy of GPS long distance positioning is still an important topic in current GPS research and development. This thesis focuses on improvement of methods for processing GPS data to detect regional crustal deformation signals.

In this chapter the background of the research is first introduced; then the GPS applications in crustal deformation research are reviewed, the problems are stated, and objectives of the current research are given; finally the outline of the thesis is given.

1.1 Research Background

Loss of life and damage to property caused by natural hazards such as earthquakes is enormous. In the current seismological studies, geomatics has come to play an increasingly important role. Project ENV#17, Natural Hazards and Disaster Monitoring, is one of the environment and marine projects supported by the Geomatics for Informed

Decisions (GEOIDE) Network of Centres of Excellence (NCE) research investment program. Its main goal is to provide information essential to theoretical deformation models which enable us to estimate the characteristics of future damaging earthquakes, especially on the west coast of Canada where earthquake activity is frequent.

As a partner of the project, the GPS research group in the Department of Geodesy and Geomatics Engineering, University of New Brunswick (UNB), led by Professor Richard B. Langley, undertook to improve GPS data analysis methods. UNB's DIfferential POsitioning Program (DIPOP) was selected for use in this study, and a project was initiated to further enhance the accuracy of the software. The work described in this thesis is a part of the project.

1.2 GPS Applications in Monitoring Regional Crustal Deformation

In recent years, the success of GPS applications in geodynamics is remarkable. The GPS applications for monitoring crustal motion are mainly in three fields:

a) global and continental plate motion and deformation analysis;

b) regional crustal motion analysis;

c) local monitoring of deformation and subsidence.

Global deformation monitoring is used in the study of global plate tectonics. Stations for global deformation monitoring are distributed worldwide with a spacing of about 1000 km or more. For example, the GPS tracking network of the International GPS Service (IGS), an international network of over 300 continuously operating permanent

GPS stations, supports global-scale scientific activities such as improving the International Terrestrial Reference Frame (ITRF), monitoring deformations of the solid Earth and variations in the liquid Earth, and in Earth rotation, determining orbits of scientific satellites and so on.

The monitoring of local deformation belongs to the field of deformation analysis in engineering surveying. In most cases the inter-point distances are very small, hence an accuracy of a few mm can be achieved, and very small deformations can be detected.

A GPS regional crustal deformation monitoring network is usually distributed with inter-point distances of a few hundred km and is installed in some seismically or volcanically active areas of high risk, like the San Andreas Fault in California in the United States, the Kanto-Tokai region in Japan, and south-western British Columbia in Canada. The study in this field has already shown significant results.

The first continuously operating regional crustal deformation monitoring GPS array in the world was established in April 1988 in Kanto-Tokai, Japan. The array consists of 10 permanent GPS stations distributed with a spacing of approximately 100 km. A time series result from 32 biweekly positions of the GPS network between April 1988 and August 1989 showed a deformation rate at a level of 1-3 cm/year over these regional scale baselines with only 16 months of data [Bock, 1991]. These early results indicated the advantage of the GPS continuous tracking capability.

In view of the known crustal deformation rates of a few cm/year or only mm/year, a relative accuracy of a few parts in 10^8 must be provided for station spacing larger than 100 km. In the 1990s, the GPS technique for measurements of long distances made significant improvements with the completion of important events. In 1993, the United

States declared the initial operating capability of the GPS system. The constellation of GPS satellites allows for a simultaneous observation of at least four GPS satellites from anywhere on the surface of the Earth at anytime. In January 1994, the International GPS Service for Geodynamics formally began to provide precise orbit information worldwide. It is now known as International GPS Service (IGS). The current IGS precise orbit accuracy based on comparisons with independent laser ranging results is better than 5 cm according to the published report of the IGS products in 2001. In the meantime, the revolution in the electronic and computer industry pushed the development of GPS. GPS receivers have become more powerful with all-satellites-in-view tracking capabilities, low-noise measurement, and low-cost and so on. Many GPS software packages now offer an automatic processing capability with a high accuracy.

Today an accuracy of 1 part in10^8 in static relative positioning is realizable; this means that a 1000 km baseline can be measured with only 1 cm error. Through recent advances in GPS techniques, it is now possible to detect regional-scale crustal deformation and to provide direct evidence for seismological studies.

The detection of crustal deformation associated with seismic or volcanic activity has been reported. The nationwide GPS array in Japan, one of the largest continuous GPS arrays in the world, successfully monitored the crustal deformation caused by some major earthquakes. They include the Hokkaido-Toho-Oki earthquake in October 1994 (M8.1), the Sanriku-Harruka-Oki earthquake in December 1994 (M7.5), and the Kobe earthquake in 1995 (M7.2). The data from this GPS array vividly recorded crustal deformation before, after, and at the time of the earthquakes and provided primary information for

constructing numerical features of the faults which caused earthquakes in those regions [Tsuji et al., 1996].

The data from GPS continuous crustal deformation monitoring also can provide evidence for geophysical theory. A recent paper [Dragert et al., 2000] from the magazine "Science" reported a silent slip event on the deep Cascadia subduction zone interface. In that area, time series results from 7 GPS site coordinates reversed their direction of daily varying trend in both latitude and longitude in the summer of 1999. No seismicity was associated with this sudden event. The detection demonstrates that the slip of the hotter and plastic part of the subduction interface zone can occur in discrete pulses or steps.

Continuous and accurate information of relative position is one of primary needs for the analysis of crustal deformation. The information is essential to refine the regional crustal deformation models and even to make long-term earthquake predictions in the region. GPS is the tool that can provide this kind of information. GPS daily solutions from the continuously operating GPS crustal deformation monitoring network had been used to estimate the velocities and strain-rate of crustal motion in the region [Chen, 1998; Khazaradze et al., 1999]. It is believed that the GPS technique has played an important role in monitoring crustal deformation

1.3 Objectives and Contributions of the Thesis

In the application of GPS to monitoring crustal deformation, there are still a few important limitations including multipath interference, unmodeled tropospheric and ionosphereic delays, and antenna phase-center-variations and uncorrected cycle slips.

These limitations are expected to be eliminated by improvements of the data analysis methods. The objective of this thesis is to detect regional crustal deformation signals of centimetre or even millimetre level by improvement of methods for processing GPS data.

The contributions of this thesis primarily consist of three parts. The first part assessed the performance of the UNB software package DIPOP. The assessment was performed by a systematical test of DIPOP for the estimation of residual tropospheric zenith delay and the correction models of solid body, ocean loading, and pole tides, the analysis of repeatability of daily solutions, and a comparison between DIPOP's and IERS's ITRF solutions. The second part was aimed at the improvement of the cycle slip detection technique. The implementation of a new method for automatically detecting cycle slips significantly improved the efficiency of data processing for a regional continuous GPS monitoring network. Finally, a 52-week-long data set was processed to estimate the crustal deformation rate. The results demonstrate the capability of DIPOP in providing high-precision GPS solutions. The recommendations suggest some studies on further improving DIPOP.

1.4 Outline of the Thesis

Chapter 1 introduces the background to the research and gives an overall review of current GPS applications for crustal deformation studies in the world, and then gives the thesis objectives.

Chapter 2 introduces background knowledge of the geological structure in western Canada: earthquake activities and plate tectonic setting in this region; briefly

describes the plate tectonics theory; and finally gives a detailed introduction to the Western Canada Deformation Array (WCDA) including its goals, configuration, equipment, and data collection.

Chapter 3 introduces the history of development of the DIfferential POsitioning Program software package and its main features; and describes its basic adjustment principle, functions, basic structure and main algorithms of three main programs (PREGO, PREDD and MPROC including post-processing program PPROC) in detail.

Chapter 4 discusses the main models involved in DIPOP including estimation of residual tropospheric delay and tidal corrections; gives the procedure and results of a test in which WCDA GPS data collected over a one-week period are processed with DIPOP and comparisons are made between the DIPOP coordinate weekly solutions and the ITRF coordinate solutions published by IERS; and finally error analysis of the DIPOP solutions and a summary of the test are given.

Chapter 5 discusses new algorithms added to PREDD for automatically detecting cycle slips; shows some test examples for demonstrating the efficiency of the new algorithms; and briefly describes the features of cycle slips detection and repair.

Chapter 6 describes the long (one-year) data set from WCDA and the estimation strategies applied to the data processing in detail; it gives the velocities of movement of 7 WCDA sites estimated by the daily solutions with respect to the reference station DRAO (Dominion Radio Astrophysical Observatory) and the corresponding statistical information of all the solutions.

Chapter 7 summarizes the thesis with conclusions and recommendations for future work.

Chapter 2

Western Canada Deformation Array

The Western Canada Deformation Array (WCDA) is a permanent regional GPS network for monitoring crustal deformation. Its purpose is to help geoscientists understand the underlying causes of earthquakes, and improve the characterization of the associated earthquake hazard in western Canada.

This chapter first introduces the earthquake activity and the geological environment of western Canada. The second section describes the WCDA network.

2.1 Earthquakes in Western Canada Region

The record published by the Geological Survey of Canada (GSC) of Natural Resources Canada (NRCan) at the Web site <http://www.pgc.nrcan.gc.ca/seismo> shows that more than 100 earthquakes with magnitude of 5 or greater occurred in western Canada in the past 70 years. And there were 5 recorded earthquakes of magnitude 7 or larger in this region in the past 300 years. Figure 2.1 from the GSC Web site <http://www.pgc.nrcan.gc.ca/seismo/recent/wc.5yr.html> displays the distribution of the earthquakes between 1996 and 2001.

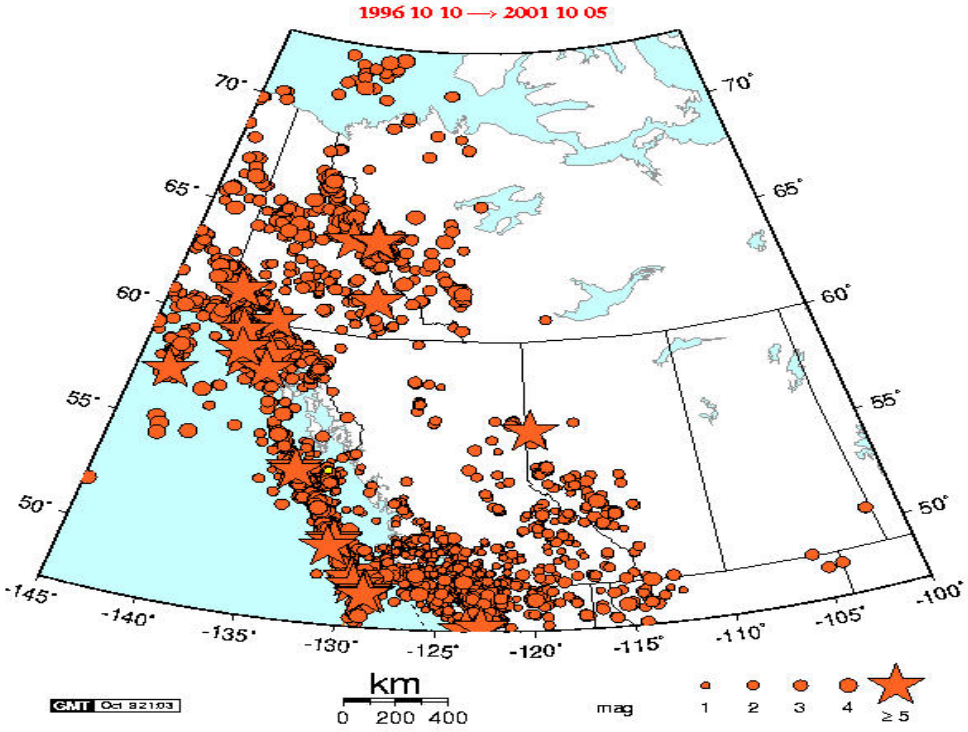

Figure 2.1 Earthquakes in western Canada between 1996 and 2001
(from the GSC Pacific Division of NRCan [October 6, 2002])

How often do the earthquakes occur in western Canada? Every Day! Scientists at the Geological Survey of Canada record and locate approximately 1000 earthquakes each year in western Canada.

Severe earthquakes and their terrible aftereffects are one of the most frightening and destructive phenomena of nature. We naturally want to know why there are so many earthquakes in the region. Since earthquakes are a result of geological structure activities, understanding the correlation of earthquakes with geological structure will be helpful for finding out an answer to the question.

2.1.1 Earthquakes and Plate Tectonics

According to plate tectonics theory, the Earth's surface is characterized by relatively aseismic units or plates carrying both continental and oceanic crust [Lambeck, 1988]. These plates are large pieces of the upper few hundred km of the Earth that move more or less as a single unit. They are formed along the oceanic ridges from uprising material and can move relative to each other through a process of crustal destruction along some boundaries of the plates and crustal creation along others. The map in Figure 2.2 from the Web site <http://eqseis.geosc.psu.edu/~cammon/HTML/Classes/IntroQuakes/Notes/> shows the major plates. These plates usually move at a velocity within a range of 1 to 15 cm per year. Today, the movement of tectonic plates can be directly measured by a variety of geodetic technologies, including Satellite Laser Ranging (SLR), Very Long Baseline Interferometry (VLBI), and Global Positioning System (GPS).

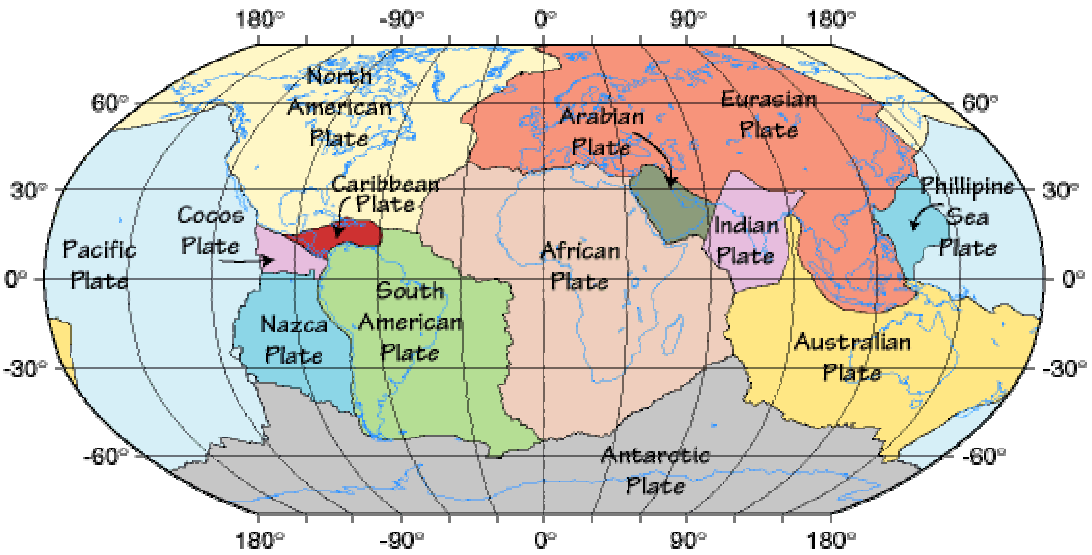

Figure 2.2 The major plates of the Earth
(from the Department of Geosciences, Pennsylvania State University, USA [July 31, 2001])

Figure 2.3 from the Web site <http://eqseis.geosc.psu.edu/~cammon/HTML/ Classes/ IntroQuakes/Notes/> locates earthquake events (dots) around the globe between 1965 and 1995. They are not evenly distributed. By comparing Figures 2.2 and 2.3, we can see that most earthquakes occurred along the boundaries between the plates. This fact indicates there is a high correlation between earthquake activity and plate tectonic movements.

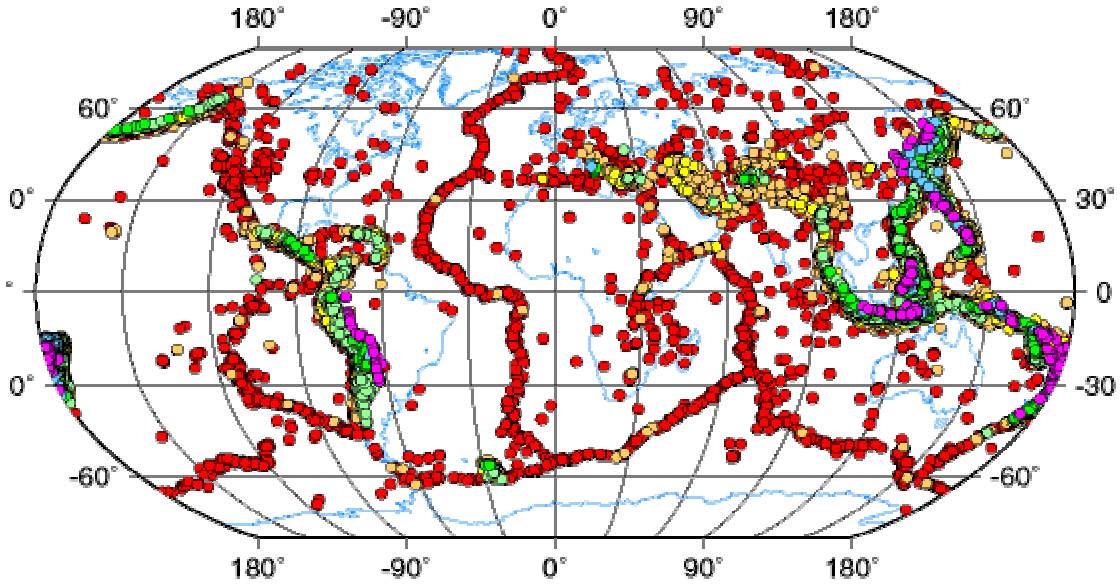

Figure 2.3 Locations of earthquakes around the globe between 1965 and 1995 (from the Department of Geosciences, Pennsylvania State University, USA [July 31, 2001])

An earthquake is a sudden movement of the Earth, caused by the abrupt release of strain that has accumulated over a long time [Shedlock and Pakiser, 1997]. For hundreds of millions of years, the Earth has been shaped as the huge plates that form the Earth's surface slowly move over, under, and past each other. Sometimes the movement is gradual. At other times, the plates are locked together, unable to release the accumulating energy. When the accumulated energy grows strong enough, the plates break free.

The plates can either slide past one another, or they can collide, or they can move apart. The western coast of Canada is one of the few areas in the world where all three of

these types of plate movements take place due to the setting of specific plate tectonics in this region.

2.1.2 Plate Tectonics Setting in Western Canada Region

The western Canada area is close to the boundary between two major plates, the North American and the Pacific plates (see Figure 2.4 from the Web site of <http://www.pgc.nrcan.gc.ca/seismo/eqinfo/plates.htm). Near to the boundary, there are a few smaller plates, such as the Juan de Fuca plate, Explorer plate, and South Gorda plate, as well as the Queen Charlotte fault and the Cascadia subduction zone. The complicated plate tectonic setting is accompanied by high earthquake activity in the area.

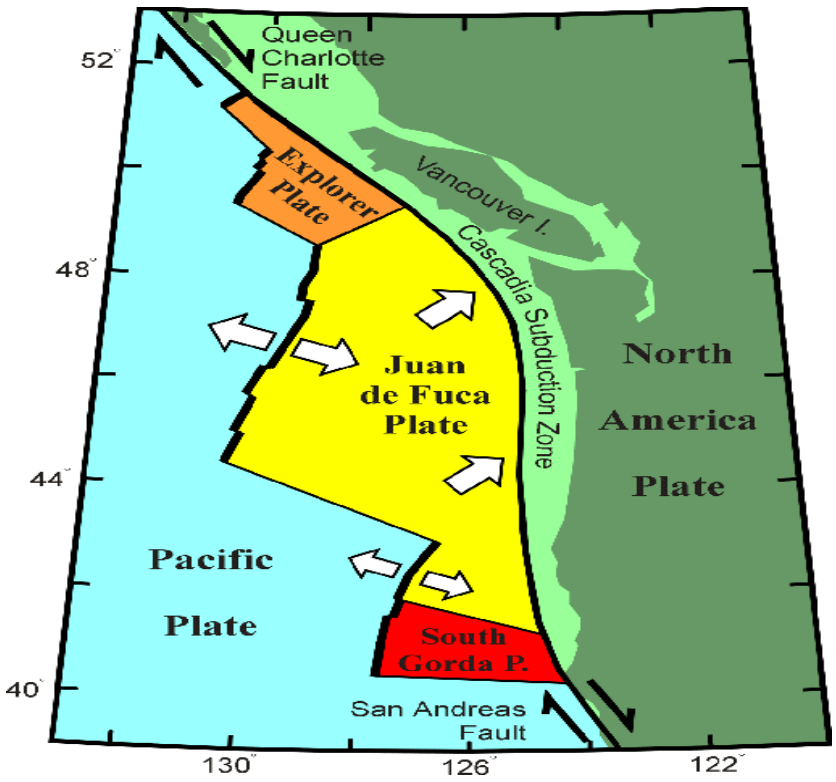

Figure 2.4 Plate tectonic setting of western Canada
(from the GSC Pacific Division of NRCan [December 31, 2001])

In fact, each earthquake indeed corresponds to particular plate tectonic regimes. Most of the earthquakes occur in areas of fractured oceanic crust, which mark boundaries of the small plates (the Juan de Fuca and Explorer plates). Earthquake activity is also high in the Cascadia subduction zone. The Juan de Fuca plate dips below the easterly neighboring North American plate. Thus, both deep (dipping plate) and shallow (overriding plate) earthquakes occur in this zone. Another region of high seismicity is defined by a zone of plate breakage or "faulting" immediately west of the Queen Charlotte Islands (the Queen Charlotte fault).

Earthquakes in western Canada occur along the faults in the offshore region; within the subducting ocean plate; and within the continental crust. Moving inland from the coast and the active plate boundaries, the frequency and size of the earthquakes decrease.

If the earthquake occurs in a populated area, it may cause many deaths, injuries and extensive property damage. If earthquakes could be predicted, many lives could be saved.

2.2 The WCDA Network

A question asked often about earthquake hazards is whether the earthquakes can be predicted. With the present state of scientific knowledge, it is not yet possible to predict earthquakes and specify in advance their exact date, time and location of occurrence. However, the continuing studies of earthquake hazards may eventually allow geoscientists to achieve the goal. In western Canada, many different types of studies are

conducted by scientists to improve the understanding of earthquake hazards. The study of contemporary crustal deformation is an important aspect of these studies.

2.2.1 Configuration of the WCDA Network

Crustal deformation is constantly taking place in response to movement associated with the Earth's plate tectonics. Because plate tectonics are global in scale, only modern space geodetic techniques, including VLBI, SLR, and GPS, can provide direct evidence for the studies of plate tectonic movement by monitoring the crustal deformation.

As part of the Canadian National Earthquake Hazards Program, the WCDA network has been established by the Geological Survey of Canada (GSC) primarily for the study of the seismic hazard in western Canada. The first site to be installed was DRAO (Penticton, B.C.) in 1991. By 2001 the WCDA network had grown to 12 sites (see Figure 2.5 and Table 2.1). The regional network spans southwestern British Columbia, which is the most seismically active, and one of the most densely populated regions in Canada. The GPS network also serves as the northern portion of the Pacific Northwest Geodetic Array (PANGA).

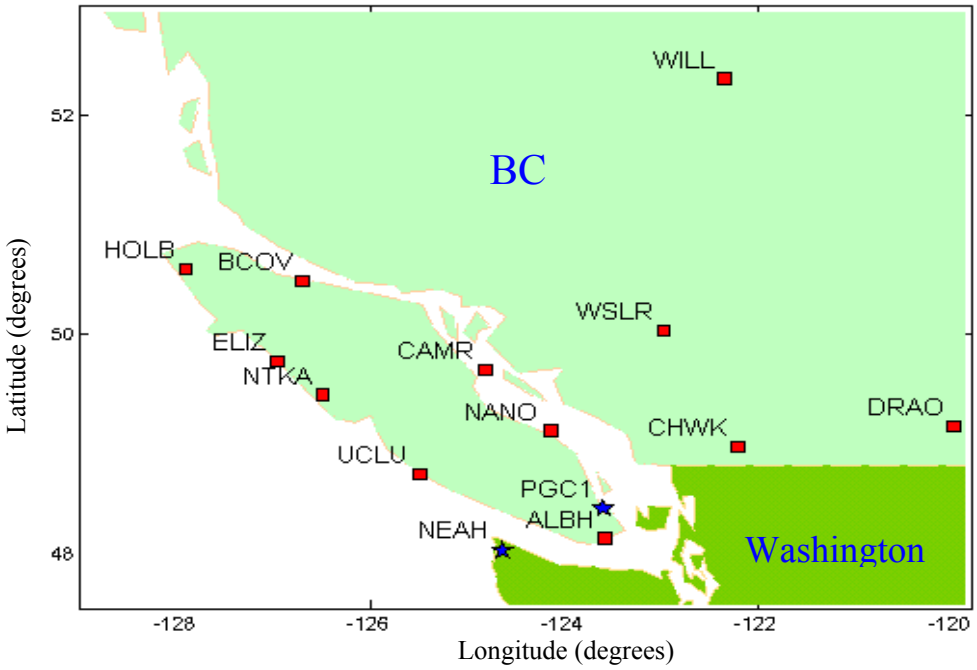

Figure 2.5 Configuration of the WCDA network (PGC1 is a site used for receiver and antenna testing. NEAH is a site operated by the University of Washington)

Table 2.1 WCDA network sites

Site	Latitude (° ′ ″)	Longitude (° ′ ″)	Starting Date	Location
DRAO	N 49 19 21.4	E 240 22 30.1	FEB 1991	Penticton, B.C.
ALBH	N 48 23 23.2	E 236 30 45.1	MAY 1992	Victoria, B.C.
HOLB	N 50 38 25.3	E 231 51 54.0	JULY 1992	Holberg, B.C.
NANO	N 49 17 41.3	E 235 54 48.7	MAY 1995	Nanoose Bay, B.C.
NEAH	N 48 17 58.2	E 235 22 30.3	OCT 1995	Neah Bay, WA, USA
UCLU	N 48 55 32.3	E 234 27 30.1	MAY 1994	Ucluelet, B.C.
WILL	N 52 14 12.3	E 237 04 43.7	SEP 1993	Williams Lake, B.C.
WSLR	N 50 07 35.5	E 237 49 55.9	SEP 1996	Whistler, B.C.
CHWK	N 49 09 21.6	E 237 59 29.8	NOV 1998	Chilliwack, B.C.
NTKA	N 49 35 32.6	E 233 23 0.2	MAY 2000	Nootka Island, B.C.
ELIZ	N 49 52 22.8	E 232 52 38.2	AUG 2000	Eliza Dome, B.C.
BCOV	N 50 59 51.4	E 233 09 26.6	NOV 2000	Beaver Cove, B.C.
PGC1	N 48 38 54.7	E 236 32 55.9	DEC 1989	Sidney, B.C.

The initial objectives of this regional array were: to provide high-quality GPS data for global geodynamic studies; to provide a precise, common reference frame for all deformation surveys carried out in this active seismic region; to serve as a strainmeter to map regional strain and monitor possible transient strain signals. The WCDA was a new tool being adopted in a program of crustal deformation studies.

For the application of GPS for monitoring regional-scale crustal deformation in western Canada, the differential positioning technique has been employed with respect to reference station DRAO. The reference site is located on the stable part of the North American (NA) plate and collocated at a VLBI site. It was chosen to be sufficiently remote from the actively deforming Cascadia subduction zone. On the other hand, the reference site is also close enough to the remote sites for elimination or significant reduction of the common errors in GPS relative positioning. The current studies indicate that the motion of DRAO referring to NA plate is insignificant [Argus and Heflin, 1995; Argus and Gordon, 1996; Larson et al., 1997]. The motions observed at the GPS remote tracking stations with the differential technique represent deformation of the surface relative to the stable reference station DRAO. The length of baselines formed with the reference station and the remote stations of the WCDA in the zone is within a range of 174 to 628 km.

2.2.2 Equipment and Data Acquisition of WCDA

Each WCDA site is equipped with a dual frequency, geodetic quality GPS receiver, atomic frequency standard, high-speed data communication and an un-interruptible

power supply. To ensure long-term reference point stability, each site is carefully monumented with a forced-centered concrete pier solidly anchored in bedrock. A GPS choke ring antenna is mounted on top of the pier using a specially constructed aluminum base that permits antenna alignment.

More detailed information on the sites can be obtained from the station log files on the Web site <http://www.pgc.emr.ca/geodyn/wcda/wcdalogs.htm>. The information in the station log files includes: site identification of the GPS monument; site location information; GPS receiver information; GPS antenna information; local site ties; frequency standard; collocation information; meteorological instrumentation; on-site, point of contact agency information; responsible agency; URL for more information; and appendix: antenna diagram.

Dual-frequency pseudorange and phase data, sampled at 30-sec intervals, are collected daily by an automated process. As part of this process, quality checks are performed routinely by three programs (GIMP8, GPSPACE, QC/TEQC) which generate statistical summaries and plots of the past day's data for each site. Data from WCDA sites are forwarded automatically (upon validation) to the Canadian Active Control System (CACS) and to IGS. The RINEX format files of observations over the last one year from the current day are available on the public server <ftp://sikanni.pgc.nrcan.gc.ca/> under the directory /pub/gpsdata/rinex.

Chapter 3

DIPOP Software Package

The DIfferential POsitioning Program (DIPOP) is a GPS software package developed at the Department of Geodesy and Geomatics Engineering, University of New Brunswick. DIPOP has been continuously upgraded with improvement of GPS and computer techniques from the original DIPOP 1.0 (1985) to the current version. Over the past 15 years or so, it has been involved in a variety of GPS studies.

The first section of this chapter reviews the history of development of the DIPOP software package. The second section describes the basic adjustment principle, functions, basic structure and main algorithms of the three main programs (PREGO, PREDD and MPROC including post-processing program PPROC). A summary is given in the third section.

3.1 Review of DIPOP Software Package Development

The first version of DIPOP, documented by Santerre et al. [1985] and Vaníček et al. [1985], was written for the HP 1000 minicomputer in 1984/85 under contract with the Geodetic Survey of Canada. All programs of the version were written in the Hewlett

Packard FTN4X Fortran language. Its design comprehensively considered various factors that might affect observing and data processing strategies at that time and later, including the satellite constellation, cost and refinement of receiver, satellites' and receivers' clock errors, ionospheric and tropospheric delays, ambiguity estimation and orbit error. The basic frame work (Figure 3.1) for development of DIPOP included: a set of preprocessors, a main processor (MPROC), and a postprocessor (PPROC). The first generation preprocessors only worked with Macrometer V-1000 and Texas Instruments TI 4100 receivers.

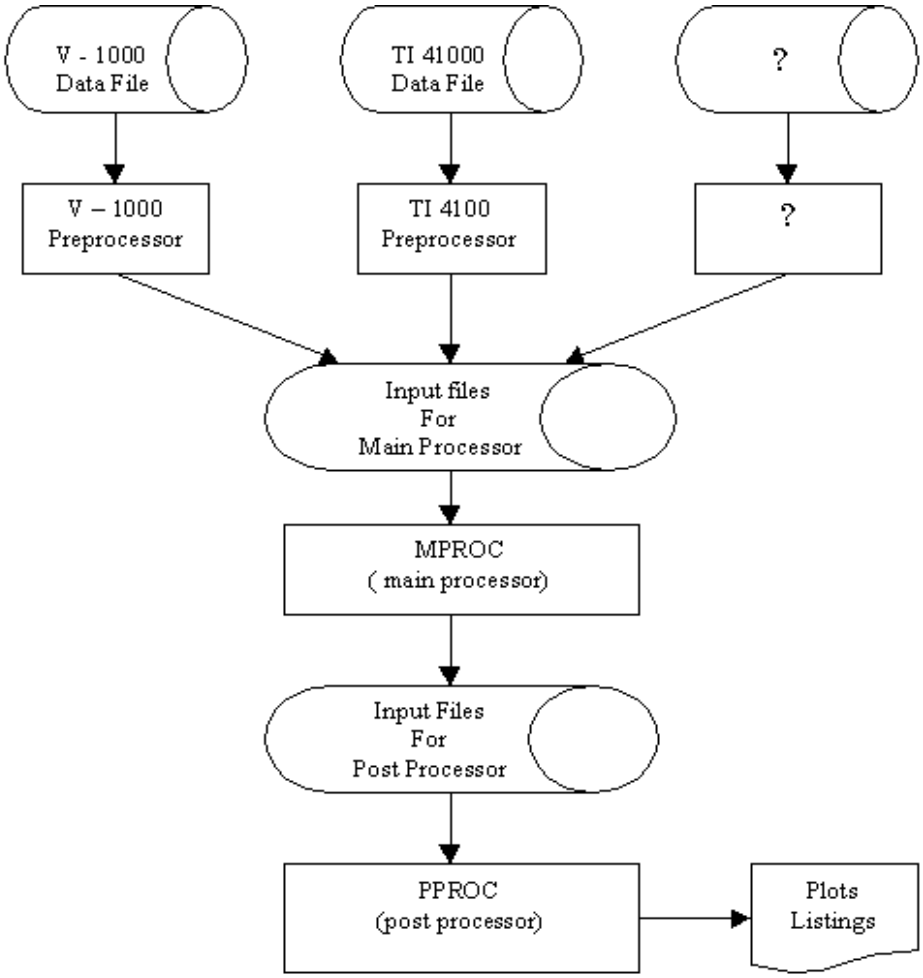

Figure 3.1 General program structure [Vaníček et al., 1985]

Two years later, a new generation, DIPOP 2.0 documented by Santerre [1987], was born. In 1989, the version 2.1, documented by Kleusberg et al. [1989], was generated. During the period of these years, DIPOP underwent extensive tests and uses and was continuously modified. The new version was written in FORTRAN 77 and implemented on the HP1000, VAX, IBM PC and Macintosh computers. The modified preprocessor for TI 4100 took advantage of the dual frequency receiver. It consisted of two main programs: PREGE and PREDD. The first one, PREGE, was used to eliminate obvious data errors and to detect and fix cycle slips in the one-way phase observations (one receiver, one satellite). In the program PREDD, phase double differences were used to detect and correct the remaining small cycle slips of the observations and the "cleaned" observations are stored in an output file for the main processor. The structure of the TI 4100 preprocessor has been kept until the current version. The main processor, MPROC, was also improved in the new version. Multiple options were added for ionospheric and tropospheric refraction corrections. Mathematical correlation between double differences of two stations was taken into account. All results from MPROC are output to files rather than printed out like in the first version. A new program (DPDIM) was created to define the parameters' dimensions during compiling MPROC and PPROC. Other modifications are detailed in the documents mentioned above.

The GPS technique has become increasingly mature and perfected during the 1990s. The satellite constellation was completed. The IGS service formally began on 1 January 1994. RINEX format is widely used. In the meantime, theoretical developments also continued at full speed. All these activities provide a good circumstance for the GPS software development. The draft version of document of third generation DIPOP was

issued in 1993 [Georgiadou et al., 1993]. After that version, DIPOP is still under development. Documentation of a formal version for the third generation DIPOP is being planed.

Besides the version used by the author, there were also some special versions of DIPOP including those by Parrot, Chen, Santos, and van der Wal (see Appendix A). They were used in different GPS applications, such as the test of GPS instruments, the analysis of crustal deformation and structural deformation, the correction of atmosphere, the orbit determination, the correction of cycle slips, and the improvement of data processing methods and so on.

The next section details the third generation DIPOP, the current version that is used by the author. In all the following sections, DIPOP denotes the current version.

3.2 DIPOP Software Package

The current DIPOP software package consists of three main programs: PREGO (PREGE), PREDD and MPROC including PPROC. All the programs of DIPOP are written in Fortran 77. Figure 3.2 gives a flowchart of the software package. It is designed to run in the shell environment of the UNIX Operation System and uses a command line user interface. Each main program has a command input file. The needed parameter values of each main program and selections of models are designated in its command file.

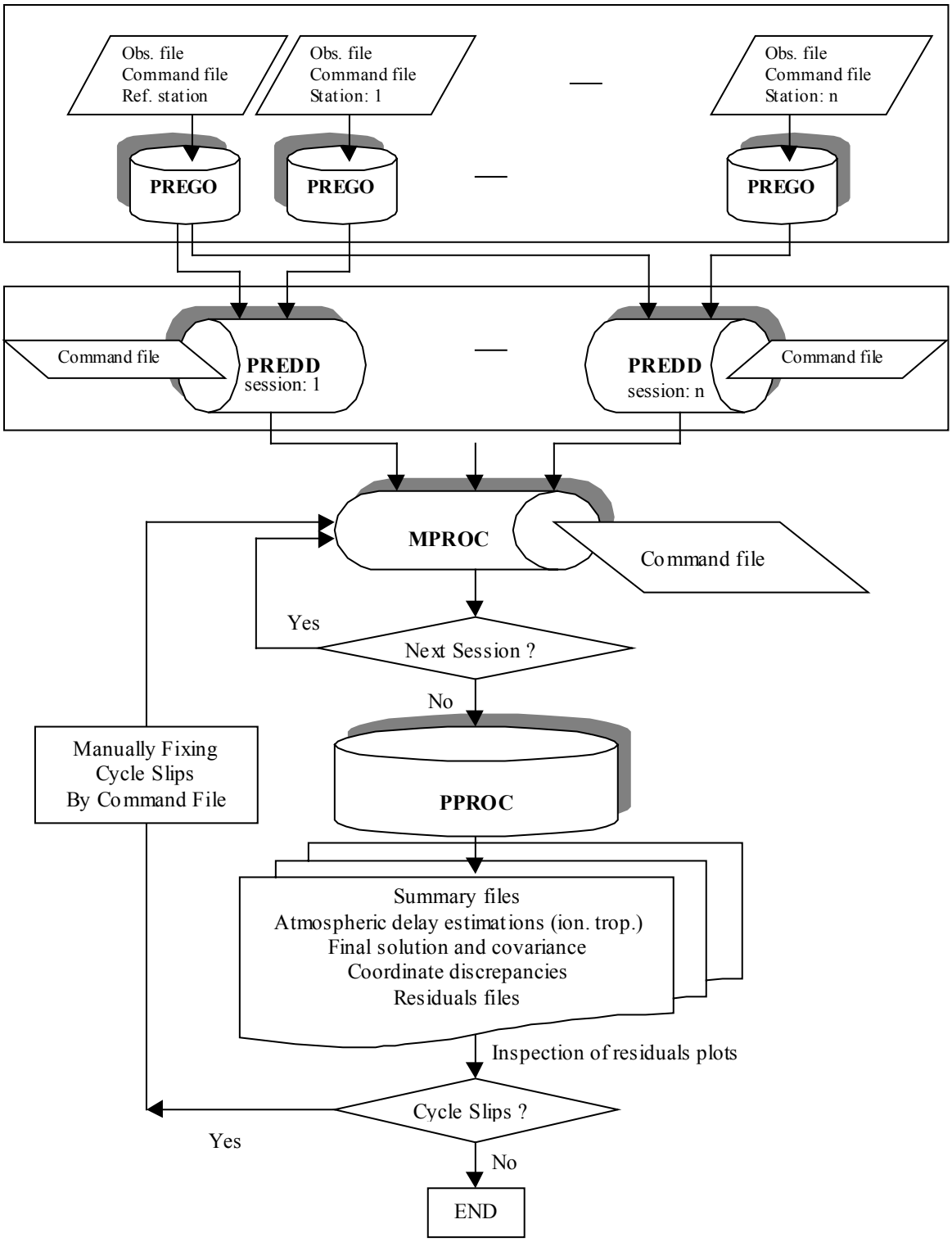

Figure 3.2 The flowchart of DIPOP

3.2.1 Principles of Adjustment in DIPOP

The equation of GPS carrier phase observations is usually expressed as:

$$\Phi_{(t)} = \lambda\ \phi_{(t)} = \rho_{(t)} + c\ (dT_{(t)} - dt_{(t-\tau)}) + d_{trop(t)} - d_{ion(t)} + \lambda\ N + \varepsilon_{(t)} \qquad (3.1)$$

where t is the nominal reception time, τ is the signal travel time from satellite to receiver, λ is carrier wavelength, $\phi_{(t)}$ is carrier phase measurement, $\Phi_{(t)}$ is the carrier phase measurement in units of distance, $\rho_{(t)}$ is satellite-to-receiver distance, c is speed of light in a vacuum, $dt_{(t-\tau)}$ is satellite clock error, $dT_{(t)}$ is receiver clock error, $d_{trop(t)}$ is tropospheric delay error, $d_{ion(t)}$ is ionospheric delay error, N is the integer carrier phase ambiguity, and $\varepsilon_{(t)}$ is random errors including measurement error in carrier phase observations and the effect of multipath and receiver noise.

In DIPOP's data analysis, the double differences of carrier phases are used. The double differences can be expressed as:

$$\Phi^{qp}_{ji\ (t)} = \lambda\ \phi^{qp}_{ji\ (t)} = \lambda\ (\phi^{q}_{j\ (t)} - \phi^{q}_{i\ (t)}) - \lambda\ (\phi^{p}_{j\ (t)} - \phi^{p}_{i\ (t)})$$

$$= \rho^{qp}_{ji\ (t)} + d^{qp}_{ji\ trop(t)} - d^{qp}_{ji\ ion(t)} + \lambda\ N^{qp}_{ji} + \varepsilon^{qp}_{ji\ (t)} \qquad (3.2)$$

where superscript p and q indicate satellite p and satellite q, and the subscript i and j represent two stations, i and j, respectively. The other terms are as defined in the above equation (3.1). It is obvious that the principal advantage of the double differences is to cancel most of the clock errors ($dt_{(t-\tau)}$ and $dT_{(t)}$) from the observations while the small clock errors caused by receiver clock drifts and satellite frequency offset are neglected.

Notice that the ambiguity N_{ji}^{qp} in equation (3.2) still keeps the character of an integer because it is simply the difference of integers. The ambiguity is estimated in the least-squares adjustment along with the coordinates of remote receivers.

For a short baseline, the effect of atmosphere delays also can be efficiently reduced using the double difference, since received signals by two near-by stations propagate almost along similar paths. But the atmospheric delays are a main error source of double difference observations in long baseline measurements.

The effects of mutipath and noise cannot be mitigated with the double difference mode or any linear combinations of observations, because they are independent of the specific receiver-satellite geometry. They have been a main factor in limiting the accuracy in GPS measurements.

3.2.2 Preprocessors: PREGO and PREDD

The goal of the preprocessors is to supply clean observations and information of satellite orbits for the main processor. The program PREGO operates on one-way single or dual frequency observations. The program is the first step for cleaning raw GPS data from single receiver. Its command file provides input and output file names, antenna information of the station, the parameters that control the quality checking and the setting of the observation time window.

PREGO performs the tasks of reading the raw data, eliminating bad observations and detecting and correcting cycle slips using a single frequency or dual frequency algorithm. A detailed description of these algorithms is given in the document*, GPS Data*

Preprocessing with DIPOP 3.0 [Georgiadou et al., 1993]. PREGO has the ability to process observations in 4 formats including UNB format, short UNB format, GSC format, and RINEX format (versions 1 and 2). In addition, PREGO produces an output file for the preprocessor PREDD and a summary file for users. Due to the receiver clock error, PREGO is mainly useful in reduction of large cycle clips to the few cycle level [Kleusberg et al., 1989].

As a continuation of preprocessing data, the program PREDD performs mainly the following tasks:

- read input data (a command file, ephemeris files, and observation files);
- scan input data for large gaps;
- edit data to perform such tasks as eliminate bad satellites and remove the observations below a specified elevation angle cutoff;
- compute satellite coordinates;
- detect, determine, and repair the remaining cycle slips;
- output clean phase double differences and satellite coordinates for the main processor.

In contrast to the analysis of one-way observations in program PREGO, the program PREDD employs phase double differences. The use of this mode makes PREDD able to detect the small cycle slips missed by PREGO due to cancellation of the impact of satellite clock and receiver clock errors. PREDD reads needed information from its command file such as input and output file names, station names, and approximate ellipsoidal coordinates of the stations. The command file also contains other parameter values used for editing data, scanning for large gaps, removing cycle slips, and setting the

elevation angle cutoff. Considering the different sensitivities of different linear combinations to cycle slips, there are multiple options for selecting different linear combinations and setting their corresponding threshold values for detecting cycle slips in the command file. Users can delete bad observations by specifying the satellite number and observation time in the command file.

Running PREDD to remove cycle slips is an automatic procedure. But threshold values for detecting cycle slips are preset in the command file specified by users. If the values are improper, falsely detecting or missing cycle slips will happen. As a result, the cycle slips will be seen in plots of the residuals from the program MPROC. According to the author's experience with DIPOP, it takes a lot of time to determine an appropriate value for the threshold of detecting cycle slips in a particular data set and is a trial-and-error process. So a filter to automatically remove cycle slips is needed in DIPOP. This is needed particularly for processing a large amount of GPS data or for production work.

3.2.3 Main Processor and Postprocessor: MPROC and PPROC

MPROC is the main processor of DIPOP. It performs one main task: sequential least-squares adjustment in baseline or in network mode using the cleaned data from the program PREDD. As a subroutine of the main program MPROC, the postprocessor PPROC is in charge of the post-processing.

The main program MPROC can estimate station coordinates, ionosphere delay and troposphere delay, and the nuisance or bias parameters (phase ambiguities, receiver clock parameters). It also computes the residuals using the final estimated parameter values.

Statistics of the adjustment results are written in a summary file. The error corrections considered in current version of DIPOP include the following terms: Earth tide, polar motion, ocean tide loading displacement, receiver clock error, ionosphere and troposphere delay.

The sections below present the models that are already applied to data processing in the main processor MPROC.

3.2.3.1 Tide Corrections

When GPS measurements require an accuracy at the cm level or better in relative positioning for medium or long baselines, various environmental effects must be taken into account. Among these effects, the deformations of the Earth induced by the tides, including solid Earth tide, pole tide and ocean loading tide, are important because they directly produce displacements of station positions. Corrections of the tide effects have been considered in the current version of DIPOP.

The solid Earth tide is the deformation of the solid Earth caused by tidal forces of the moon and the sun. At low altitudes, the Earth's surface is typically displaced through a range of 40 cm in a little more than 6 hours due to the deformation. The solid Earth displacement can be computed to an accuracy of about 2 mm. The remaining uncertainty is caused by the effects of lateral variations in Earth structure and inelasticity at tidal periods [Baker et al., 1995].

The effect on station coordinates induced by the Earth solid tide is most conveniently modeled as variations in the standard geopotential coefficients expressed as spherical

harmonic functions of time. The site displacements caused by the tides of spherical harmonic degree and order (n, m) are characterized by the Love Number h_{nm} and Shida Number l_{nm}. The effective values of these numbers depend on station latitude and tidal frequency [Wahr, 1981]. The dependence is a consequence of the ellipticity and rotation of the Earth, and includes a strong frequency dependence within the diurnal band. A further frequency dependence, which is most pronounced in the long period tidal band, arises from the mantle anelasticity which leads to corrections to the elastic Earth Love Number; these corrections have a small imaginary part and cause the tidal displacements to lag slightly behind the tide generating potential. All these effects need to be taken into account when an accuracy of 1 cm or better is desired in positioning. Consequently the anelastic Earth model is recommended for use in precise data analysis [McCarthy, 1996].

The vector Δ of the displacements on a spherical Earth expressed in a topocentric system is given by equation [Bock, 1995]:

$$\Delta = \sum_i \left[\delta_1^{(i)}, \delta_2^{(i)}, \delta_3^{(i)}\right]^T \tag{3.3}$$

$$\delta_1^{(i)} = \frac{h_i U_i}{g}, \qquad \delta_2^{(i)} = \frac{l_i \cos\phi_s \left(\frac{\partial U_i}{\partial \lambda_s}\right)}{g}, \qquad \delta_3^{(i)} = \frac{l_i \left(\frac{\partial U_i}{\partial \phi_s}\right)}{g}.$$

In the equation, $i = 2, 3$ (2 for Moon and 3 for Sun), U_i is the tidal potential for a station due to a perturbing object (the Sun or the Moon), ϕ_s and λ_s are geocentric latitude and east longitude of the Moon or the Earth respectively, h_i and l_i are vertical Love Numbers and the corresponding horizontal Shida Numbers respectively, and g is the gravity acceleration of the Earth.

$$g = GM_{\oplus} / \mathbf{r}_s^2 \tag{3.4}$$

where the $GM_{\oplus}$ is gravitational parameter for the Earth, $\mathbf{r}_s$ is the coordinate vector from the geocentre to the station.

The correction of the solid Earth tide in DIPOP is computed with a subroutine program provided by Dehant et al. in June, 1996 at the ftp serer <ftpserver.oma.be>, subdirectory /pub/astro/dehant/IERS/ (anonymous-ftp system). The effect of solid tide can be modeled to an accuracy of within 2 mm. The detailed information about the computation and use of parameter values is described in the IERS Technical Note 21 [McCarthy, 1996].

The ocean loading tide local site displacement is understood as an effect of elastic deformation of the Earth in response to time-varying surface loads. The reference point of zero deformation is the joint mass center of the solid Earth and the loads, while the sites are attached to the solid Earth. The convention implies that the rigid body change of the solid Earth that counterbalances the motion of the load's mass center is not contained in the local displacement model.

The ocean loading tide is the elastic response of the Earth's crust to the ocean tide on the Earth's surface and causes a local deformation. The deformation due to the ocean tide has a range of more than 10 cm for vertical displacement in some near-ocean locations. When mm positioning accuracy is required, even GPS measurements made 500 to 1000 km from the ocean require ocean loading corrections [Baker et al., 1995].

To model the ocean loading tide deformation at a particular site, an elastic Earth model is used and the response of the Earth to the surface mass load is computed. The

loading tide deformation is clearly site dependent because it changes with the spatial distribution of the ocean tides with respect to the observation site, and both the nearby and distant ocean tides are important to the calculation. Let Δc denote a displacement vector (radial, west-east, and south-north) at a particular site and time t. The displacement vector due to the ocean loading tide is expressed in the form:

$$\Delta c = \sum_j \alpha_j \cos(\omega_j t + \chi_j - \psi_j) \tag{3.5}$$

where j is an order number of tidal components (in the current version of DIPOP, j # 11). An explanation of the 11 constituents is given in Table 3.1 [Baker et al., 1995]. Based on the periodic characteristic of these constituents, they are divided into the semi-diurnal tides, diurnal tides and long period tides. ω_j and χ_j are the frequency and astronomical argument of tide constituent j, and α_j and ψ_j are the amplitude and Greenwich phase lag of tidal constituent j respectively. ω_j and χ_j can be determined from the solar and lunar ephemeris information.

In DIPOP, the effect of the ocean loading tide is computed by reading from a file containing the amplitude and phase of the tidal harmonic coefficients of the ocean loading correction. The coefficients of ocean tide loading can be obtained from the free Web site, <http://www.oso.chalmers.se/~loading/>, by providing the coordinates of a station and selecting an ocean loading model; or computed with the software LOADSDP [Pagiatakis, 1992]. The version 5.03 of LOADSDP can be obtained from the ftp server <geod.nrcan.gc.ca> in a directory called /pub/GSD/spiros/. The software allows users to use only the FES95.2 global ocean tide model, or integrate this global model with a regional ocean tide model to calculate parameters of the ocean tide correction when you

have a more accurate regional model. The regional model usually represented by cells of $0.5^{\circ} \times 0.5^{\circ}$ or smaller size is used to supplement the $1^{\circ} \times 1^{\circ}$ global model. For principal geodetic sites in Canada and the Northern United States, the enhanced ocean tide loading parameters are available on the ftp site <geod.nrcan.gc.ca> in a directory called /home/ftp/pub/GSD/Tides [Lamber et al., 1998].

Table 3.1 The main tidal harmonics

Tide Symbol	Tide Type	Period (Solar Time)
M_2	Semidurnal tide, principal lunar	12.42 hours
S_2	Semidurnal tide, principal solar	12.00 hours
N_2	Semidurnal tide, major lunar elliptical	12.66 hours
K_2	Semidurnal tide, luni-solar declinational	11.97 hours
K_1	Diurnal tide, luni-solar declinational	23.93 hours
O_1	Diurnal tide, principal lunar	25.82 hours
P_1	Diurnal tide, principal solar	24.07 hours
Q_1	Diurnal tide, major lunar elliptical	26.80 hours*
M_f	Long-period tide, lunar fortnightly	13.66 days
M_m	Long-period tide, lunar monthly	27.55 days
S_{ea}	Long-period tide, solar semiannual	182.62 days

* Q_1 is from Lambeck, 1988. The others are from Baker et al., 1995

Pole tide is the elastic response of the Earth's crust to shifts in the pole of rotation. Tides are raised by the variation in the orientation of the rotation axis relative to the crust; and further tides are raised by the changes in the speed of rotation of which the major components would be annual and semi-annual variations, as well as a variation on the decade time scale. The variation of station coordinates caused by the pole tide should not be ignored in the data analysis of precise GPS measurements. Expressions for pole tide

displacement in the direction of geocentric spherical latitude, longitude and radius are given by Wahr [1985]:

$$d_\phi = -\frac{\omega^2 R}{g}\cos 2\phi\left(x_p \cos\lambda + y_p \sin\lambda\right)l_2 \tag{3.6}$$

$$d_\lambda = -\frac{\omega^2 R}{g}\sin\phi\left(-x_p \sin\lambda + y_p \cos\lambda\right)l_2 \tag{3.7}$$

$$d_r = -\frac{\omega^2 R}{g}\sin\phi\cos\phi\left(x_p \cos\lambda + y_p \sin\lambda\right)h_2 \tag{3.8}$$

where ω is the rotation rate of the Earth, x_p and y_p represent displacement from the mean pole, g is the surface acceleration due to gravity and h and l are the vertical and horizontal quadrupole Love Number and Shida Number respectively.

In DIPOP, $l_2 = 0.0836$ and $h_2 = 0.6027$ based on the IERS conventions (1996); and the parameters (x_p and y_p) of polar motion are from the bulletins published by IERS. Taking into account the variation of x_p and y_p, at most 0.8 arcsec, the maximum radial displacement is approximately 25 mm, and the maximum horizontal displacement is about 8 mm [McCarthy, 1996].

3.2.3.2 Atmospheric Delays: ionospheric delay and tropospheric delay

The propagation speed of GPS signals does not equal the vacuum light speed while they are traveling in the Earth's atmospheric envelope. The varying propagation speed leads to a delay in excess of the free-space or vacuum delay of the signals. This delay is called the atmospheric delay. Based on the physical properties of the atmosphere, the Earth's

atmosphere is divided into several distinct layers. They include ionosphere, mesosphere, stratosphere, and troposphere.

Ionospheric delay The ionosphere is the first atmospheric layer encountered during the propagation of the GPS signals from the satellites to a receiver. This region is characterized by a significant number of free electrons and positively charged atoms and molecules. The free electrons affect the propagation of radio waves, and thus affect the signals from the GPS satellites.

Because the ionosphere is a dispersive medium for radio waves, the propagation velocity depends on the frequency of the waves. This means that a user of a dual frequency GPS receiver can essentially eliminate the ionospheric delay with dual frequency observables. The well-known ionosphere-free linear combination serves this purpose, especially for long baseline measurements. The ionospheric delay can be almost completely removed with the linear combination as long as the effects from higher order terms (>1 order) of the refractive index of ionosphere are negligible (mm level or less). Based on equation (3.1), the ionosphere-free combination is expressed in units of length as

$$\Phi_{IF}(t) = fc_1 \Phi_{1(t)} + fc_2 \Phi_{2(t)} \tag{3.9}$$

$$= \rho_{(t)} + c\{dT_{(t)} - dt_{(t-\tau)}\} + d_{trop(t)} + fc_1 \lambda_1 N_1 + fc_2 \lambda_2 N_2 + \varepsilon_{IF}$$

$$fc_1 = \frac{f_1^2}{f_1^2 - f_2^2} \qquad fc_2 = \frac{-f_2^2}{f_1^2 - f_2^2}$$

where f_1 and f_2 represent the carrier frequencies on L1 and L2, λ_1 and λ_2 are the carrier wavelength on L1 and L2 , c is the vacuum light speed and N_1 and N_2 are the L1 and L2

phase ambiguities respectively. The other terms are defined as in equation (3.1). However the linear combination is not suitable for short distance relative positioning because the combination increases the noise level caused by multipath and noise. Therefore, for short baselines it may be preferable to only use single-frequency observations rather than the ionosphere-free combination.

For the users of DIPOP, using only double differences of a single frequency observable or using the ionosphere-free combination of dual frequency observables to eliminate the effect of ionospheric refraction are both available in measurement adjustment.

Tropospheric delay The lowest layer of the Earth's atmosphere is the troposphere where a lot of neutral atoms and molecules exist. When the radio signals pass through the troposphere, the signals are refracted. The refraction delays the propagation of the radio signals. There is also some effect in the stratosphere, so it is the best to generally use the term “neutral atmosphere delay”. Since the bulk of effect occurs in the troposphere, many use the term “troposphere delay”. The tropospheric delay for GPS signals can be about 2.4 meters in the zenith direction and grows with increasing zenith angle [Brunner and Welsch, 1993]. The tropospheric delay does not depend on the carrier frequency due to its non-dispersive nature. So the tropospheric delay cannot be measured using the GPS signals themselves. It is recognized as a major error in precise GPS positioning applications.

The tropospheric delay consists of two parts: "dry" or hydrostatic and "wet" or non-hydrostatic components. The dry term contributes about 90% of the total delay.

Hydrostatic delay can be obtained from surface pressure only with an accuracy of a few mm. Unlike the dry delay, the wet delay is highly variable, both spatially and temporally, and model prediction using surface meteorology yields an accuracy no better than 1-2 cm, depending on the atmospheric conditions [Langley, 1997]. Although the wet contribution is only about 10% of the total, it is still an accuracy limitation in precise GPS positioning, especially for the vertical position component. An error of a cm in modeling the tropospheric zenith delay can result in vertical position error of about 3 cm [Brunner and Welsch, 1993].

Since the tropospheric delay is elevation angle dependent, the tropospheric delay at a certain elevation angle is expressed as a product of the tropospheric zenith delay and a mapping function that maps the increase in delay with an increasing zenith angle. The mapping function relates the vertical delay to the delay at a particular elevation angle. Such mapping functions typically do not depend on azimuth, because atmospheric layers are assumed to be spherically symmetric.

The total tropospheric delay at an elevation angle ε is usually expressed as

$$d_{trop} = d^z_{dry} \cdot m_{dry}(\varepsilon) + d^z_{wet} \cdot m_{wet}(\varepsilon) \tag{3.10}$$

where d^z_{dry} and d^z_{wet} are the dry and wet delays in the zenith direction, $m_{dry}(\varepsilon)$ and $m_{wet}(\varepsilon)$ are mapping functions corresponding to the dry and wet delays respectively. In some cases, a single mapping function can be used for both components. Scientists have published a succession of tropospheric prediction models and mapping functions to model the tropospheric delay during the past 30 years. Table 3.2 gives all the zenith delay prediction models and the mapping functions included in DIPOP.

Table 3.2 The models of tropospheric zenith delay and the mapping functions in DIPOP

Dry Zenith Model	Wet Zenith Model	Dry Mapping Function	Wet Mapping Function
Hopfield	Hopfield	Hopfield	Hopfield
Saastamoinen	Saastamoinen	Saastamoinen	
	Ifadis	Lanly	Ifadis
	Askne&Nordius	Niell	Niell
		Davis	
		Chao	Chao
		Csec	Csec
		Herring	Herring
		Goad&Goodman	Goad&Goodman

Since the present models cannot fully predict the tropospheric delay, especially the wet component, an estimation of the residual tropospheric zenith delay, the difference between the value predicted from a sophistical model and the actual zenith delay, is usually involved in GPS data analysis. The residual zenith delay can be estimated for observations spanning many hours, an hour or less per site, or using a stochastic model such as a random walk process. Only the first way is taken in the main processor of the current version of DIPOP although van der Wal (1995) experimented with stochastic estimation of residual tropospheric delay using DIPOP. Considering larger errors caused by tropospheric delay from lower elevation angles, an approach to down-weight the observations at low elevation angles using mapping function is provided in the least-squares adjustment of DIPOP. How to efficiently remove the effect of the tropospheric delay using DIPOP is discussed in the next chapter.

3.2.3.3 Measurement Weighting

There are two modes of weighting observations in the least-squares adjustment of DIPOP. The two modes are based on similar principals to down-weight the observations at low elevation angles.

Using the mapping function to determine weights of observations at each epoch is one of the two modes. The approach's improvement is particularly obvious for the vertical component of position solutions when the observations at lower elevation angles have to be used without estimation of the tropospheric delay. The weighted position solutions by mapping functions have smaller bias than the unweighted solutions due to an unmodeled tropospheric delay [Collins and Langley, 1998]. The weight *w(t)* for an observation at epoch t in DIPOP yields the inverse of the square of the combined mapping functions related to the elevation angle at the epoch. The calculation of the weight follows the equation:

$$w(t) = \left(\frac{zenithd_{trop}(t)}{totald_{trop}(t)} \right)^2 \tag{3.11}$$

where $zenithd_{trop}(t)$ and $totald_{trop}(t)$ are the tropospheric delay in the zenith direction and the total tropospheric delay respectively. The zenith models and mapping functions available in DIPOP predict the zenith delay and the total delay.

The second mode uses the measured carrier-to-noise power density ratios (C/N0) from the original data to calculate the phase variance of each observation and so estimate their

weights. In DIPOP, the phase variance is computed using a formula driven by Langley (1997)

$$\sigma_{\phi}^{2} = C \cdot 10^{-\frac{C/N0}{10}} \tag{3.12}$$

where σ_{ϕ}^{2} is the variance of the phase observation (m^2), C is the model parameter (m^2Hz), *C/N0* is the measured carrier-to-noise-power-density ratio in unit of dB-Hz. Since the measured C/N0 values directly express the quality of individual GPS signal, the weights of the GPS observations are actually determined by the quality of data.

The two modes reduce some physical correlation in the measurement to a certain degree besides the mathematical correlation of double difference observations, which is taken into account in DIPOP.

3.2.3.4 Linear Combinations of Carrier Phase Observables

The linear combinations of dual frequency observables are involved in different studies and applications based on their different characteristics. For example, the ionosphere-free combination is used to reduce the effect of ionospheric delay since the ionospheric delay is frequency dependent; the widelane combination is useful when trying to resolve ambiguities; the narrowlane has the property of reducing the noise; and the geometry-free combination is particularly useful for monitoring the ionosphere.

If symbol $\phi_{LC}(t)$ represents the linear combination of carrier phase observables, the equation of the combination can be expressed as:

$$\phi_{LC}(t) = I \cdot \phi_1(t) + J \cdot \phi_2(t) \tag{3.13}$$

where I and J are integer numbers, $\phi_1(t)$ and $\phi_2(t)$ are carrier phase observations in cycles on L1 and L2 at the epoch t. Let the $\lambda_{LC,}$ λ_1 and λ_2 represent the wavelengths of the combination and the carrier phases on L1 and L2 respectively, and the $f_{LC,}$ f_1 and f_2 represent the frequencies of the combination and the carrier phases on L1 and L2 respectively. The effective wavelength and frequency of the combination are defined by following expressions:

$$\lambda_{LC} = \frac{\lambda_1 \cdot \lambda_2}{I \cdot \lambda_1 + J \cdot \lambda_2} \qquad f_{LC} = I \cdot f_1 + J \cdot f_2 \tag{3.14}$$

In general, the combinations for which I and J have different signs are called the widelane observables, and for which I and J have same signs are called the narrowlane observables. Because the specific observable ($I = 1, J = -1$) and ($I = 1, J = 1$) are the most important of all the widelane and narrowlane observables, they are usually referred to simply as the widelane and narrowlane observables.

Table 3.3 gives all the linear combinations involved in the main processor of DIPOP. A discussion of GPS inter-frequency carrier phase combinations can be read in a paper written by Collins [1999] who created the linear combination part of the programs.

Table 3.3 The linear combinations of carrier phase observables

I	J	Combination Observables
1	0	Carrier phase on L1
0	1	Carrier phase on L2
77	-60	Ionosphere-free
1	-1	Widelane
1	1	Narrowlane
-1	2	Alternative widelane 1
-2	3	Alternative widelane 2
-3	4	Alternative widelane 3
4	-5	Alternative widelane 4
-7	9	Extra widelane
4	-3	Narrowlane 1
5	-4	Narrowlane 2
9	-7	Extra narrowlane

3.2.3.5 Least-squares Adjustment

The main processor of DIPOP provides a batch sequential least-squares adjustment of estimated parameters. Batch means one session can be divided into a few small independent observation files with the same time interval depending on the user's requirements and each file has an independent solution in the least-squares adjustment. This option for batch processing can be used to simulate rapid static processing. The time length of batch sessions, which is represented by number of epochs, is input from the command file of the main program.

For static GPS relative positioning, DIPOP provides an algorithm of sequential least-squares adjustment for each session. The algorithm allows users to get a series solution of

all the estimated parameters at each epoch specified by the users. The specific epoch is realized by setting an interval (a number of epochs) in the command file for evaluating the nuisance parameters or for tropospheric estimation. During the whole adjustment, a sequential solution is produced once each interval. The interval should be larger than the sampling interval of observations and large enough to satisfy requirements of the sequential solutions. All the information about the sequential and final solutions of the session is written in the output files by the post processor.

3.2.3.6 Cycle Slip Editing

The main processor of DIPOP provides an opportunity to repair the remaining cycle slips as a supplement of the preprocessor PREDD. The cycle slips may be missed by preprocessors or are incorrectly fixed by PREDD. The procedure is completed by a manual interaction with DIPOP.

The postprocessor produces a double difference residuals file in compact format that can be viewed by GT, a graphical software tool developed by University NAVSTAR Consortium (UNAVCO). The residuals plots can help a user to discover remaining cycle slips in double difference observations. If a cycle slip occurs in a residual plot, the user can estimate number of cycles of the jump by examining the residual plot. The number will be input in the command file of the main processor together with the corresponding satellite number and epoch of the cycle slip.

The slip should appear in two plots unless the satellite is either the first or last in the list of satellite pairs at the particular epoch. The sign of the cycle slip follows a regulation

that if the satellite with the cycle slip is the first one of the satellite pair, the sign is positive, otherwise it is negative. Note that manual cycle slip editing is only practical in the case of a few cycle slips. If there are many cycle slips in the residual plots, the best way is to go back to PREDD and adjust the threshold values.

3.2.3.7 Postprocessor: PPROC

Although the program PPROC is designed as a subroutine of the main program MPROC, the program PPROC as the postprocessor has an independent function. Its task is to record all the results of the estimated parameters and their statistical information into a summary file in an easily understood form. Contents of the summary file contain the station coordinates and derived values (baseline components and length) together with their respective standard deviations as well as the inverse of the normal equation matrix. This file also presents a standard deviation and a mean of double difference residuals and some information from the command file of the main program. In addition, the program produces a file of double difference residuals in a compact format that can be viewed with the graphical software tool GT and the residuals plots of double difference observations can be displaced in a window of GT. This file is very useful for checking the final results' quality. A file including residual tropospheric or ionospheric delays at each epoch is output if users require estimate of the delays using an option in the command file of the main program.

3.3 Summary

The main purpose of this chapter is to introduce the software package DIPOP, especially for the models and algorithms involved in the main processor. Considering mm-level relative positioning precision, this chapter addresses the usage of the technique of double differences of carrier phases and details the correction models of main systematic errors including tropospheric delay, ionospheric delay, and the tidal effects. A test with WCDA data for the models in DIPOP is presented in the next chapter.

Chapter 4

A Test of Data Processing with DIPOP

In order to meet the requirement of the accuracy for WCDA data analysis, the performance of the GPS software DIPOP was verified by a test with a data set from the WCDA network covering a one-week period. The test focused on the determination of proper adjustment models in DIPOP for future data analysis and evaluation of the accuracy of the DIPOP solutions.

This chapter consists of 5 sections. The first section gives some considerations in regard to the test followed by the discussions of estimation methods for residual tropospheric delay and tidal effects on GPS measurement in sections 2 and 3. Section 4 presents the processing results of the WCDA data over one week. The last section gives a summary of the test.

4.1 Some Considerations

Since the rate of crustal deformation in the region of WCDA is only of the order of 1 cm per year or less, high precision processing software is required to extract the deformation

signals. According to the requirement, the test of DIPOP mainly addresses the following two aspects:

1) determine an approach to efficiently eliminate the errors in GPS relative positioning with DIPOP;
2) evaluate the performance of DIPOP software by processing a data set from 7 WCDA baselines over a one-week period.

As discussed in Chapter 3, in the least-squares positioning model using double differences, the errors of the receiver and satellite clocks are eliminated. When the precise ephemeris is applied in data analysis, the errors affecting GPS measurement are mainly caused by the ionospheric and tropospheric delays, tidal displacements, and multipath and receiver noise.

The ionosphere-free combination can be used to efficiently remove the effect of ionospheric delay due to the use of dual frequency observations, thus the ionospheric delay is not a main concern of the test. However since the current tropospheric delay empirical models including the mapping functions cannot attain the accuracy of 1 cm by themselves, the remaining part of the tropospheric delay not predicted by the models is still a main error source, which is usually estimated by introducing unknown parameters within the sequential least-squares algorithm. Over the past years, multiple prediction models and different modes for estimating the residual tropospheric zenith delay have been implemented in DIPOP for different research purposes. Determining a proper prediction model and estimation mode of the residual delay for the WCDA data analysis was one of the main objectives of the test. Besides the corrections of the solid Earth tide

and the pole tide, the effect of the ocean loading tide is discussed since the WCDA network sites are quite near the Pacific Ocean.

There are a number of research groups who are processing the data of the WCDA network in different ways. So besides the evaluation of the results' precision from DIPOP, a cross-comparison between the independent solutions from DIPOP and another organization, ITRF position solutions published by IERS, was performed to further qualify the accuracy of DIPOP.

4.2 Estimation of Residual Tropospheric Zenith Delay

In the command file of DIPOP's main processor, there are four options dealing with the tropospheric delay: the zenith delay model and mapping function, the estimation of residual tropospheric zenith delay of stations, the fitting order of residual zenith delay estimation within a sequential interval, and the sequential interval length of tropospheric estimation. This section gives a discussion of the four options; the longest WCDA baseline, DAHL (627 km) from the reference station DRAO to remote station HOLB, was used as an example. The 24-hour observation files over one-week were separately processed in a baseline mode with DIPOP.

4.2.1 Prediction Models of Tropospheric Zenith Delay and Mapping Functions

The tropospheric zenith delay empirical model predicts delay as a function of surface temperature, pressure and relative humidity. Thus the model accuracy mainly depends on

the meteorological data at the time of the GPS measurement as well as model itself. But in most cases, it is difficult to get accurate meteorological data. So if there are inaccurate or even no meteorological data, a standard atmosphere is usually used. Usually such a standard atmosphere is created by defining reference temperature, pressure, and humidity at sea level and then using the height of the GPS site as a sole variable to calculate the meteorological values for a site. Due to the absence of meteorological data for the tested baseline, standard reference values at the sea level were used initially to model tropospheric zenith delay in the test.

Various zenith delay models are currently available, but most of them are not suitable for precise geodetic data analysis. Of all the zenith delay models, the Saastamoinen zenith delay model is one of the relatively more accurate models. Mendes and Langley (1995) found that the Saastamoinen dry zenith delay model was generally accurate to the mm level with accurate surface weather measurements. The error in the Saastamoinen wet zenith delay model driven by surface measurements falls within the 2-5 cm range depending on latitude**.**

The Saastamoinen dry and wet zenith delay models is described as:

$$T_{dry}{}^{z} = 10^{-6} K R P / g_m \tag{4.1}$$

$$T_{wet}{}^{z} = 0.002277\ (1255 / T + 0.05)\, e \tag{4.2}$$

where in equation 4.1, K is a refractivity coefficient, R is the gas constant for dry air, P is the site pressure, and g_m is the local gravity; in equation 4.2, T is surface temperature, e is the surface water vapor pressure and can be estimated from either numerical model or a statistical model with temperature and relative humidity. The model (dry + wet) is less

sensitive to temperature error compared with other models. In DIPOP, the following expression [Santerre, 1987] are used to calculate e

$$e = RH \cdot \exp(-3.72465 + 2.13166 \cdot 10^{-1} T - 2.56908 \cdot 10^{-4} T^2) \tag{4.3}$$

where RH (%) is relative humidity, T is surface temperature.

The Saastamoinen zenith delay model must be combined with mapping functions. Of all the mapping functions, no tropospheric mapping function exists for every application and all ranges of elevation angles. However, Mendes and Langley (1994) recommended the Niell mapping functions after they assessed the accuracy of most of the available mapping functions using ray-tracing through an extensive radiosonde data set for different elevation angles starting at 3 degrees. In another paper, they concluded that the Niell mapping functions are the best choice in cases where meteorological data is not reliable or unavailable due to its independence from meteorological data [Mendes and Langley, 2000].

The form of the Niell mapping function is defined as below:

$$m(\varepsilon) = \frac{1 + \dfrac{a}{1 + \dfrac{b}{1 + c}}}{\sin(\varepsilon) + \dfrac{a}{\sin(\varepsilon) + \dfrac{b}{\sin(\varepsilon) + c}}} \tag{4.4}$$

where ε is the elevation angle, a, b, and c are empirical coefficients determined separately for the dry and wet mapping functions. The coefficients for the Niell dry mapping function depend on the latitude and day of year, and for the Niell wet mapping function depend on the latitude of stations only. The Saastamoinen dry and wet zenith delay models and the Niell dry and wet mapping functions were used in the test herein.

4.2.2 Parameter Estimation of Residual Tropospheric Zenith Delay

The command file of the main program has an option defining the residual tropospheric zenith delay as an unknown parameter. Users can specify the mode of the tropospheric parameter estimation. Table 4.1 gives descriptions of all the types of the tropospheric parameter estimation in DIPOP.

Table 4.1 Options of estimating residual tropospheric zenith delay in DIPOP

Option	Description
0	No residual zenith delay estimation
1	Estimating at remote station only: assuming that the residual delay at one station is zero and then estimating the delay at the other station.
2	Estimating absolute tropospheric delays at both stations. Not for short baselines because the elevation angles from the two stations to any particular satellite will be very similar. This will cause almost complete correlation between the two estimated parameters.
3	Estimating one common residual delay of both sites: assuming that the two stations have the same residual delay.
4	Estimating a common and offset delay: considering the unmodeled portions of the zenith delay at the two stations to include one common parameter and one unique parameter.
5	Estimating the relative difference between the two stations.

For data processing of long baselines, a good choice is to simultaneously estimate the residual delays at the two stations of a baseline as two unknown parameters in adjustment, like option 2. However due to the usage of double difference data, a strong mathematical correlation between the partial derivatives of tropospheric delay at the two ends of a baseline appears when the baselines are short because the elevation angles from the two

stations to any particular satellite will be very similar. This will cause almost complete correlation between the two estimated tropospheric parameters. The solution of the problem is to fix the tropospheric delay at the reference station and only to estimate the relative delay at the remote station. This is option 1.

If we assume that the two stations have the same tropospheric delay, as in option 3, the same prediction models and mapping functions are used at both the stations. So option 3 is not suitable for long baselines because the atmospheric conditions at the ends of a long baseline are different. Option 4 is an extension of option 3. Comparing with above options (1, 2, 3, and 4), option 5 is simpler and mode flexible. It can be used for both long and short baselines.

For a test on a long baseline, here only are the computed results from the options 0, 2, and 5. Table 4.2 gives the mean and root-mean-square (RMS) of the double difference residuals. The mean and RMS are the averages of 7 daily solutions for the baseline (DAHL: 627km). In Figure 4.1, the three plots graphically show the double difference residuals of a pair of satellites using the three options.

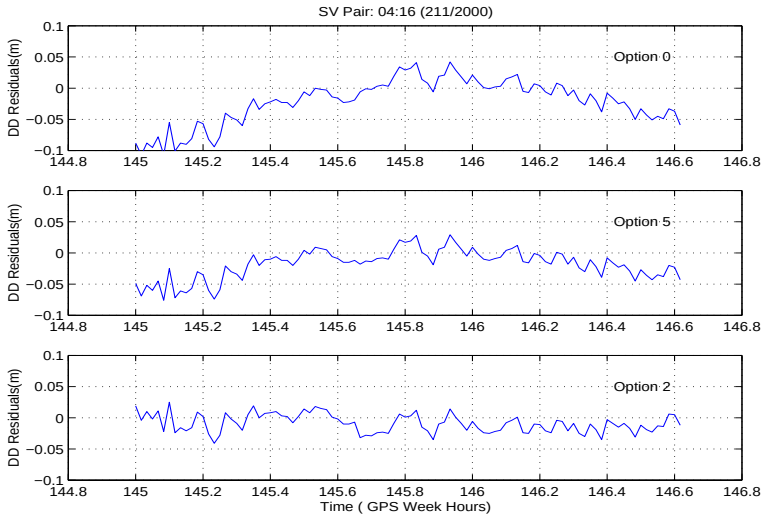

Figure 4.1 Residuals plots of double difference in estimating tropospheric zenith delay

Table 4.2 Statistics of the baseline DAHL over 7 days for different residual tropospheric zenith estimation

Option	Average of 7 Daily Solutions		
	Remote Site HOLB Height (m ± mm)	DD Residuals Mean (mm)	DD Residuals RMS (mm)
0	559.6757 ± 0.52	-0.11	30.27
5	559.6705 ± 0.69	0.10	21.71
2	559.6856 ± 0.57	0.11	11.42

The results in Table 4.2 reveal that the RMS terms are remarkably reduced by estimating the residual tropospheric zenith delay, and the RMS of the third mode (option 2) makes an improvement of about 60 percent compared with the option 0. From the three plots in Figure 4.1, we can find that estimating the residual zenith delay can efficiently mitigate the systematic error term caused by the residual tropospheric delay and option 2 has the best performance among the three tested options. The test suggests the estimation of the residual tropospheric delay can significantly reduce the effects of residual tropospheric delay and failure to estimate residual tropospheric delay may result in an error of cm level in the height component. The results show the option 2 is the best choice in relative positioning on the long baselines.

4.2.3 Modeling Residual Tropospheric Zenith Delay within a Sequential Interval

As mentioned in Chapter 3, users can model the residual tropospheric zenith delay using a constant term or a first order linear fitting within a sequential interval in the adjustment. In Figure 4.2, the two plots display variations of tropospheric zenith delay estimated by DIPOP at the two stations DRAO and HOLB on day 211, respectively. The fitting

interval of a 100 minutes interval was used in this test. The tropospheric zenith delay in the plots is sum of the prediction from Saastamoinen (dry and wet) models and the estimation of the residual zenith delay. As expected, the mean of the first order linear fitting is almost equal to estimate of the constant fitting within a sequential interval except the first and last intervals. Due to ignoring the correlation between the residual delays in sequential intervals, discontinuities occur between the two sequential intervals. So evaluating the correlation is a future task in the study of tropospheric delay estimation in DIPOP. It should be possible to make the estimate piece-wise continuous.

Table 4.3 gives the statistics results from the two modeling modes, the averages of the mean and RMS values of double difference residuals from 7 days. The mean and RMS values from the first order linear fitting are both smaller than those from the constant fitting. From Figure 4.3, which shows an example for the residuals plots of double differences of a pair satellites, we can see that a bias near the right end occurring in the first plot is mitigated by the first order linear fitting. The results indicate that the first order linear fitting is more efficient in reducing the effect of the residual tropospheric delay.

Table 4.3 Statistics of the baseline DAHL during 7 days for fitting residual zenith delay within a sequential interval

	Order	Average of 7 Daily Solutions	
		Mean (mm)	RMS (mm)
Constant	0	0.11	11.42
Linear Fitting	1	0.08	9.98

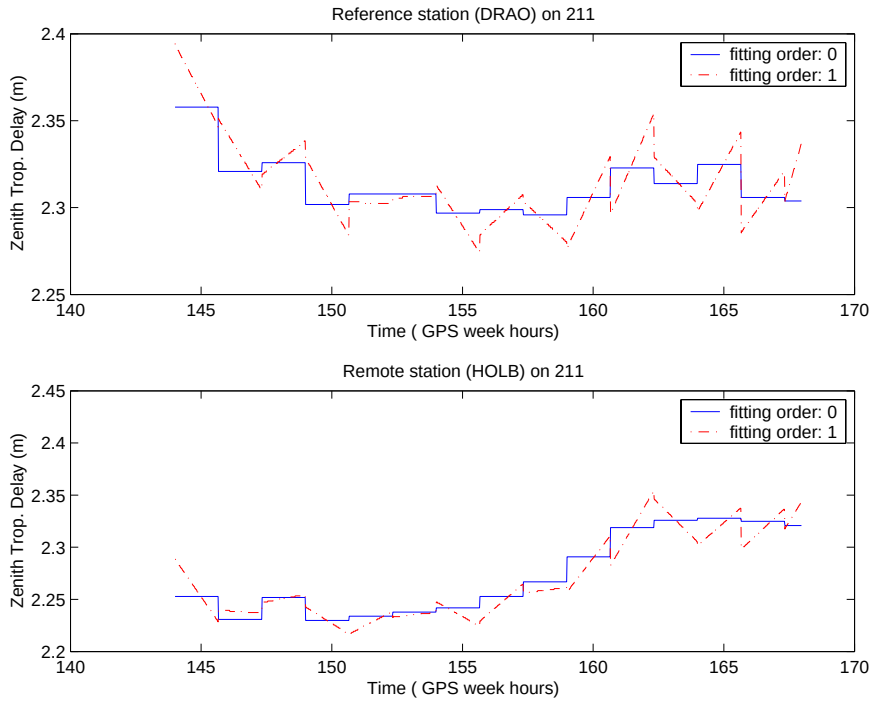

Figure 4.2 Tropospheric zenith delays at the two stations, DRAO and HOLB

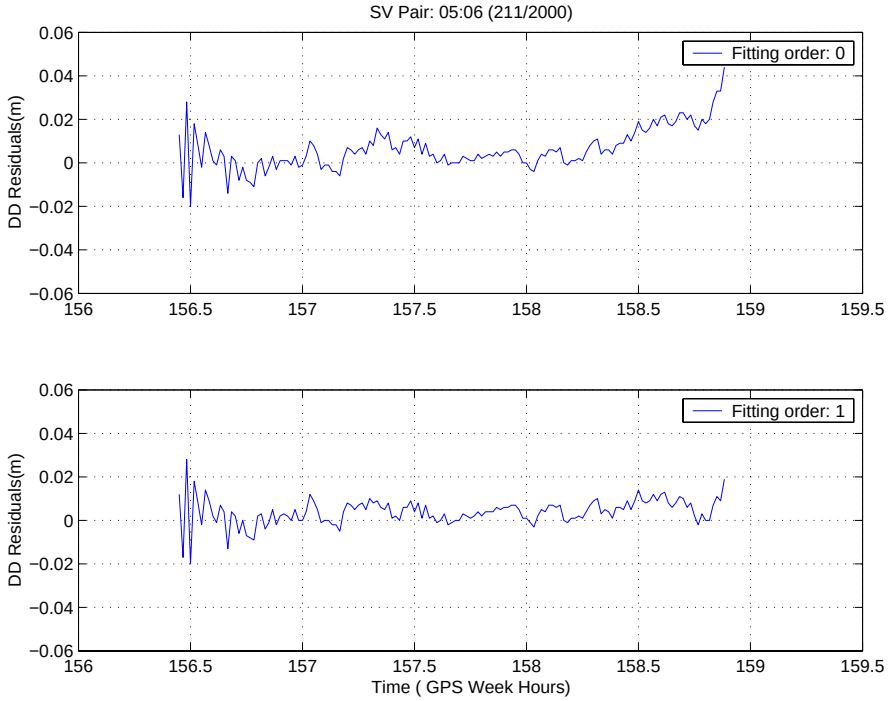

Figure 4.3 Residuals of double difference for modeling residual tropospheric zenith delay in sequential intervals

4.2.4 Sequential Intervals for the Estimation of Residual Tropospheric Zenith Delay

How do we set the interval length of sequential solutions for estimating the residual tropospheric zenith delay? Theoretically, the more redundant observations within an interval, the better the GPS sequential solutions. However, the tropospheric zenith delay can vary significantly with time especially in the wet component; estimation of tropospheric zenith delay with long sequential intervals is not reasonable to model the residual tropospheric delay. In order to examine the effect of estimation interval for the sequential estimation of the residual tropospheric delay, five different intervals (45, 100, 300, 600 and 900 minutes) were selected for a test.

Table 4.4 gives the averaged mean and RMS values of double difference residuals from the five sequential intervals over 7 days. In Figure 4.4, each plot displays an example of double difference residuals with respect to the 5 different intervals. The RMS values of double difference observations in Table 4.4 decrease with the decrease of the interval length, the differences among the weekly height solutions are at a range 1.6 - 3.9 mm. Figure 4.4 also shows the systematic error in residuals is better mitigated with a smaller interval. But considering the effect of the geometric distribution of satellites and the number of redundancy observations on the positioning accuracy, the sequential interval length cannot be too small. For example, when the cutoff angle of elevation is set to higher than 10 degrees, the satellite geometry may be very poor within a period shorter than 30 minutes. Such a situation has sometimes occurred during the author's work,

which used sequential intervals shorter than 30 minutes with a cutoff angle of 15 degrees. Through this test, a sequential interval of 30–40 minutes or even longer is suggested when the data sampling interval is 1 minute and the elevation angle cutoff is 15 degrees.

Table 4.4 Statistics of the solutions at different sequential intervals for the baseline DAHL over 7 days

Interval (min)	Average of 7 Daily Solutions		
	Remote Site HOLB Height (m ± mm)	DD Residuals Mean (mm)	DD Residuals RMS (mm)
45	559.5892 ± 0.56	0.10	8.53
100	559.5876 ± 0.52	0.08	9.98
300	559.5844 ± 0.59	0.16	11.59
600	559.5846 ± 0.63	0.17	12.47
900	559.5843 ± 0.70	0.15	13.79

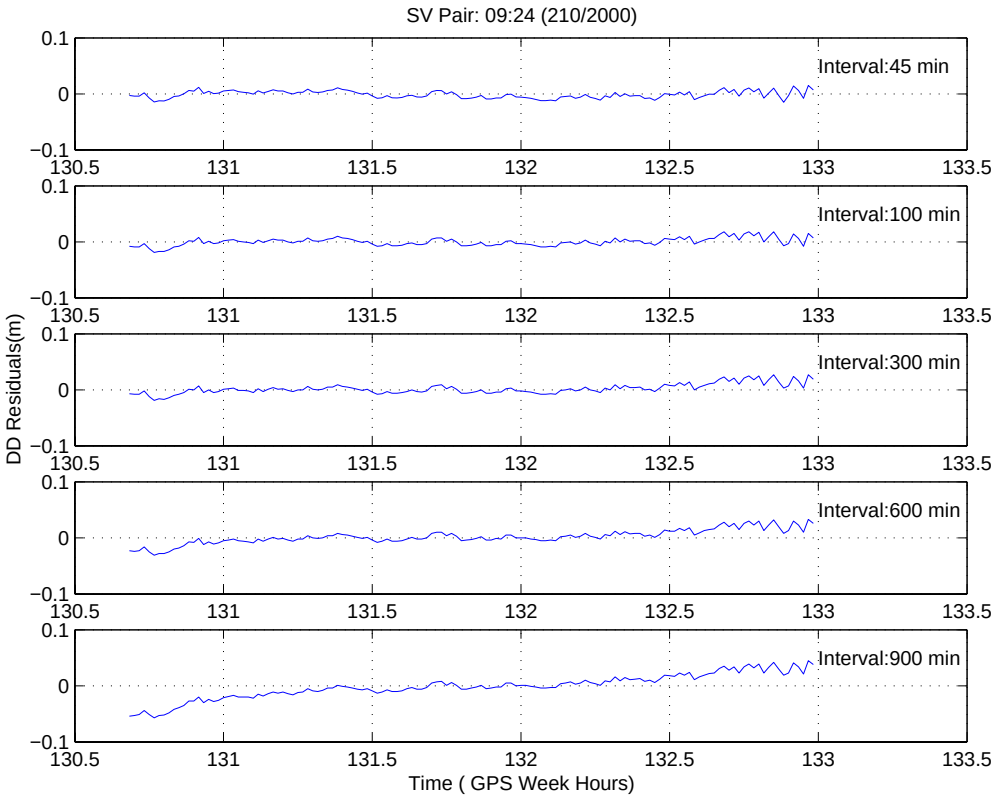

Figure 4.4 Residuals of the double differences for different intervals

4.3 Tide Corrections

The effects of tides including the solid Earth tide, the ocean loading tide, and the pole tide cannot be ignored in precise GPS positioning. Due to the improvement of the prediction methods of the effects, now it is possible to accurately evaluate and correct for them [McCarthy, 1996; Lambert et al., 1998].

The models of the tide corrections in DIPOP have been described in Chapter 3. The coefficients of the ocean loading tide correction computed by the program LOADSDP [Pagiatakis, 1992]. In order to examine these tidal effects on static relative positioning, the solutions with and without the tidal corrections are computed and compared to each other. Table 4.5 gives differences between the two sets of averaged solutions over 7 days for the height component and length of the baseline DAHL from the reference station DRAO to the remote station HOLB. Table 4.6 shows the mean and standard deviation of double difference residuals in the two cases.

Table 4.5 Averaged height and length differences of the solutions with tide corrections minus without tide corrections over 7 days (DAHL)

Tide Correction	Averaged Difference over 7 days(mm)	
	Differential Height	Baseline Length
Ocean Loading Tide	1.7	-0.2
Pole Tide	-0.8	0.4
Solid Earth Tide	3.0	3.0

Table 4.6 Averaged mean and RMS of the double difference residuals with tide corrections and without tide corrections over 7 days (DAHL)

Tide Correction	Average Over 7 Days(mm)			
	With Tide Correction		Without Tide Correction	
	Mean	RMS	Mean	RMS
Ocean Loading Tide	0.09	10.42	0.14	10.30
Pole Tide	0.08	10.41	0.08	10.41
Solid Earth Tide	0.05	10.14	0.08	10.41

The results of Table 4.5 show that the solid Earth tide has the most significant effect among the three types of tides; and the effects from the pole tide and ocean loading tide on the height component are larger than that on the length component. The effects of solid Earth tide and ocean loading tide on the height component are of the order of 1.0-3.0 mm; and the effects of pole tide on the height component and baseline length are less than 1 mm. As shown in the results of Table 4.6, the three corrections do not make significant changes to the RMS values of daily 24-hour solutions. The values of RMSs in Table 4.6 show a difference of less than 0.5 mm between the two solutions. The reason is that the main effects of the ocean loading tide and the solid Earth tide are from diurnal and semi-diurnal bands which average close to zero over the period of 24 hours. And although the pole tide can cause a displacement of 1-2 cm on the vertical direction, its effect becomes insignificant since the vertical displacement is absorbed by the estimated residual tropospheric zenith delay parameter in the adjustment.

The results indicate that using the daily 24-hour observations and estimating the residual tropospheric zenith delay in adjustment can mitigate the tidal effects on the GPS positioning accuracy. However, failure to apply the daily tide corrections will result in an error at the mm level in the vertical component of the baseline. If data sets shorter than 24

hours or results of long time series of daily data sets are analyzed, the effects of the tides will be more evident if they are not corrected.

4.4 Experience with WCDA Data

4.4.1 Data Processing Strategy

Data sets from the WCDA network, a total of 49 sessions (7 baselines × 7 days from 23 to 29 June 2000, see Table 4.7), were processed in the test. The strategy of data processing was determined based on the previous discussion. The double difference carrier phases were processed in baseline mode for static relative positioning.

The main estimation strategy used in the data processing was:

- Reference station: DRAO with a priori standard deviation of 10^{-6} meters;
- Remote stations: ALBH, HOLB, NEAH, NANO, UCLU, WILL and WSLR, all with a priori standard deviation of 100 meters;
- Reference frame: ITRF97 at 1997.0;
- Daily reference epoch: the middle epoch of current day of observations;
- Precise ephemeris: IGS final orbit (fixed) in SP3 format;
- Elevation angle cutoff: 15 degrees;
- Sampling interval: 60 seconds;
- Linear combination of observables: ionosphere-free;

- Parameters estimated: remote station coordinates, carrier phase ambiguities (not fixed), absolute residual troposphere zenith delay at two stations at 100 minute sequential intervals with the first order linear fitting;
- Tropospheric delay modeling: Saastamoinen model for zenith delay (dry and wet) with standard sea level atmospheric values combined with Niell mapping function (dry and wet); standard atmosphere at sea level: Pressure: 1013.25 mbar, Temperature: 15.0 ^{o}C, Relative humidity: 50 %;
- Tidal corrections: the solid Earth tide, the ocean loading tide, and the pole tide;
- Observation correlation: only mathematical correlation.

Table 4.7 Tested data sets

Baseline	Station (Reference–Remote)	Baseline Length (km)	Observing Date (day/year)	Observing Period (hour)	Sampling Interval (second)
DAAB	DRAO – ALBH	302	205 – 211 / 2000	24	60
DAHL	DARO – HOLB	627	205 – 211 / 2000	24	60
DANA	DARO – NEAH	384	205 – 211 / 2000	24	60
DANN	DARO – NANO	324	205 – 211 / 2000	24	60
DAUL	DARO – UCLU	434	205 – 211 / 2000	24	60
DAWL	DARO – WILL	370	205 – 211 / 2000	24	60
DAWS	DARO – WSLR	254	205 – 211 / 2000	24	60

The reference station DRAO is located on the North American plate and is relatively stable compared to other sites in the WCDA network. As one of the IGS global fundamental stations, its position at an epoch and velocity in ITRF are published by IERS. Since from 04 June 2000 all IGS products, including the IGS orbits, are based on the IGS realization of the ITRF97 reference frame, all the WCDA station coordinates discussed were in ITRF97. Since the ITRF position solutions from IERS are only considered valid

for a specified epoch due to tectonic plate motion, for any other epoch they must be estimated using the corresponding ITRF velocity solution from IERS.

In this experiment, the coordinates of the reference station DRAO were computed using the following equation

$$X(t) = X(t_0) + V \cdot (t - t_0) \tag{4.5}$$

where $X(t_0)$ is the station position at the reference epoch t_0, V is the corresponding movement velocity of station, $X(t)$ is the station position at the specific epoch t.

For the tested WCDA data set (from 205/2000 to 211/2000), the most recent ITRF solutions from IERS, the ITRF2000 solutions, were used to calculate the coordinates of DRAO. After the velocities and coordinates of DRAO from IERS's ITRF2000 solutions at epoch 1997.0 were converted into ITRF97 with ITRF transformation parameters (see Table 4.8), the coordinates of DRAO at the specific epoch (the middle epoch of current day of observations) in ITRF97 were obtained using equation 4.5.

The values in Table 4.8 suggest that the velocity of DRAO is less than 2 cm/year with respect to ITRF97 and the accuracy of the solutions is at a level of 1-2 mm for coordinates and at a level of less than 1 mm per year for velocities in the three axis directions respectively.

Table 4.8 The position and velocities of DRAO at epoch 1997.0 in ITRF97 converted from ITRF2000 solutions of IERS at epoch 1997.0

Station	Position at epoch 1997.0 in ITRF97 (m)		
	X / σ_X	Y / σ_Y	Z / σ_Z
DRAO	-2059164.6805 / 0.001	-3621108.3935 / 0.001	4814432.3680 / 0.002
	Velocity in ITRF97 (m/year)		
	Vx / σ_{Vx}	Vy / σ_{Vy}	Vz / σ_{Vz}
	-0.0161 / 0.0003	-0.0026 / 0.0004	-0.0081 / 0.0006

4.4.2 Summary of Results

In order to inspect the repeatability of the daily solutions from DIPOP, Figures 4.5-4.11 graphically give the daily variations of length and height components of each baseline referring to the average of 7 daily solutions with respect to the reference station DRAO. The average value of the 7 daily solutions is represented with a horizontal line in each plot. The vertical impulses in each plot represent the difference of the daily solutions from the average value. Tables 4.9 and 4.10 give summaries including the maximum, the minimum, and the standard deviation of the daily variations for the 7 baselines. Relative precision along each baseline length is also given in Table 4.10. Table 4.11 provides a summary of pseudorange multipath plus noise on L1 and L2 carriers at the 8 WCDA GPS stations over the test period. The table only reports their mean effects over the week on signals at elevation angles above the cutoff angle (15^o) based on the estimation of pseudorange multipath plus noise using software QC/TEQC.

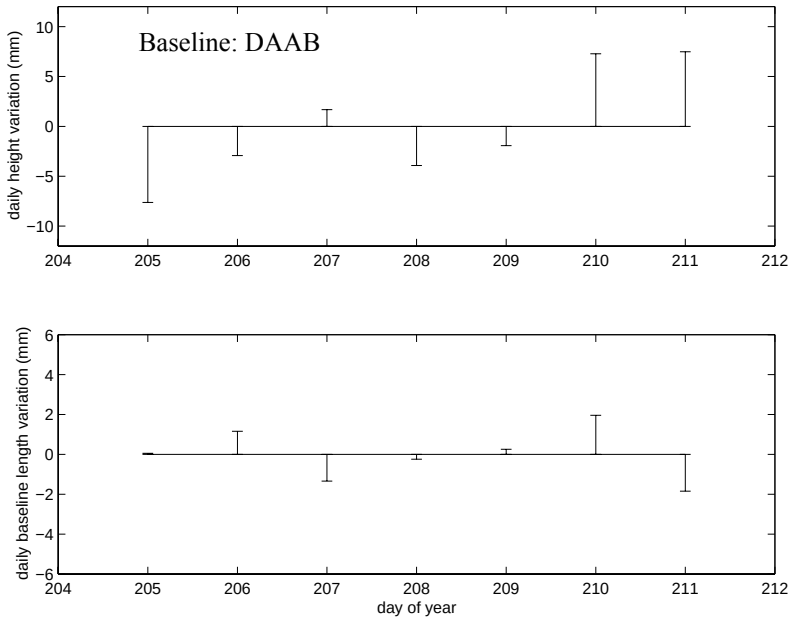

Figure 4.5 Daily variations of length and relative height solutions for baseline DAAB (Referring to the mean of the 7 daily solutions)

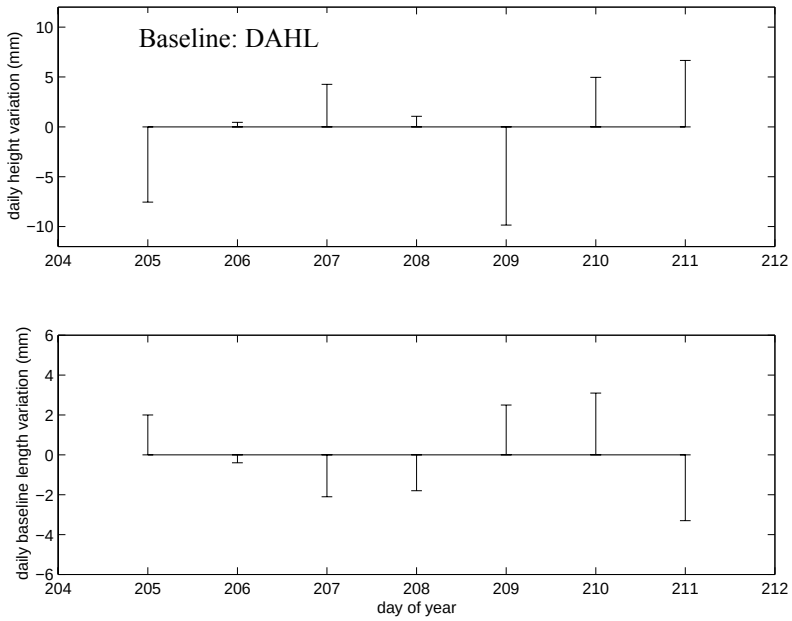

Figure 4.6 Daily variations of length and relative height solutions for baseline DAHL (Referring to the mean of the 7 daily solutions)

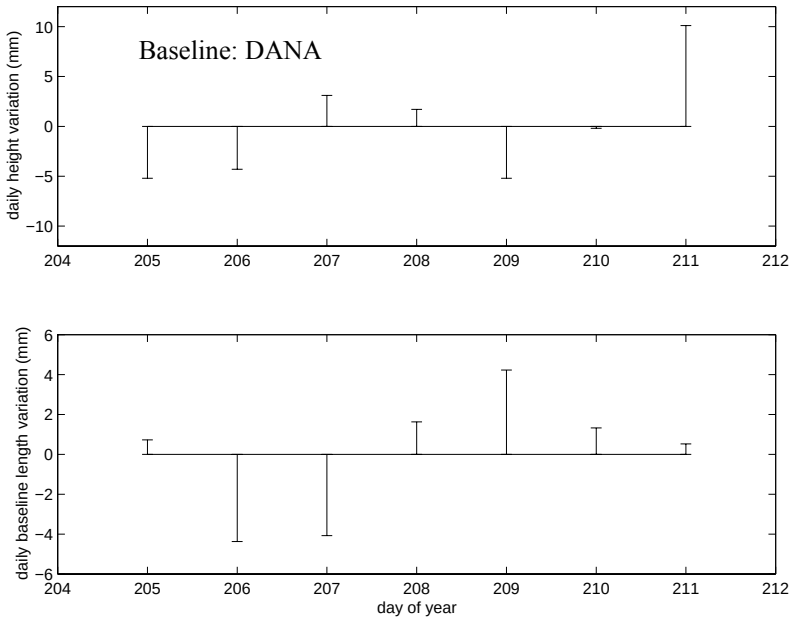

Figure 4.7 Daily variations of length and relative height solutions for baseline DANA (Referring to the mean of the 7 daily solutions)

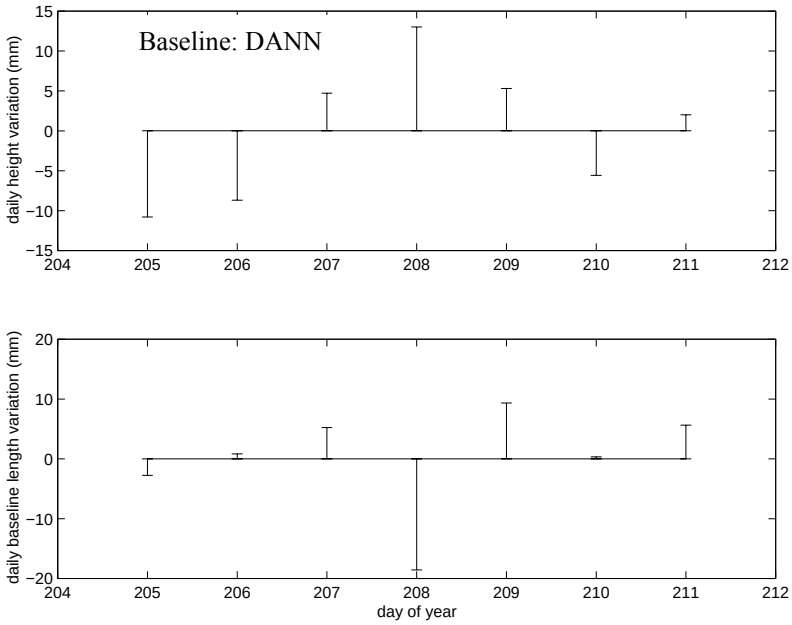

Figure 4.8 Daily variations of length and relative height solutions for baseline DANN (Referring to the mean of the 7 daily solutions)

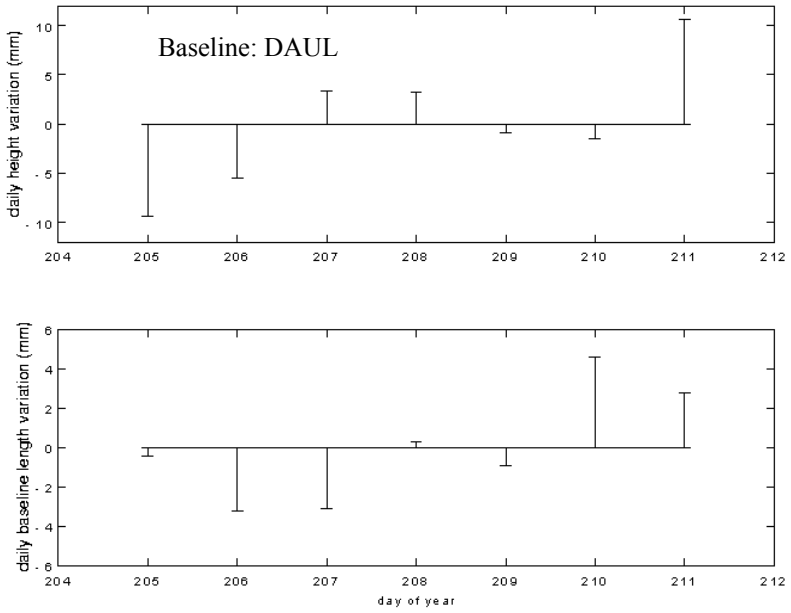

Figure 4.9 Daily variations of length and relative height solutions for baseline DAUL (Referring to the mean of the 7 daily solutions)

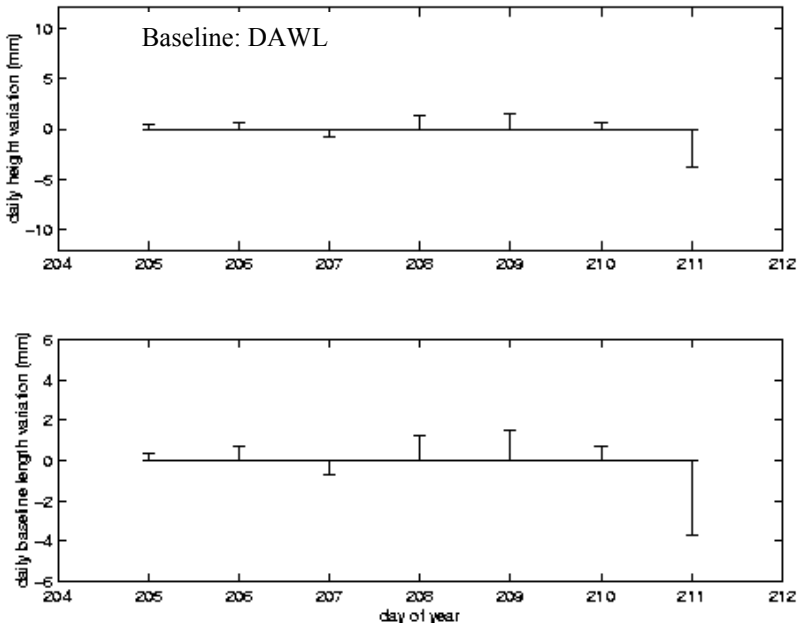

Figure 4.10 Daily variations of length and relative height solutions for baseline DAWL (Referring to the mean of the 7 daily solutions)

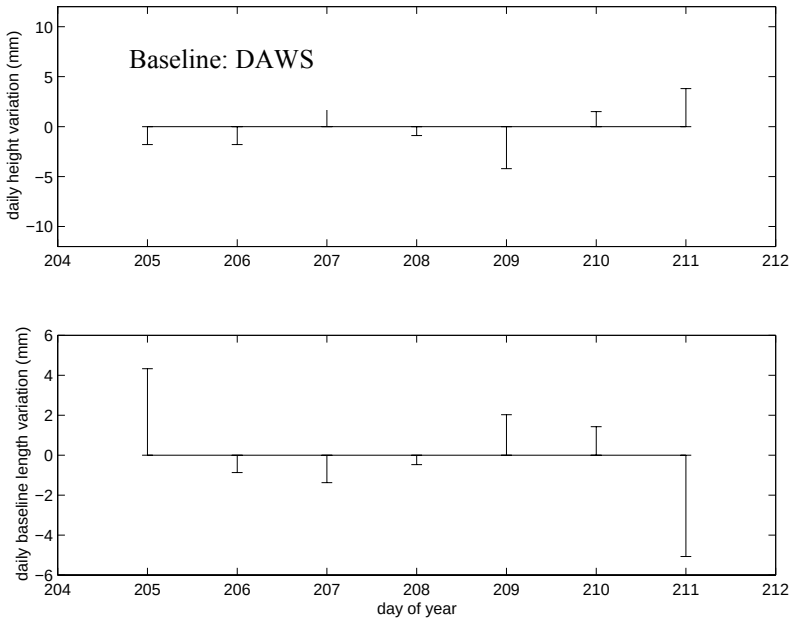

Figure 4.11 Daily variations of length and relative height solutions for baseline DAWS (Referring to the mean of the 7 daily solutions)

Table 4.9 Statistics of daily relative height variation referring to the mean of 7 daily solutions and standard deviation of the daily variations in three components of baseline

Baseline	Daily Height Variation		Daily Variation Std (mm)		
	Max(mm)	Min(mm)	Height	Latitude	Longitude
DAAB	7.5	-7.6	5.7	4.1	2.6
DAHL	6.7	-9.8	6.4	3.2	2.4
DANA	10.1	-5.2	5.6	5.0	4.0
DANN	13.0	-10.8	8.6	9.1	5.4
DAUL	10.6	-9.4	6.5	3.3	3.0
DAWL	8.3	-9.0	6.4	1.3	3.3
DAWS	3.8	-4.2	3.0	3.3	2.1

The height solution has the worst standard deviation of daily variation among three baseline components. The maximum of the daily height variations is 13 mm for the baseline DANN referring to its mean and the baseline length also has the maximum departure of 19 mm from its mean length. The worst relative precision of baseline length

is that for baseline DANN: 0.03 PPM. For other baselines, their standard deviations of daily height, latitude, longitude and length solutions are within a range from 1 mm to 7 mm. Their relative precision of the baseline lengths are better than 0.01PPM, within a range of 0.004-0.008 PPM. The preliminary test results from DIPOP show the repeatability of daily variation are better than 1 cm referring to the average of 7 daily solutions for all 3 baseline components and baseline length.

Table 4.10 Statistics of daily baseline length variation referring to the mean of 7 daily length solutions and standard deviation of the relative variations

Baseline	Baseline Length Daily Variation (mm)			Relative Precision (0.01PPM)
	Max	Min	Std	
DAAB	2.0	-1.8	1.3	0.43
DAHL	3.1	-3.3	2.5	0.40
DANA	4.2	-4.3	3.1	0.81
DANN	9.3	-18.8	9.1	2.81
DAUL	4.5	-3.2	2.9	0.67
DAWL	4.3	-5.1	3.0	0.81
DAWS	1.5	-3.7	1.8	0.71

Table 4.11 Averaged pseudorange multipath plus noise over 7 days at 8 WCDA stations

Station	Pseudorange Multipath + Noise (m)	
	L1	L2
DRAO	0.19	0.21
ALBH	0.24	0.18
HOLB	0.11	0.16
NEAH	0.31	0.32
NANO	0.27	0.52
UCLU	0.24	0.49
WILL	0.30	0.56
WSLR	0.22	0.22

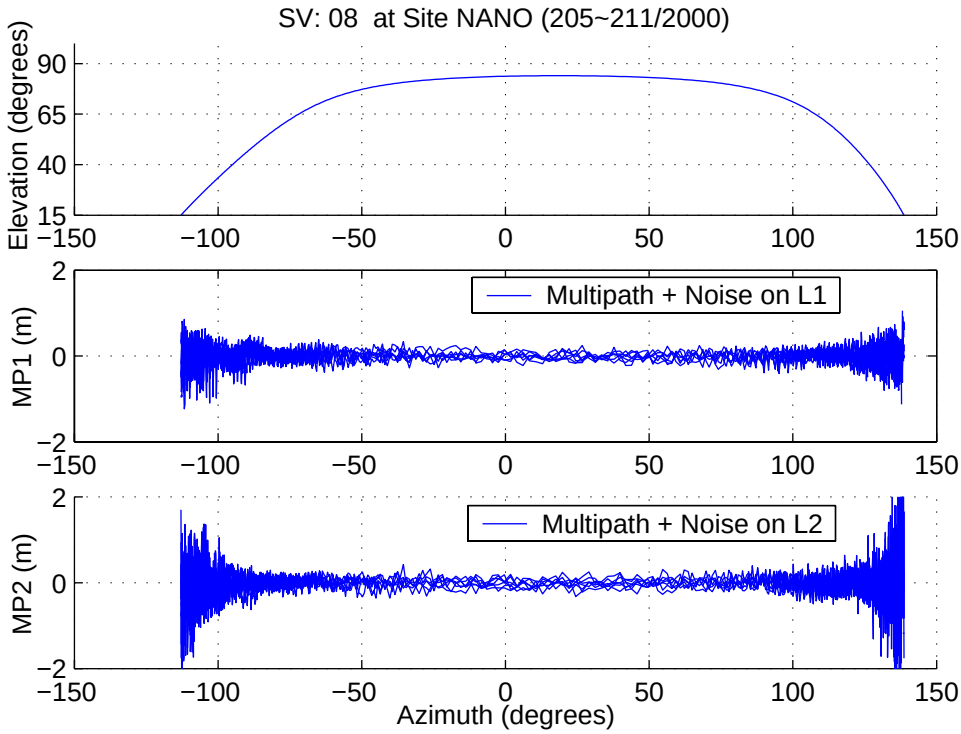

Figure 4.12 Multipath plus noise at site NANO (205-211/2000)

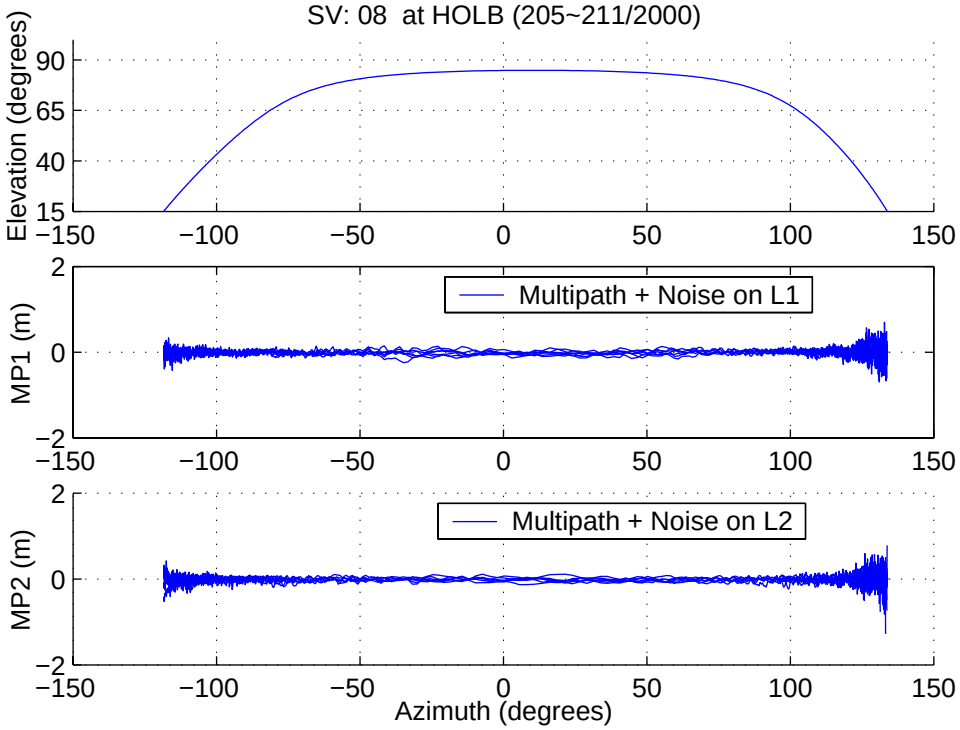

Figure 4.13 Multipath plus noise at site HOLB (205-211/2000)

To learn the reason why the results of the baseline DANN are worse than those of other baselines, the multipath effects were considered as a potential error resource. The averaged mutipath on L1 and L2 at each remote site calculated by TEQC/QC are given in Table 11. The highest multipath plus noise level shows at the sites NANO and WILL. We also find two baselines formed with NANO and WILL have worse repeatability of daily solutions. These results show that the variation of daily solutions increases with increase of the multipath and noises (see Tables 4.9, 4.10, and 4.11). Figures 4.12 and 4.13 display two examples of multipath at the remote sites NANO and HOLB, respectively. Some of the multipath features obviously occur in Figures 4.12 for the site NANO.

Although the main factors cannot be completely determined by the preliminary results, a study of how to mitigate the multipath effect will facilitate the identification of a "no-multipath error" and reduce the multipath effect on DIPOP solutions.

4.4.3 Comparisons of Results

The ITRF solutions published by IERS contain coordinates and velocities of GPS stations at a reference epoch in an ITRF. In WCDA network, there are six sites on the list of the ITRF2000 solutions of IERS. These sites include the reference station DRAO, and five remote stations: ALBH, HOLB, UCLU, WILL, and WSLR. So in the following comparison, the coordinate solutions of the five baselines, DAAB, DAHL, DAUL, DAWL, and DAWS are taken for the following discussion.

In order to compare the solutions from DIPOP with ITRF solutions from IERS, the ITRF2000 solutions of the five remote stations from IERS were transformed into ITRF97

at 1997.0. The ITRF2000 solutions were downloaded from IERS Web site <http://lareg.ensg.ign.fr/ITRF/ITRF2000/results/ITRF2000_GPS.SSC>. The transformed results including station position and velocity solutions are given in Tables 4.12 and 4.13 respectively. Table 4.14 gives the accuracy of the IERS's ITRF2000 solutions at epoch 1997.0.

Table 4.12 The positions at epoch 1997.0 in ITRF97 converted from ITRF2000 solutions of IERS

Station	Position (m)		
	X	Y	Z
DRAO	-2059164.6805	-3621108.3935	4814432.3680
ALBH	-2341332.8829	-3539049.5124	4745791.3599
HOLB	-2503040.4132	-3188233.3348	4908701.5521
UCLU	-2440669.0501	-3416437.0752	4785136.8549
WILL	-2084258.0055	-3313872.9870	5019853.0873
WSLR	-2227013.6138	-3439649.1122	4872522.2401

Table 4.13 The velocities in ITRF97 converted from ITRF2000 solutions of IERS

Station	Velocity in ITRF97 (m/year)		
	Vx	Vy	Vz
DRAO	-0.0161	-0.0026	-0.0081
ALBH	-0.0101	-0.0023	-0.0078
HOLB	-0.0137	-0.0003	-0.0096
UCLU	-0.0022	0.0018	-0.0091
WILL	-0.0175	-0.0027	-0.0079
WSLR	-0.0116	0.0012	-0.0130

Table 4.14 Accuracy of ITRF2000 solutions at epoch 1997.0 from IERS

Station	Position Sigma(m)			Velocity Sigma(m/year)		
	X	Y	Z	Vx	Vy	Vz
DRAO	0.001	0.001	0.002	0.0003	0.0004	0.0006
ALBH	0.001	0.001	0.002	0.0004	0.0006	0.0007
HOLB	0.011	0.012	0.015	0.0047	0.0054	0.0070
UCLU	0.014	0.016	0.019	0.0064	0.0076	0.0092
WILL	0.002	0.002	0.003	0.0007	0.0009	0.0013
WSLR	0.013	0.016	0.019	0.0064	0.0079	0.0095

Since the motion velocities of the remote stations are less 2 cm/year in ITRF97 (see Table 4.13), their motion during the tested one-week period was ignored in this discussion. The average of 7 DIPOP's daily position solutions of each remote station was used as its weekly solutions. The reference epoch of the weekly solutions was set at epoch 208.5 of 2000, the middle epoch of the tested one-week period. By using equation (4.5), the weekly position solution of DIPOP at epoch 1997.0 in ITRF97 was calculated. Table 4.15 gives the weekly position solutions of the five remote stations at epoch 1997.0 in ITRF97.

Table 4.15 The weekly position solutions from DIPOP at epoch 1997.0 in ITRF97

Station	Position at epoch 1997.0 in ITRF97 (m)		
	X	Y	Z
ALBH	-2341332.8912	-3539049.5113	4745791.3679
HOLB	-2503040.4259	-3188233.3289	4908701.5546
UCLU	-2440669.0529	-3416437.0702	4785136.8510
WILL	-2084258.0076	-3313872.9807	5019853.0790
WSLR	-2227013.6152	-3439649.1099	4872522.2262

The comparison between DIPOP and IERS coordinates was conducted by computing the coordinate differences in three axis directions (X-, Y-, and Z-axis) and baseline length

differences between the weekly solutions of DIPOP and the ITRF solutions of IERS at epoch 1997.0 in ITRF97. The differences of position solutions, the DIPOP solutions (in Table 4.15) minus the IERS solutions (in Table 4.14), are summarized in Table 4.16. In this table, Dx, Dy and Dz denote of the differences of the two sets of position solutions in X-, Y-, and Z-axis directions respectively; the differences in latitude (+N), longitude (+E) and height (+up) are presented with Dϕ, Dλ, and Dh in this table, respectively. At the same time, the differences of baseline length solutions and their relative errors referring to the solutions of IERS are given in Table 4.17.

Table 4.16 Comparison of absolute position solutions at epoch 1997.0 in ITRF97 (DIPOP minus IERS)

Station	Coordinate Solution Difference (mm)					
	Dx	Dy	Dz	Dϕ	Dλ	Dh
ALBH	-8.3	1.1	8.0	2.6	-7.5	8.4
HOLB	-12.7	5.9	2.5	-0.9	-13.7	3.9
UCLU	-2.7	5.0	-3.9	-0.7	-5.2	-4.6
WILL	-2.1	6.3	-8.3	-1.7	-5.1	-9.1
WSLR	-1.4	2.3	-13.9	-7.9	-2.5	-11.4

Table 4.17 Comparison of baseline length solutions at epoch 1997.0 in ITRF97 referring to DRAO (DIPOP minus IERS)

Baseline	Baseline Length (m)	Difference of Baseline Length Solution	
		Absolute (mm)	Relative (PPM)
DAAB	301768	-6.2	0.02
DAHL	627131	-13.5	0.02
UCLU	433929	-5.1	0.01
WILL	370433	-7.7	0.02
WSLR	253920	5.2	0.02

The comparison suggests that the consistency of the two sets of absolute coordinate solutions is better than 1.5 cm for X-, Y-, and Z-axis directions. The coordinate differences show all negative in X-axis direction and all positive in Y-axis direction. The two sets of solutions in the latitude, longitude, and height components agree to better than 1.5 cm. The differences of baseline length solutions show that the baseline length solutions from DIPOP are larger than those from IERS except the baseline WSLR. The relative difference of the baseline length solutions shows a scale difference of 1 - 2 parts in 10^8. The comparisons show that the level of coordinate conformity between the IERS ITRF2000 and DIPOP solutions is of the order of a few cm.

4.4.4 The Error Budget

In this section, we only discuss the potential error sources related to the data analysis methods. The main error sources include multipath interference, tropospheric delay, and antenna phase center offset.

4.4.4.1 Multipath Effects

Mutipath is the phenomenon whereby a signal arrives at a receiver's antenna by way of two or more different paths [Langley, 1997]. The difference in path lengths causes the signals to interfere (with each other) at the antenna and to contribute error to the observables. In comparison with the effect of the multipath on the pseudorange, the carrier phase is affected at a lower level and the effect is always within a range of ±5 cm.

In order to mitigate the multipath effects from data collected at lower elevation angles, an elevation angle cutoff of 15^o was used in all data analyses reported here. Nevertheless, the multipath still shows significant effects on the accuracy of DIPOP's solutions. The test results indicate that multipath is a potential main error source affecting DIPOP's accuracy. In addition, the usage of the relatively high elevation angle cutoff ($\geq 15^o$) may cause a high correlation between tropospheric zenith delay and height estimations, thereby degrading the accuracy of height estimations. An attempt to solve simultaneously for the tropospheric delay and heights will be aided by using observations at low elevation angles ($<15^o$).

Considering all the factors, it is necessary to develop an efficient method to mitigate the effect of multipath in DIPOP. It will be also helpful for improving the accuracy of height solutions due to the use of the observations from the low elevation angles.

4.4.4.2 Tropospheric Delay

Theoretically, the tropospheric delay should vary continuously with time. However, as shown in Figure 4.2, the tropospheric zenith delay estimated by sequential least-squares adjustment in DIPOP is not continuous and some obvious discontinuities occur between the consecutive intervals. This is a result of the failure to consider the correlation between two successive sequential tropospheric delay estimates.

It is therefore more reasonable to model the residual tropospheric zenith delay by a stochastic model, in which we treat the unknown residual zenith delay as a time-varying parameter. The model is characterized by an empirical variance, which constrains the

zenith delay changes by a time correlation. Such a model has shown good results in comparison with direct water vapor radiometer (WVR) measurements [Brunner and Welsch, 1993].

Although the stochastic model had been used to estimate residual tropospheric delay in a previous test version of DIPOP [van der Wal, 1995], implementation of the stochastic model in the current formal version of DIPOP is a top priority in the DIPOP's further improvements, especially for the users of high precise GPS positioning.

4.4.4.3 Phase Center Corrections

In GPS data analysis, there are two corrections for antenna phase centers. One is for phase center offset of the satellites' transmitting antennas; the other one is for the offset of the receiver antenna.

The offset between the GPS ephemeris reference point (mass center) and the phase center of the satellite transmitting antenna is reported in a summary file of the IGS precise ephemerides for each GPS week. For the tested week, the antenna phase center offset in satellite body-fixed reference frame is reported in the file (IGS10667.SUM) as: Block II/IIA: 0.279 0.000 1.023 X, Y, Z (in satellite body-fixed reference frame) in meters.

In DIPOP's adjustment, the coordinates of satellites from the IGS precise ephemerides are held fixed as exact known parameters without the offset correction. As a result, the geometry offset will directly affect the accuracy of DIPOP solutions, especially when the offset is large. But the effect is reduced in difference solutions on short baselines.

The offset of the receiver antenna is from the inconsistency of its antenna phase center and the control point mark leading to the antenna phase center variation (PCV). The PCV is primarily caused by the non-spherical phase-response pattern of the antenna. The phase center depends on the direction of the incident angle of the incoming signals and is azimuth- and elevation-dependent. For a particular antenna, the L1 and L2 frequencies may have different phase center properties, and consequently may have no common phase center.

If we assume that the L1 and L2 phase centers of the antenna are not variable or their variation can be completely neglected like the current treatment in DIPOP, the corrections of the antenna offset will be easily made by adding constants, the L1 and L2 mean phase center offsets computed basing on the diagram of the specific antenna, to the coordinate of the receiver antenna. But this correction is not recommended for highly-precise and large-scale GPS applications. The magnitude of PCV typically usually spans a range of mm to cm. The neglect of this antenna behavior can lead to baseline errors between mm and cm and can even reach up to 10 cm for the height component. Wübbena (1996) suggested that it is necessary to correct the absolute PCV within regional and global networks, even if they use the same antenna type. Otherwise, a systematic error can reach up to several cm or bias the baseline length in some parts of 10^{-8}, respectively [Wübbena et al., 1996].

For the data analysis of the WCDA network, the corrections of PCV should be considered in DIPOP's future improvements.

4.5 Summary

Based on the above results of the tests discussed in this chapter, it can be concluded that the repeatability of WCDA daily solutions over a one-week period from DIPOP is better than 1 cm for three components of baseline solutions, and also better than 1 cm for baseline length solutions. The daily variation from the average of 7 daily solutions for three components of baseline and baseline length is within a range of 1 cm except for the baseline DANN. The relative precision of baseline lengths is better than 0.01 PPM except for the baseline DANN. The comparisons between DIPOP's and the IERS's solutions suggest that DIPOP is capable of providing a comparable accuracy to that of other GPS software in static relative positioning, and processing the data from the WCDA network with DIPOP should be able to detect the crustal deformation in the WCDA area.

We believe that the accuracy of the DIPOP solution can be further enhanced by using some better or new data processing methods which can reduce the multipath effects, estimate the continuous residual tropospheric delay, and correct the offsets due to antenna phase center variations.

For the characteristics of the WCDA network, another data set over a one-year period from WCDA was used in Chapter 6 to further assess DIPOP’s performance in order to detect the crustal deformation signals in the region.

Chapter 5

Cycle Slip Detection

Repairing cycle slips of observations is an essential task in GPS data preprocessing. In general, the procedure of repairing cycle slips is divided into three steps: The first is to detect cycle slips; then the number of cycle jumps must be determined; and finally the phase data must be repaired using the determined cycle slips. The correct detection of cycle slips is a pre-requisite of successfully removing them. This chapter focuses on the technique of cycle slip detection in data pre-processing. The beginning of this chapter is a brief description of the basic features of cycle slips. The second section gives an introduction to the algorithm involved in PREDD. The main part of this chapter is the third section. It proposes an improved method for automatically detecting cycle slips in PREDD. Some test examples are given.

5.1 Cycle Slips

A cycle slip is a sudden jump in the carrier phase observations by an integer number of cycles. Cycle slips are caused by the loss of lock of the phase tracking loop. Loss of lock

may occur briefly between two measurement epochs, or may last several minutes or more if the satellite signals cannot reach the antenna.

It is a characteristic of cycle slips that the fractional portion of the phase is not affected by the discontinuity in the observation sequence and all observations taken after the cycle slip are shifted by the same integer amount. It is quite possible for several cycle slips to occur in one observation sequence. For each slip, there is one additional jump in the double difference sequence. However, only one epoch of the triple differences is affected by a cycle slip since the triple difference is a difference of double differences between two sequential epochs (see Figure 5.1). This feature of the triple differences is usually used to locate the positions of the cycle slips in an observation sequence.

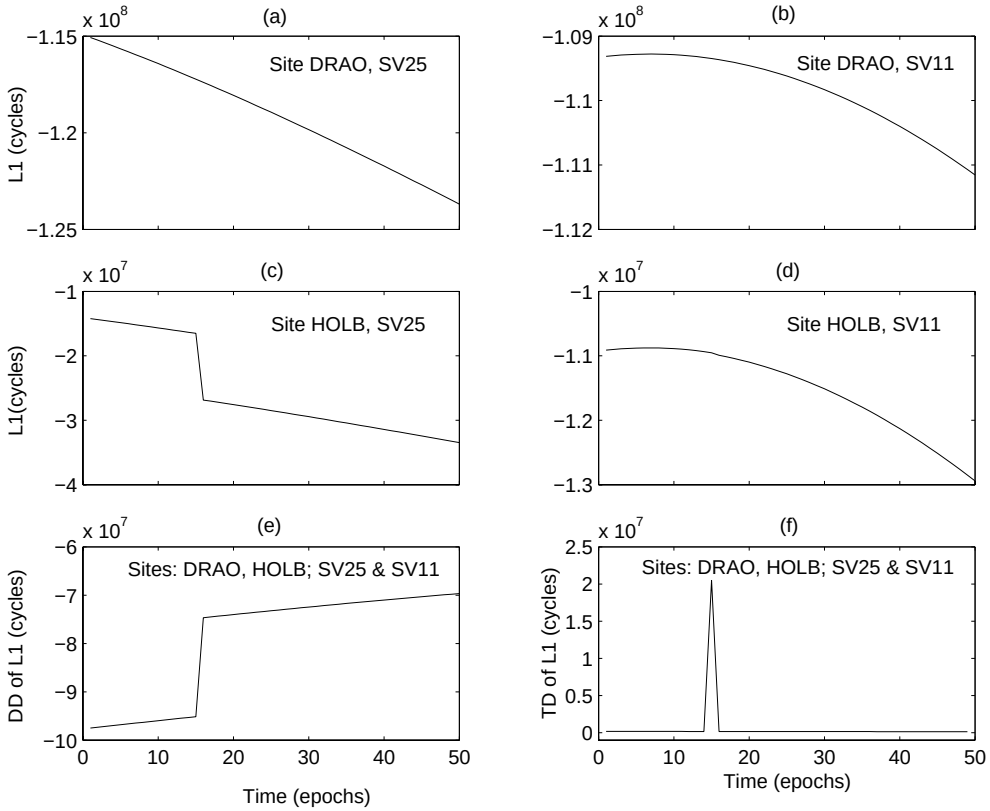

Figure 5.1 Carrier phase observations (L1) on 205/2001 ((a), (b), (c), and (d)) and the Double Differences (e) and Triple Differences (f)

For users of dual-frequency carrier phase observations, there are additional difficulties in data analysis. A cycle slip in linear combinations of L1 and L2 measurements is a combination of cycle slips in both L1 and L2 carrier phases; and it is not an integer for the ionosphere-free observable. The ambiguity change caused by the combined cycle slips of L1 and L2 carrier phases can be very small; it could be less than 1 cm or even close to zero. In fact, a small jump may be buried in the noise of observations if the noise is at a sufficiently high level.

Table 5.1 shows small changes of ambiguities in column 1 and their effects on the ionosphere-free, widelane, narrowlane, and geometry-free observations in column 2, 3, 4, and 5 respectively. Note that sometime a change is very small (the bold numbers) for a combination whereas larger changes for other combinations are caused with the same changes of the L1 and L2 ambiguities. The phenomenon indicates that the different combinations have different sensitivities to cycle slips. If one uses only one combination in repairing cycle slips, there is the possibility of missing a few cycle slips.

Table 5.1 Effects of small cycle slips on phase ambiguity

$\in N_1$ $\in N_2$ (cycles)	Combined Ambiguity (cm)			
	Ionosphere-free	Widelane	Narrowlane	Geometry-free
1 1	10.7	**0.0**	21.4	-5.4
2 2	21.4	**0.0**	42.8	-10.8
2 3	-16.4	-86.2	53.5	-35.2
3 3	32.1	**0.0**	64.2	-16.2
4 3	80.6	86.2	74.9	2.8
4 5	5.0	-86.2	96.3	-46.0
5 6	15.7	-86.2	117.7	-51.4
7 9	**-0.7**	-172.4	171.2	-86.7
9 7	171.8	172.4	171.2	**0.3**
10 8	182.5	172.4	172.3	-5.1

As a remedy, using multiple combinations at the same time can reduce the probability of missing a small combination of cycle slips. Figure 5.2 and Figure 5.3 give examples showing the sensitivities of four combinations including ionosphere-free, widelane, narrowlane, and geometry-free combinations to cycle slips. Figure 5.2 shows change rate of a double difference sequence and Figure 5.3 shows the double difference sequence. In Figure 5.2, we can see obviously a high spike exceeding 4 sigma in the two plots for the ionosphere-free and widelane combinations; a spike lower than 4 sigma occurs in the plot for the geometry-free combination; but there is no spike in the plot for the narrowlane combination. In Figure 5.3, the jumps marked with a "|" occur in the three plots for the ionosphere-free, widelane, and geometry-free combinations.

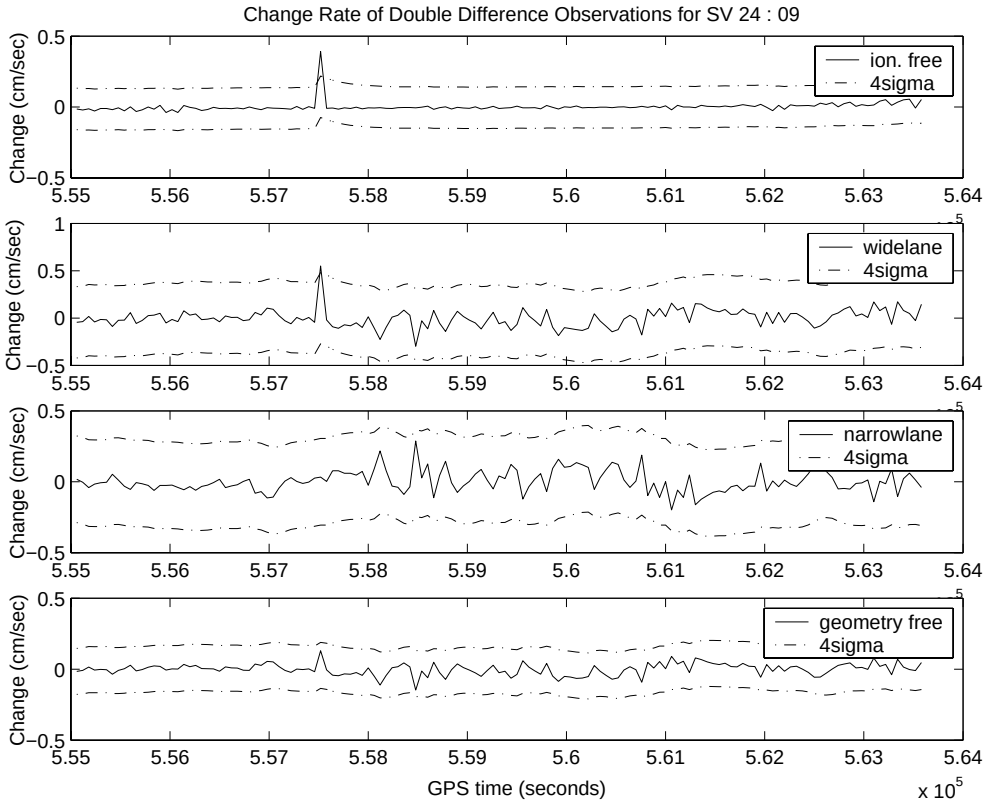

Figure 5.2 Change rate of double difference observations

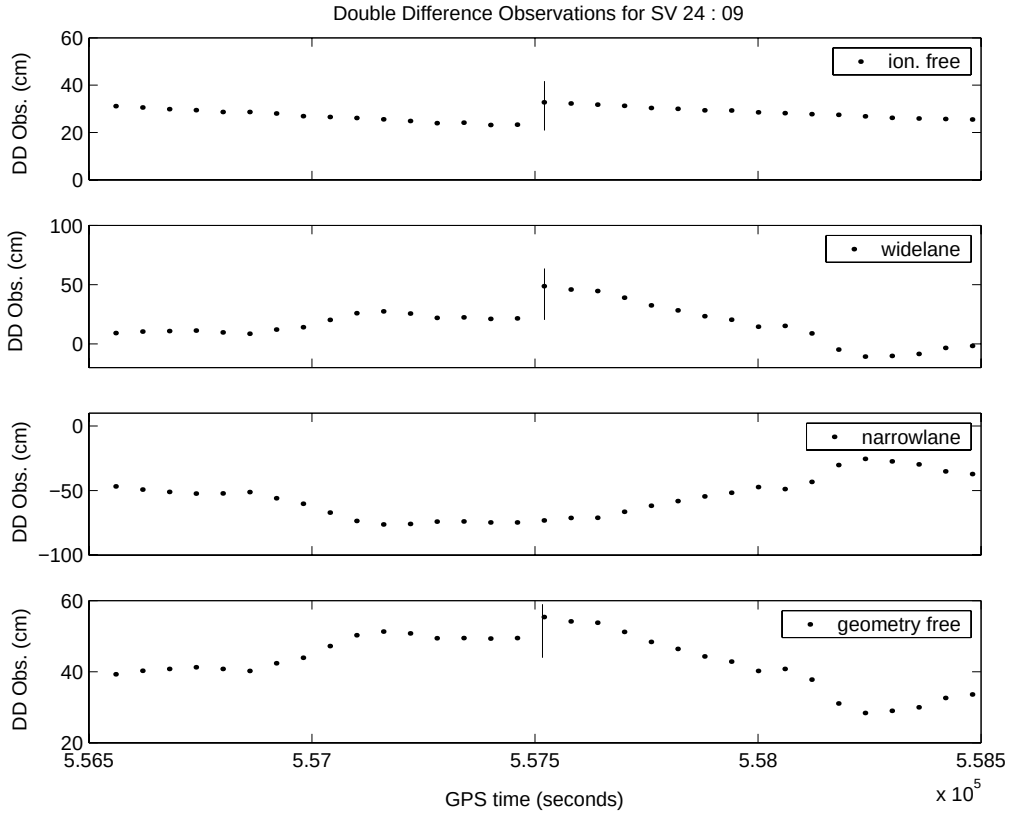

Figure 5.3 Double difference observations

A cycle slip may be limited to one cycle, or could be millions of cycles. Sometime a cycle slip of a few cycles could induce an error at cm level in a GPS position determination. Undoubtedly, cycle slips should be completely removed before computing the solution of a least-squares adjustment in order to reach cm-level accuracy. However, there is no unique method for eliminating cycle slips; available procedures are not guaranteed to work in all cases [Leick, 1995]. If any jump is not discovered before the least-squares adjustment is performed, the double difference residuals will show the jump at the epoch where the slip occurs. In such a case, a visual inspection of the residuals might be necessary in detecting the cycle slip. Many precision GPS software packages including DIPOP provide a visual helper for repairing cycle slips.

Larger cycle slips are more easily found and fixed in comparison with smaller ones. The preprocessor PREDD carries on the task to fix the small cycle slips (a few cycles) after PREGO removes the lager ones. The following sections focus on the algorithm of detecting the small cycle slip in PREDD.

5.2 Algorithm of Cycle Slip Detection in PREDD

Since a data set will have been processed in the program PREGO, all cycle slips detected in program PREDD are expected to be small. So double differences are used in PREDD in order to remove the effects of the receiver's clock error from the observable.

The algorithm of cycle slip detection applied in PREDD uses a straight line fit over 5 data points in the time difference series. The time difference series is similar to the triple difference, but related to the sampling interval of sequential observations. It is the change rate of the double difference sequence with the sampling interval.

To detect a cycle slip, the difference between the next data point and the value predicted by the straight-line fit or median value from the first 5 observations of the time difference series is compared to a certain threshold value. If the difference is larger than the threshold value, a cycle slip is declared. Otherwise no cycle slip is assumed to exist at the data point. The procedure shifts epoch by epoch and is repeated until the end of the time difference series is reached [Georgiadou et al., 1993].

Repairing cycle slips in PREDD is accomplished automatically once the threshold value for detecting slips is preset in the command file. How to find a value for the threshold of cycle slip detection has been discussed in the DIPOP literature. A 6 cm

criterion was recommended for the ionosphere-free combination in order to reduce the number of falsely detected cycle slips. The threshold value is based on a noise level of 2 cm in the ionosphere-free dual frequency combination [Georgiadou et al., 1993].

However, different data sets have different noise levels due to differences in receiver option or measurement environment, and so the preset threshold should vary with the noise level of the data sets. The command file of PREDD provides multiple options for detecting cycle slips. The algorithms for repairing cycle slips are available for both the single and dual frequency carrier phases. Users can specify the types of observations for single frequency or observation combinations, and for dual frequency observations and their corresponding threshold values for each data set. Table 5.2 describes each option for detecting cycle slips in PREDD. Considering the different sensitivities of the four combinations to cycle slips, the author added an option "4" for dual frequency phases.

Table 5.2 Multiple choices of observations for detecting cycle slips in PREDD

Option		Description
Single Frequency	1	Using L1 observations only
	2	Using L2 observations only
Dual Frequency	0	Using L1 and L2 observations separately
	1	Using ionosphere-free and widelane combinations
	2	Using ionosphere-free and geometry-free combinations
	3	Using narrowlane and widelane combinations
	4	Using ionosphere-free, widelane, geometry-free, and narrowlane combinations

In addition, the noise and other errors such as ionospheric delay and multipath will be amplified to different degrees due to the combinations of dual frequency observations used in the detection of cycle slips. An overview of GPS inter-frequency carrier phase combinations by Collins [1999] includes a detailed discussion about the combination

characteristics. Table 5.3 cites some results from the discussion in order to illustrate the effects of the combinations. The geometry-free combination is not included in the table. These values of Table 5.3 give an upper limit of the amplifications. In this discussion, the noise is propagated as a random error, while the ionospheric delay and multipath are propagated as biases in the results.

Table 5.3 Linear combination characteristics

Combination	λ_{LC} (cm)	$\lambda_{L1} / \lambda_{LC}$	Amplification (cycles)		
			Noise	Ion. Delay	Multipath
Ionosphere-free	0.6	30.25	104.15	0	34.25
Widelane	86.2	0.22	1.54	-0.28	0.50
Narrowlane	10.7	1.78	1.54	2.28	0.50

Considering all the related factors, users have to examine the noise level for each combination of each data set before setting the threshold value in the command file of PREDD. Otherwise choosing a too low criterion may increase the probability of falsely detecting cycle slips; or a too high value may miss a large number of cycle slips. It is undoubted that setting the threshold values by the examination of data outside DIPOP raises difficulties for users of DIPOP. In order to improve this situation, a method to automatically detect cycle slips inside PREDD has been devised and is introduced in the next section.

5.3 Method of Automatically Detecting Cycle Slips

The method of automatically detecting cycle slips is actually used to perform three tasks:

1) to examine the noise level of time difference series for determining the threshold value of detecting cycle slips;
2) to set the threshold value for detecting cycle slips;
3) to rule out the probability of falsely detecting cycle slips.

This section details the principles of the method and its realization in PREDD.

5.3.1 Examination of Noise Level

Since the noise levels of the double difference data from every pair of satellites are different, the examination of the noise level should be carried out whenever a pair of new satellites is introduced. As mentioned above, the time difference series formed by the rate of change of a double difference sequence has the same features as the triple difference sequence. It has a major advantage in that cycle slips are mapped as individual outliers. The individual outliers can be detected and corrected using sophisticated algorithms.

Due to the cancellation of the most common systematic errors such as clock errors of satellites and receivers, orbit error, and most of the effects from atmospheric refraction in the time difference sequence, the time difference series can be treated as a stochastic process. The stochastic process mainly consists of the random errors of observations and the effect from multipath interference. Since the atmospheric effect is time and space dependent, its partial effect still remains in the change rate series of double differences.

The data displayed in Figure 5.4 basically resembles these characteristics mentioned above. This figure clearly demonstrates that the data at low elevation angles, near the beginning and end of the data series, are subject to more noise over the 2.5-hour period.

This is a typical characteristic of multipath and noise. Such noise levels usually induce some troubles for detection of cycle slips. In addition, a small bias caused by an unknown systematic error term exists in each plot.

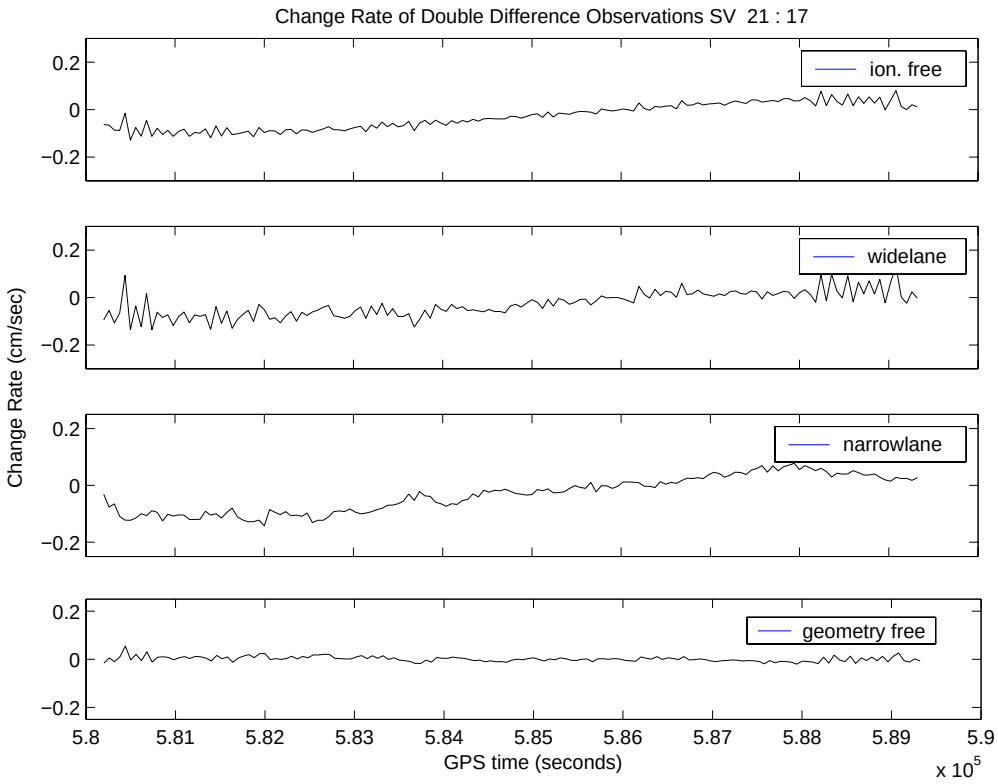

Figure 5.4 Time difference series of double differences

For this time difference series, a normal distribution can be first presumed [Tiberius et al., 1999]. The normal distribution is completely described by the two parameters: the mean and variance of the time difference series. The variance measures the spread of the probability density in the sense that it gives the expected value of the squared deviations from the mean [Mikhail and Ackerman, 1982]. The square root of the variance is usually given the name standard deviation (σ). The noise level of the time difference series can be measured by its standard deviation.

However, due to the effects of multipath and small systematic errors, the time difference series is not a stationary stochastic process; its mean is not a constant. So a moving average filter is more suitable to compute the mean of time difference series over a certain window at each epoch instead of the single total mean. The general expression for the moving average filter of one side is:

$$\bar{x}_t = \bar{x}_{t-1} + \frac{1}{t_{win}}(x_t - x_{t-1}) \tag{5.1}$$

where x_t is the observation at epoch t, $\bar{x}_t$ and $\bar{x}_{t-1}$ are the mean of time difference series x at epoch t and t-1, t_{win} is the window width of moving average filter. The average at epoch t is based on the most recent set of values within the window. The value of $\bar{x}_t$ is calculated using its previous value $\bar{x}_{t-1}$ as reference. The moving average but not the

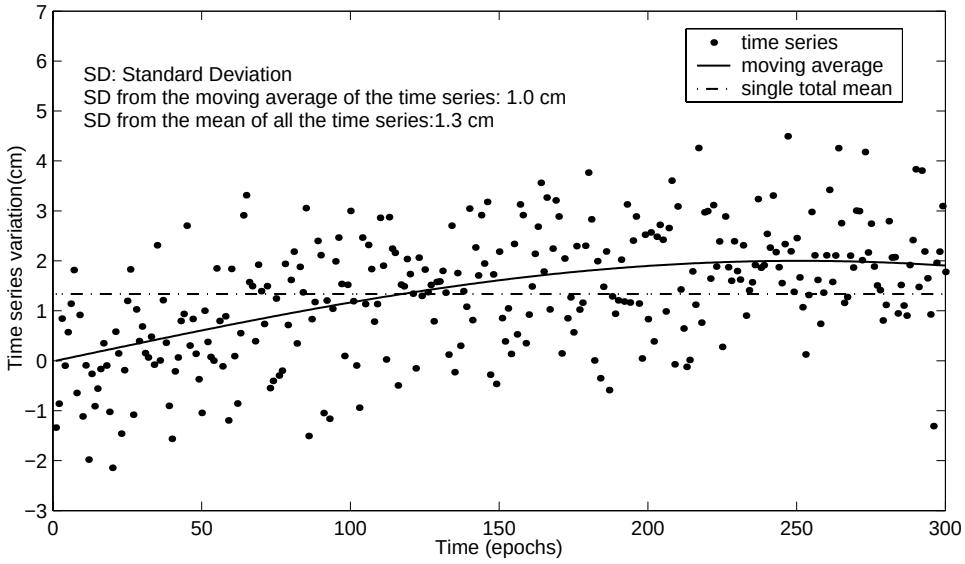

Figure 5.5 The moving average and mean of the time series

From a statistical point of view, the samples with cycle slips in the time difference series cannot be considered as belonging to the same normal distribution of the cycle-slip free in observations. The observations with cycle slips should not be used together with other observations to compute the noise level of the time difference series.

How should we detect or reject the observations with cycle slips? For a normal distribution, in about 99.73% ~99.99% of all cases the observations fall within $3\sigma \sim 4\sigma$ of the mean (see Table 5.4). Therefore, 3σ or 4σ is usually taken as the limit to what can be regarded as random errors. Statistically, large errors cannot be avoided, but their occurrences are unlikely. In order to get a true noise level without the effect of cycle slips, any deviations larger than 4σ from the moving average are considered as occurrences of cycle slips. The rejection avoids the probability of falsely amplifying the noise level due to large cycle slips. If the deviation caused by a small cycle slip is within a range of 4σ, it will still be kept in the time difference series. But the contribution from the small cycle slip to the overall noise level is usually very small in the time differences series.

Table 5.4 Selected values from the normal distribution

	0.6745σ	1σ	1.6449σ	2σ	2.3263σ	3σ	4σ
Probability (%)	50.00	68.27	90.00	95.45	98.00	99.73	99.99

After the effect of the probable large cycle slips is eliminated, the noise level can be directly obtained by computing the standard deviation of the time difference series. The examination of the noise level of the time difference series in PREDD is realized by a subroutine, SETTHOLD. The subroutine carries out the task of computing the noise level of the time difference series.

5.3.2 Setting Threshold Values

After determining the noise level, a threshold value is set at 4 times the noise level for detecting cycle slips based on the distribution characteristics of the noise. However, statistically, a small probability does not mean that the event has no chances to occur. In other words, it is still possible that an error that is not caused by a cycle slip may occur in practice. In that case, a mistake will occur if a judgement is made only based on the principle of the threshold value.

Figure 5.6 gives examples in this case. As the figure shows, both a cycle slip and large noise spike can produce peaks in the time difference series. In order to avoid the false detection of a cycle slip, a judgement directly following the detection will be used to

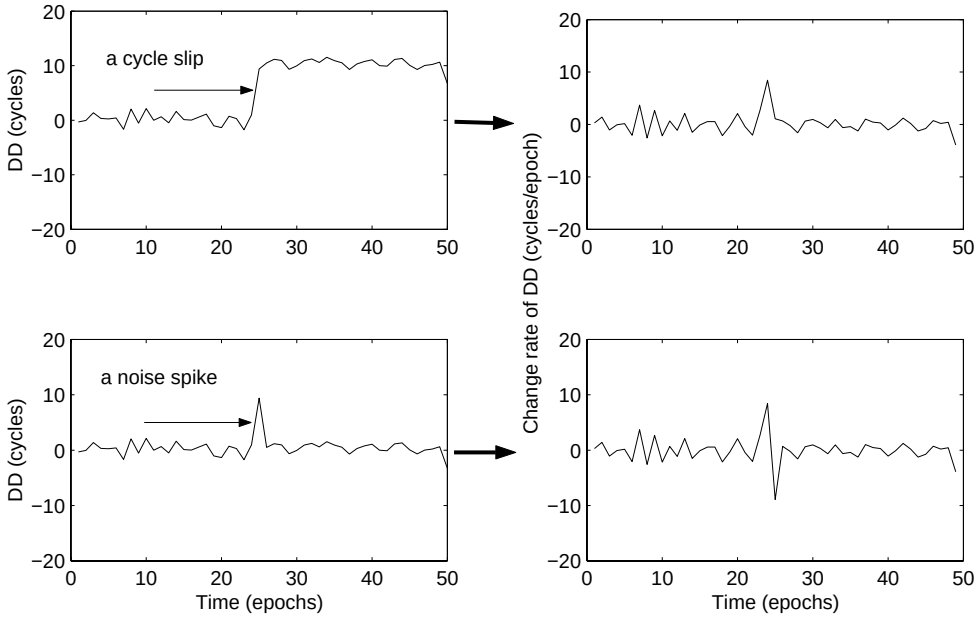

Figure 5.6 Occurrences of a cycle slip and a noise peak in the double difference series and time difference series

5.3.3 Ruling out the Probability of Falsely Detecting Cycle Slips

From the discussions in the last section, we know that there are two possible occurrences: a cycle slip or a large noise spike, when the difference between predicted value and practical value is larger than the threshold value. In order to solve the problem of falsely detecting cycle slips, it is necessary to understand the difference between the cycle slip and the noise. Their difference is that a cycle slip makes all observations taken after the cycle slip shifted by the same integer amount; but a noise spike is a single occurrence and does not affect the observations at other epochs.

According to their different characteristics, a method was designed to distinguish noise spikes from cycle slips. The basic principle of the method is to compare a difference between two predicted values. The one (O_{fore}) is predicted forwards using 5 data points from the double difference sequence before the tested epoch, the other one (O_{back}) is predicted backwards using 5 points from the double difference sequence after the tested epoch. Figure 5.7 illustrates the idea of the method. If absolute value of the difference ($|O_{fore} - O_{back}|$) is greater than 3 times the local noise value, a cycle slip is declared found. Otherwise, it is a large noise peak. Note that the predicted value is computed by a linear fitting backwards or forwards using the 5 observations before or after the tested data point.

There is an exception to the prediction. If the tested data point is located within the last 5 epochs of the time difference series, the backward prediction is the median from the data points after the tested epoch; or the median is itself if the tested data point is at the

last epoch. Since the median is obtained by arranging the values of time difference series in their order of magnitude, it is more suitable for a discrete time sequence than the mean.

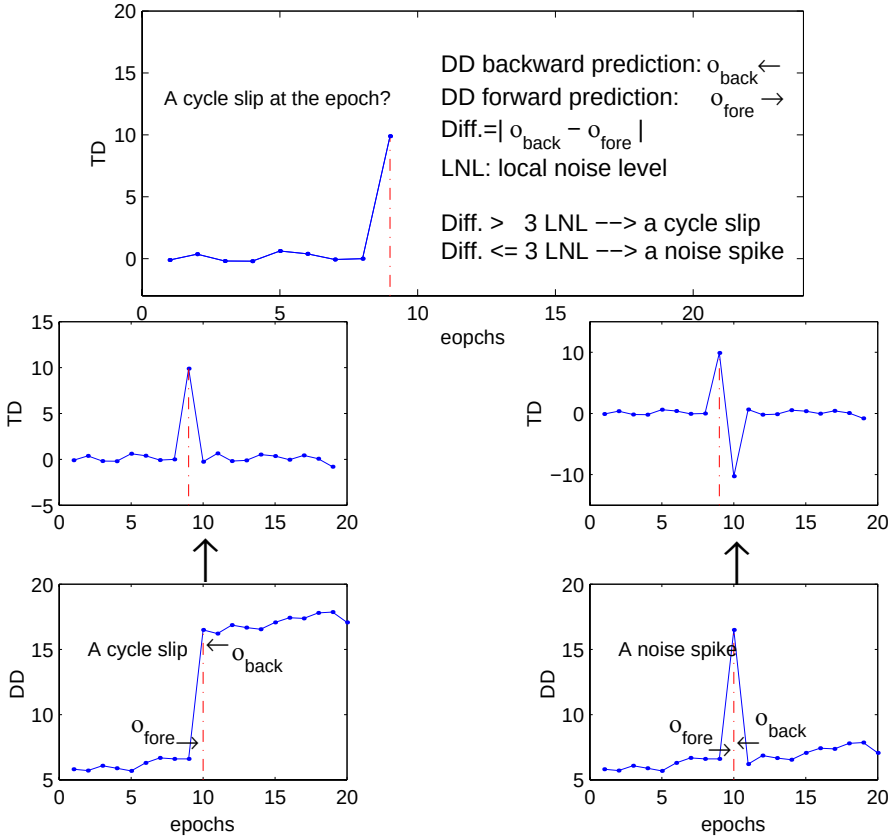

Figure 5.7 Principle of distinguishing a cycle slip and a noise spike

Figures 5.8 – 5.13 graphically give examples of the detection of cycle slips. The sign, "|", in the plots denotes an occurrence of a cycle slip at that epoch. The Figures 5.8, 5.10 and 5.12 display the time difference series of double differences; the Figures 5.9, 5.11 and 5.13 display the corresponding double difference series.

In the plots of the six figures, the signs "|", marked at the epochs where peaks exceed the ±4σ borderline, indicate a found cycle slip. Figure 5.8 shows that the four combinations have different sensitivities to cycle slips. According to Figure 5.9, there should be two cycle slips in the data series. Except for the widelane combination, only

one is found in the other combinations. Thus the usage of different combinations can indeed reduce the probability of missing cycle slips.

Figures 5.8 - 5.9 display an example with true cycle slips. Figures 5.10-5.11 display an example of avoiding a false cycle slip. In Figure 5.11, the data sequence shows significant noise; but no jump exists. It indicates that the data set should not have cycle slips. We can see there are no "|" marks for cycle slips in Figure 5.10 although a value exceed the $\pm 4\sigma$ threshold. So in that case, the algorithm is successful. Figures 5.12-5.13 show an example of the most normal case. The four combinations all correctly detect a cycle slip at the same epoch; in each plot of their double difference series, an obvious jump occurs at the epoch.

Since the author focused on the data analysis of long baselines, all the discussions and the examples shown here are from the combinations of dual frequency observations. Whatever observations are used in PREDD, the principle of detecting cycle slips should be same.

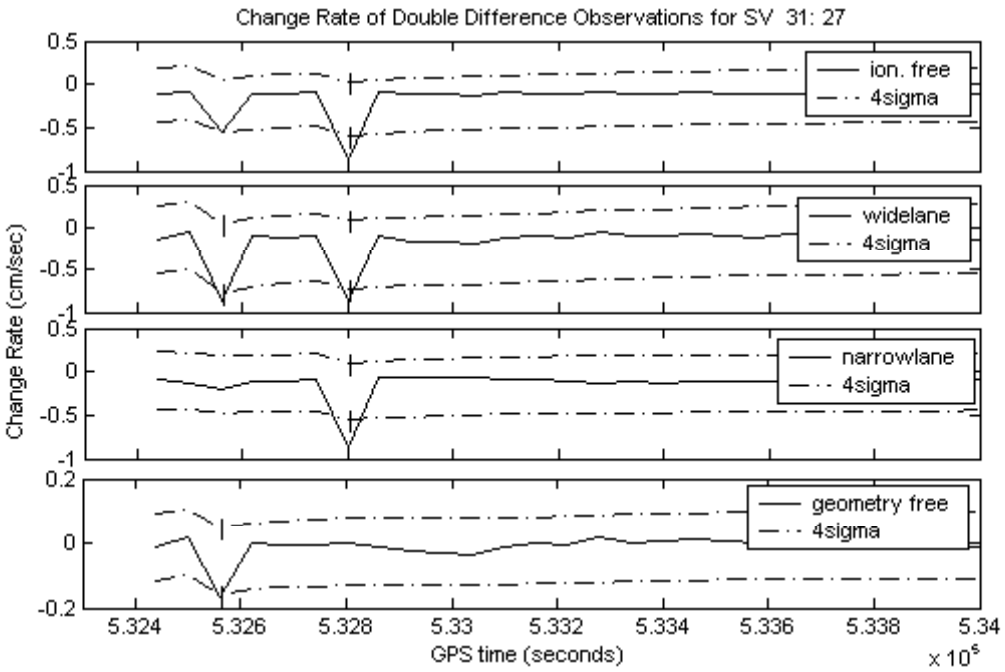

Figure 5.8 Time difference series of the four combinations with different sensitivities to cycle slips

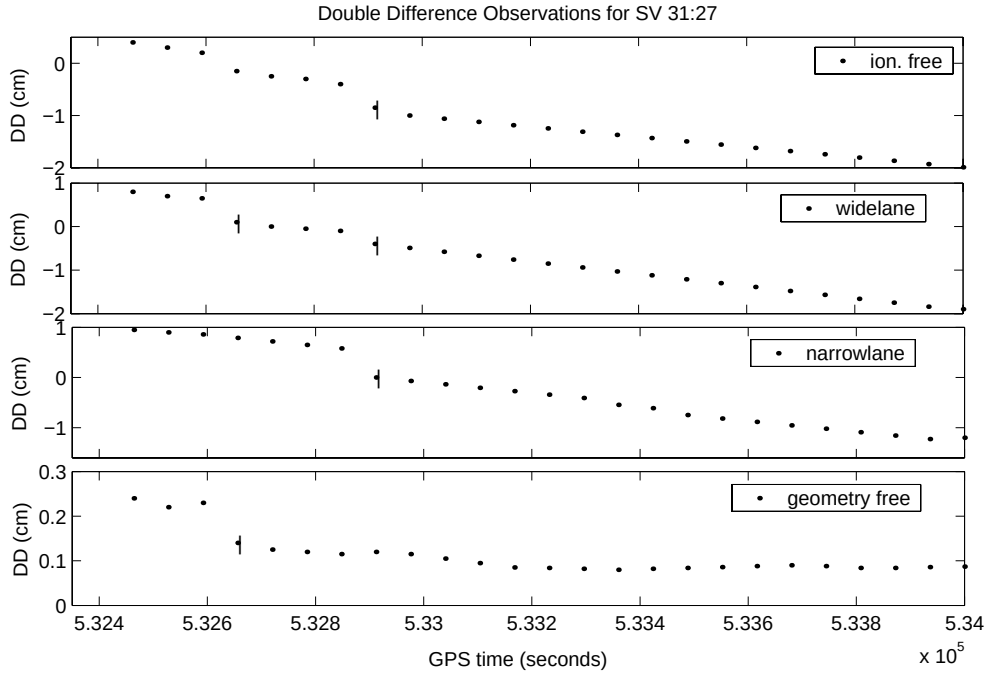

Figure 5.9 Double differences of the four combinations with different sensitivities to cycle slips

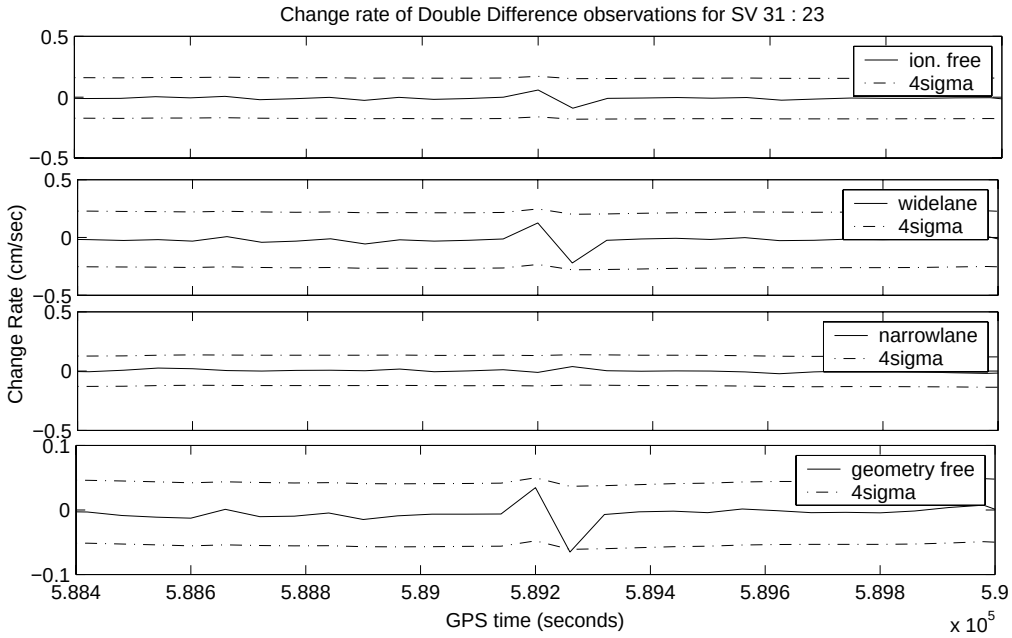

Figure 5.10 Time difference series of the four combinations with a large noise spike

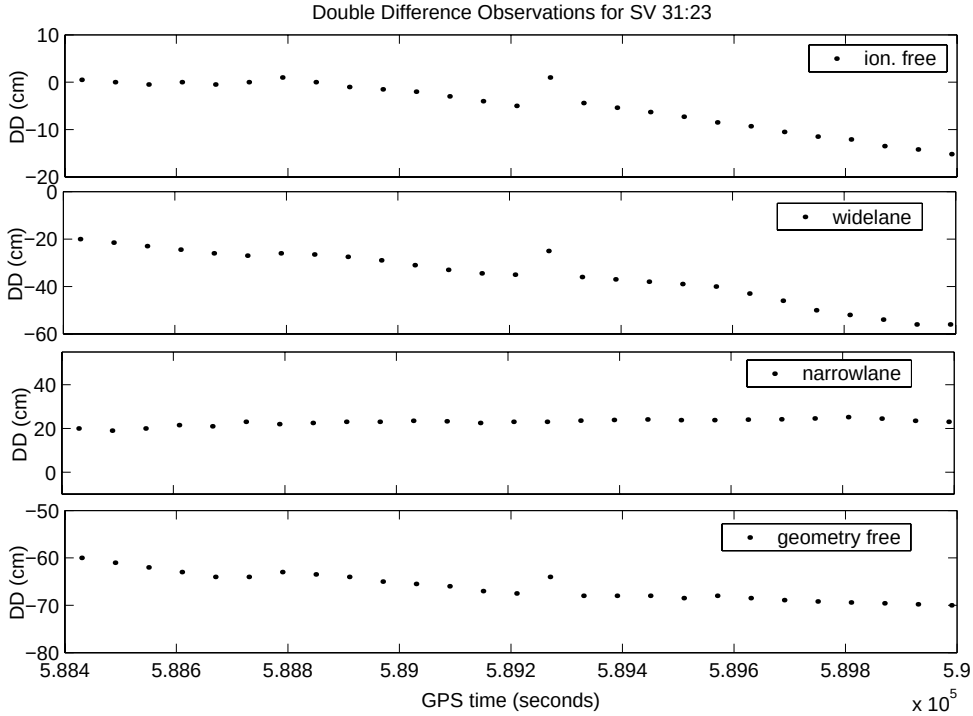

Figure 5.11 Double differences of the four combinations with a large noise spike

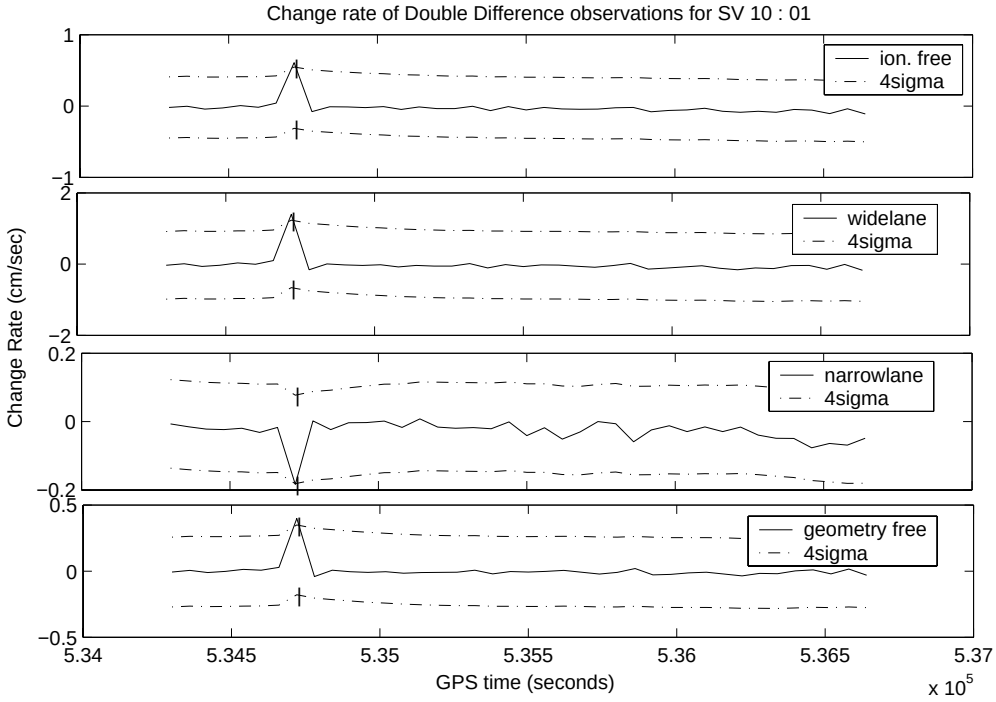

Figure 5.12 Time difference series of the four combinations with a detected cycle slip

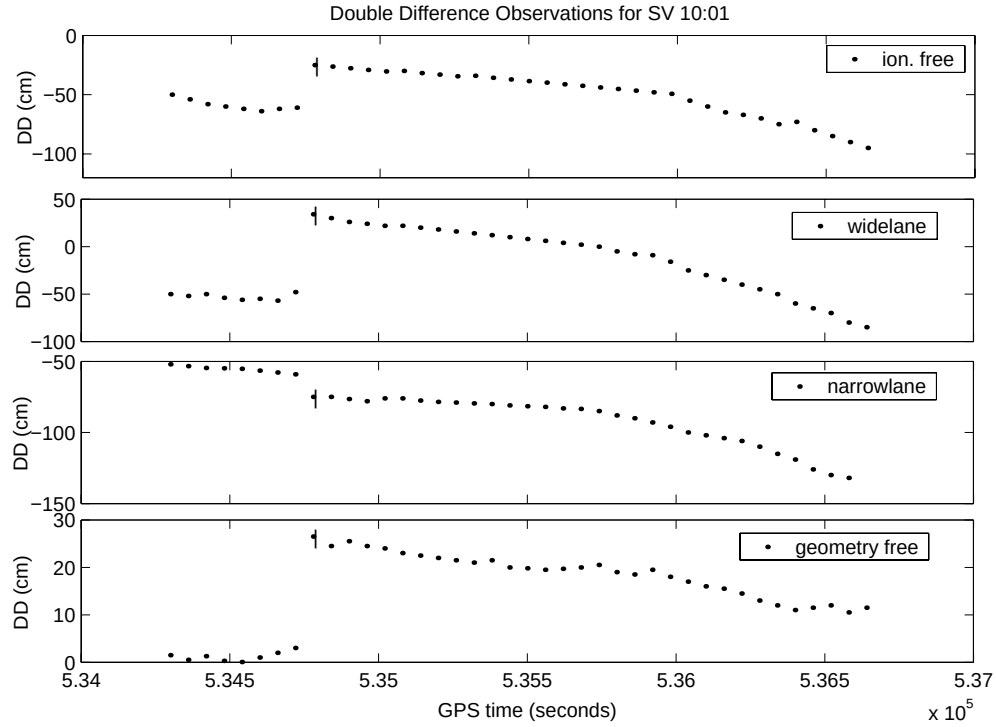

Figure 5.13 Double differences of the four combinations with a cycle slip

5.4 Summary

The method to automatically detect cycle slips is realized with three added subroutines in PREDD. The three subroutines are

- SETSHOLD.F: to set threshold values for detecting cycle slips by examining the noise level of time difference series;
- STDNOISE.F: to compute the standard deviation of a time difference series;
- ISSLIPS.F: to rule out a false detection of cycle slip.

The study suggests that in order to avoid missing the detection of cycle slips, the multiple combinations for dual frequency phases should be used in detection of cycle slips for long baselines. In most cases, using two combinations can detect all cycle slips for long baselines. But the visual inspection of residuals is still a useful and safe way for finally checking if all cycle slips have been fixed.

However, for a short baseline, using L1 and L2 observations separately to detect the cycle slips is more suitable in order to reduce the probability of falsely detecting cycle slips due to amplifying the noise because the common error can almost completely be canceled by the double difference.

Cycle slips much larger than the noise level are easy to correctly identify. During the author's study, the most complicated case was found to be when the jump caused by a cycle slip has a same level as the noise or when the noise level is very high. Then the probability of falsely detecting cycle slips increases. It is necessary to improve the program ISSLIPS further.

The purpose of improving the technique of detecting cycle slips is to raise the efficiency of DIPOP. From the current study, the initial purpose has been achieved. But the cycle slip has a complicated behavior. Events can still conspire to cause the false detection of cycle slips or to miss a cycle slip. A future study for correct detection of cycle slips is recommended.

Chapter 6

Velocity Estimations

Typically the use of GPS in the study of crustal deformation involves monitoring changes of site coordinates via continuous observation. The purpose of this chapter is to evaluate DIPOP's performance to extract crustal deformation signals by an analysis of a position time series from three WCDA GPS stations for a period of 52 weeks.

After an introduction to the data sets, this chapter describes the methods used in velocity estimations of the GPS stations from the positioning time series; then the results of velocity estimations and their statistics are given and discussed.

6.1 Introduction

6.1.1 GPS Data Sets

Due to time constraints, only daily data from three WCDA baselines over a period of 52 weeks were processed with DIPOP in this discussion. The three baselines are the baseline (302 km), ALBH – DRAO, the longest one (627 km), HOLB – DRAO, and the baseline

(434 km), UCLU – DRAO, that shows a reported movement velocity of about 1 cm per year in the WCDA network (Dragert, et al., 2001).

The daily GPS observation RINEX files of the four sites over 52 weeks from October 30, 2000 to October 27, 2001 were downloaded from the WCDA Web site <http://www.pgc.nrcan.gc.ca/geodyn/wcda/wcdadata.htm>. The Web site provides the past one year data from the current day for the WCDA GPS stations except the station NEAH which is operated by the University of Washington. Information about the processed data sets with DIPOP is summarized in Table 6.1.

Table 6.1 Daily data sets for estimation of movement velocity

Baseline	Remote-Reference Station	Length (km)	Observing Date (day/year)	Sampling Interval (sec)
DAAB	ALBH – DRAO	302	304/2000 – 300/2001	60
DAHL	HOLB – DRAO	627	304/2000 – 300/2001	60
DAUL	UCLU – DRAO	434	304/2000 – 300/2001	60

6.1.2 Method of Velocity Estimations

The estimation of crustal movement rate is essentially a procedure of linear regression. The algorithm of weighted least squares has been used in the linear regression to determine the crustal deformation rates of GPS observation stations (e.g. Khazaradze et al., 1999).

6.1.2.1 Weighted Least Squares Fitting

The least squares fitting can be used to find the relationship between an independent variable x, such as a time tag, and a dependent variable y, such as a position coordinate of a GPS station, from a set of their measurement values (x_i, y_i, i = 1, 2, 3, ...). The relationship of x and y is mathematically expressed in terms of a linear dependence on a set of constant parameters, $(A_1, A_2, A_3, \Lambda, A_m)$, which are to be determined:

$$y = F(x) = A_1 + A_2 x + A_3 x^2 + \Lambda + A_m x^{m-1} \tag{6.1}$$

There are two main applications of the fitting. One is to determine what the functional relationship between x and y is. The other one, used more frequently, is to use a known functional relationship of x and y to find the best set of the parameters $(A_1, A_2, A_3, \Lambda, A_m)$ to fit the set of data (x, y). Determination of an annual linear trend term from a position time series of daily solutions belongs to the second case.

In the weighted least squares fitting, the unknown parameters are estimated by finding the values for the parameters that minimize the sum of the squared deviation between the measured values and the functional predictions. At the same time, each term in the weighted least squares procedure includes an additional weight that determines how much each measurement in the data set influences the final parameter estimates.

Assume that the independent variables x are known quite accurately, but that the dependent variables y have standard errors (σ_i, i=1, 2, 3, ...) associated with them, then the weights (w_i) of individual pairs ($x_{i,}$, y_i) are defined as

$$w_i \propto \frac{1}{\sigma_i^{\,2}} \tag{6.2}$$

If there is a total of *n* measurements, the principle of the weighted least squares regression can be defined by minimizing

$$Q = \sum_{i=1}^{n} w_i \left\{ y_i - F(x_i) \right\}^2 \tag{6.3}$$

Necessary conditions for Q to be a minimum are that the partial derivatives with respect to the parameters are equal to zero.

$$\frac{\partial Q}{\partial A_i} = 0, \qquad i = 1, 2, \Lambda\ , m \tag{6.4}$$

These equations can be expressed in the form of a single matrix equation

$$\boldsymbol{M}\,\boldsymbol{A} = \boldsymbol{Y} \tag{6.5}$$

where $$M_{jk} = \sum_{i=1}^{n} w_i\, f_j(x_i)\, f_k(x_i)$$

$$Y_j = \sum_{i=1}^{n} w_i f_j(x_i) y_i$$

$$f_j(x_i) = x_i^{\,j-1} \quad f_k(x_i) = x_i^{\,k-1} \qquad j,k = 1,2,\ldots,m \quad i = 1,2,\ldots,n$$

Then the unknown parameters, $(A_1,\ A_2,\ A_3, \Lambda\ , A_m)$, are found by inversion of the square symmetric matrix $\boldsymbol{M}$

$$\boldsymbol{A} = \boldsymbol{M}^{-1}\,\boldsymbol{Y} \tag{6.6}$$

In the application of the linear velocity estimations of position time series, the expression (6.1) can be simplified as

$$F(x) = A_1 + A_2 x \tag{6.7}$$

And the weights are defined by variances associated with the daily solutions as

$$w_i = \frac{\frac{1}{\sigma_i^{\,2}}}{\sum_{k=1}^{n} \frac{1}{\sigma_k^{\,2}}} \tag{6.8}$$

The slope A_2 in euqation (6.7) denotes the desired linear movement rate of a site.

6.1.2.2 Assessments of Linear Fitting

For assessments of the quality of the linear fitting, a value r^2 called **the coefficient of determination** is involved. It is a quantity measuring the goodness-of-fit of the linear regression. The value r^2 can be computed by the following formulas

$$r^2 = \frac{SSR}{SST}\ , \qquad SSR = \sum_{i=1}^{n} (\hat{y}_i - \bar{y})^2\ , \qquad SST = \sum_{i=1}^{n} (y_i - \bar{y})^2 \tag{6.9}$$

where y_i is the i^{th} value of y, $\bar{y}$ is the mean of all y values and $\hat{y}_i$ is the predicted value from the best fitting line. SSR is the sum of squared deviations of predicted values by the linear regression model from the mean value. SST is the sum of squared deviation of individual measurements from the mean. Figure 6.1 demonstrates the computation of r^2. The value r^2 reports how much of the total variance in y is "explained" by the rate term in the linear regression model. It is a fraction between 0.0 and 1.0, and has no units. A r^2 value of 0.0 means that there is no linear relationship between x and y, and the best-fit line is a horizontal line going through the mean value $\bar{y}$. When r^2 equals 1.0, all points lie exactly on a straight line with no scatter. Figure 6.2 gives four examples of linear regression with different values of r^2.

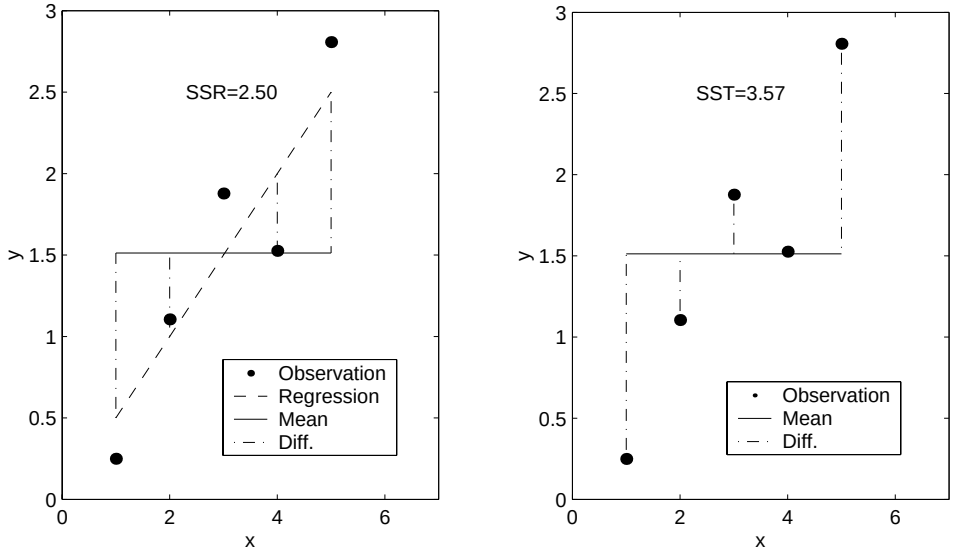

Figure 6.1 The computation of r^2

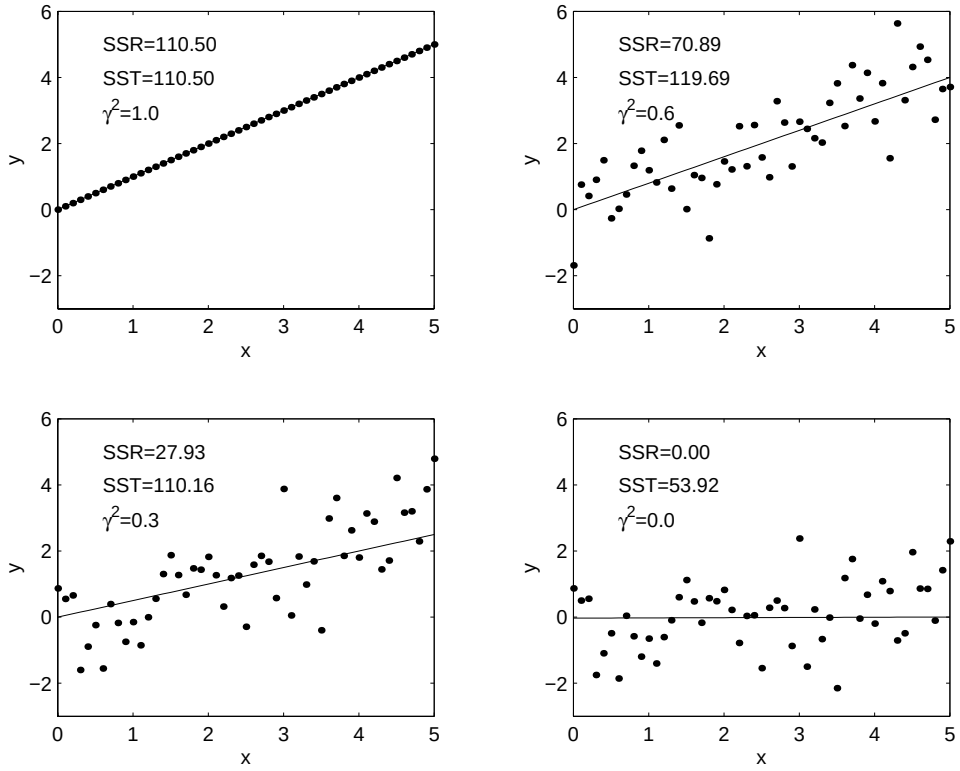

Figure 6.2 r^2 and linear regression fitting

The simplified linear regression assumes that y is linearly dependent on x, and then finds the slope and intercept that make a straight line come as close as possible to the observation data. In other words, using daily solutions to estimate the movement rate is based on the assumption that there is a linear relationship between the daily solutions and time. When r^2 is very small or even close to zero, the results from the linear fitting obviously are questionable. Is the slope or the crustal movement rate significantly different than zero? An F-test may help us answer this question. The F-test is usually used to test a hypothesis via a ratio of two variances. The results of the F-test tell us, with a certain of degree of confidence, whether or not there is linear relationship between x and y. The significance of the linear regression is evaluated using the following F-statistic:

$$F = \frac{SSR / df(SSR)}{SSE / df(SSE)}, \quad SSE = SST - SSR \tag{6.10}$$

where $df(SSR) = g - 1$, is the number of degrees of freedom for SSR which is equal to the number (g) of coefficients in the linear regression equation minus 1. SSE is the sum of squared deviations of actual values from predicted values. $df(SSE) = n - g$, is the number of degrees of freeedom for the error sum of squares SSE which is equal to the number of observations (n) minus g.

In the F-test, the null hypothesis is that the slope of the fitting line is equal to zero. If the tested statistic value (F) from the equation (6.9) falls within a critical region from the F distribution function, then the null hypothesis is rejected. Else, the null hypothesis is accepted; the slope from the linear regression is zero. As a consequence of accepting the null hypothesis, the annual variation rate of the position time series is set to zero.

The F-test can be two-tailed or one-tailed [Snedecor and Cochran, 1989]. Their choice is determined by the problem. The two-tailed version tests against the alternative that the standard deviations are not equal. The one-tailed version only tests in one direction, that is the standard deviation from the first sequence is either greater than or less than (but not both) the second sequence standard deviation. At the same time, the F-test is referred to a significance level, α**,** which is used as a criterion for rejecting the null hypothesis. The lower α, the more the data diverge from the null hypothesis. The choice of α is somewhat arbitrary. In practice, values of 0.1, 0.05, and 0.01 are most commonly used. In this research, the two-tailed F-test is employed with a significance level of 0.05 (α=0.05).

6.2 Time Series and Velocity Estimations

All the daily solutions were produced with DIPOP using the same processing strategy as described in section 4.4.1. The velocity vectors of the time series in three directions (latitude, longitude, and vertical) and along baseline length were determined by the weighted least squares linear regression described in the last section. The results of velocity estimations of the three baselines and relative statistical results are given in Tables 6.2 – 6.5. Figures 6.3 – 6.5 graphically display the time series of three baselines from 304/2000 to 300/2001, the computed linear fitting results including annual movement rate, error and RMS, and their corresponding best-fitting lines.

The results of the linear regression shows that the sites ALBH and UCLU have displayed significant relative displacement with respect to the reference station DRAO. Their displacements reach 10.9±0.62 (mm/year) in the direction of $E33^0N$ and

13.9±0.82(mm/year) in the direction of E30^{0}N, respectively. The displacement for the site HOLB is 3.8±0.5(mm/year) to the North. For the vertical components, the site HOLB has the largest value, -7.8±1.0(mm/year); and the movement rates of UCLU and ALBH are 0 and 2.6 ±0.9mm/year in the height component, respectively. Tables 6.2-6.5 show that the RMS for the baseline DAAB is the smallest of the three baselines and the RMS for the longest baseline DAHL is the largest. Among the three components: latitude, longitude and height, the height component has the lowest r^2 value and the highest RMS level; on the contrary, the latitude component has the highest r^2 value and the lowest RMS level.

According to the discussions in the last section, a slope of zero is determined in the linear regression of movement velocity if the null hypothesis for the F-test is accepted. In this case, the number in the tables is denoted with the bold font. In all the F-tests, there are three F-tests not rejecting the null hypothesis (see Tables 6.2-6.5). At the same time, we can find that the r^2 values associating with them are all very small (less than 0.01) compared with other components. The estimated deformation variation trends at stations ALBH and UCLU with respect to DRAO are basically in agreement with the results of other crustal deformation studies in the WCDA area [Dragert, et al., 2001].

The results of the three baselines for 52 weeks indicate that the software DIPOP has the capability to detect the mm-level variations of the crustal deformation signals.

Table 6.2 Variations in latitude (+North)

Baseline	Velocity (mm/yr)	1σ (mm/yr)	r^2	RMS (mm)	F-Test H_0: Vel.=0
DAAB	5.8	0.4	0.3969	1.8	Reject
DAHL	3.8	0.5	0.1764	2.3	Reject
DAUL	7.0	0.4	0.4356	2.1	Reject

Table 6.3 Variations in longitude (+East)

Baseline	Velocity (mm/yr)	1σ (mm/yr)	r^2	RMS (mm)	F-Test H_0: Vel.=0
DAAB	9.2	0.6	0.3364	3.5	Rejected
DAHL	0.0**(-0.2)**	**(0.7)**	**(0.0064)**	**(5.1)**	**Accepted**
DAUL	12.0	0.7	0.3721	4.4	Rejected

Table 6.4 Variations in height (+Up)

Baseline	Velocity (mm/yr)	1σ (mm/yr)	r^2	RMS (mm)	F-Test H_0: Vel.=0
DAAB	2.6	0.9	0.0256	5.2	Rejected
DAHL	-7.8	1.0	0.0841	6.9	Rejected
DAUL	0.0**(-1.9)**	**(1.0)**	**(0.0064)**	**(9.4)**	**Accepted**

Table 6.5 Variations in baseline length

Baseline	Velocity (mm/yr)	1σ (mm/yr)	r^2	RMS (mm)	F-Test H_0: Vel.=0
DAAB	-10.9	0.6	0.4356	3.6	Rejected
DAHL	0.0**(-0.1)**	**(0.7)**	**(0.0009)**	**(5.0)**	**Accepted**
DAUL	-13.1	0.7	0.4096	4.5	Rejected

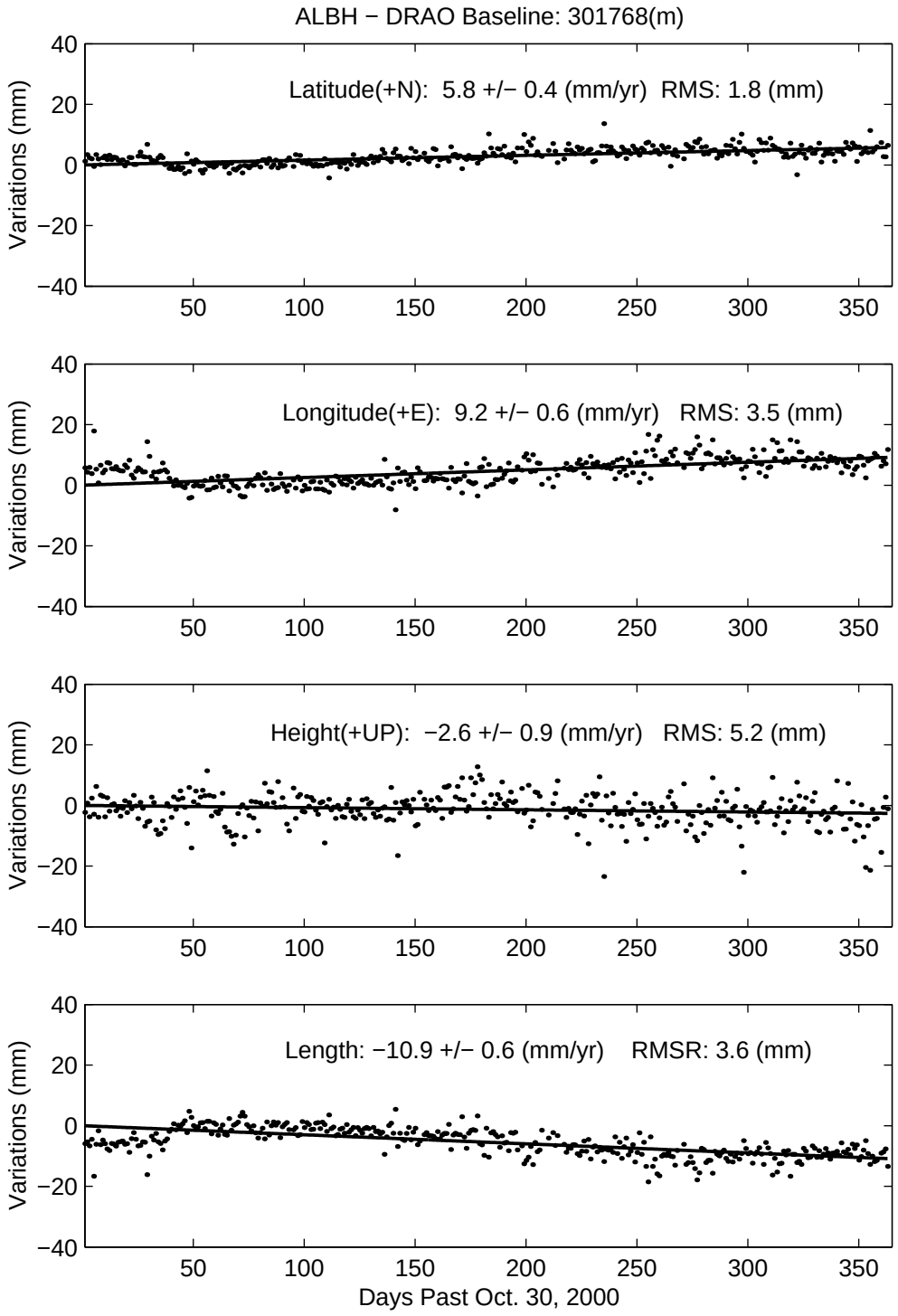

Figure 6.3 Time series of variations at ALBH with respect to DRAO in latitude (+N), longitude (+E) and height (+up) and of the baseline DAAB length

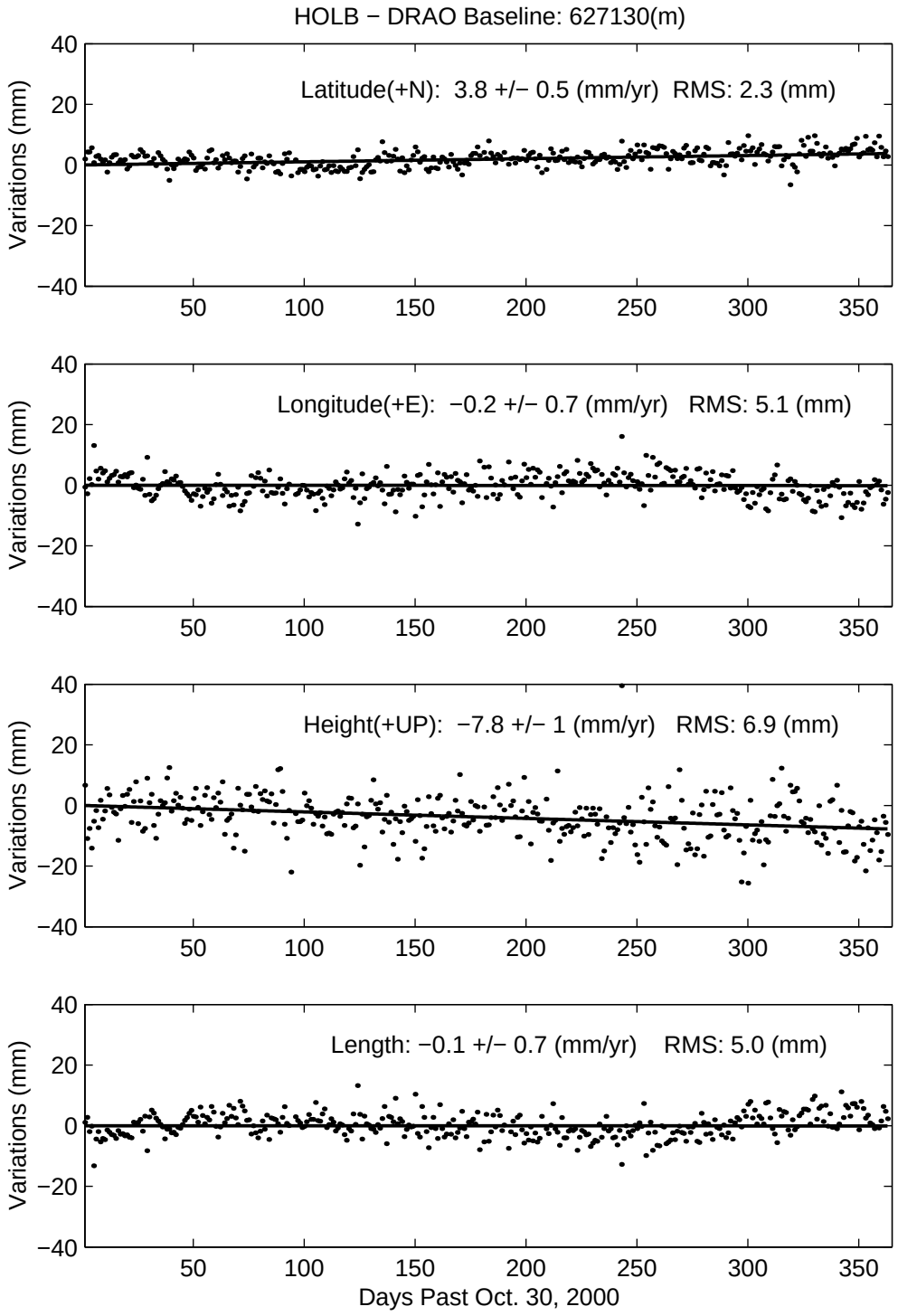

Figure 6.4 Time series of variations at HOLB with respect to DRAO in latitude (+N), longitude (+E) and height (+up) and of the baseline DAHL length

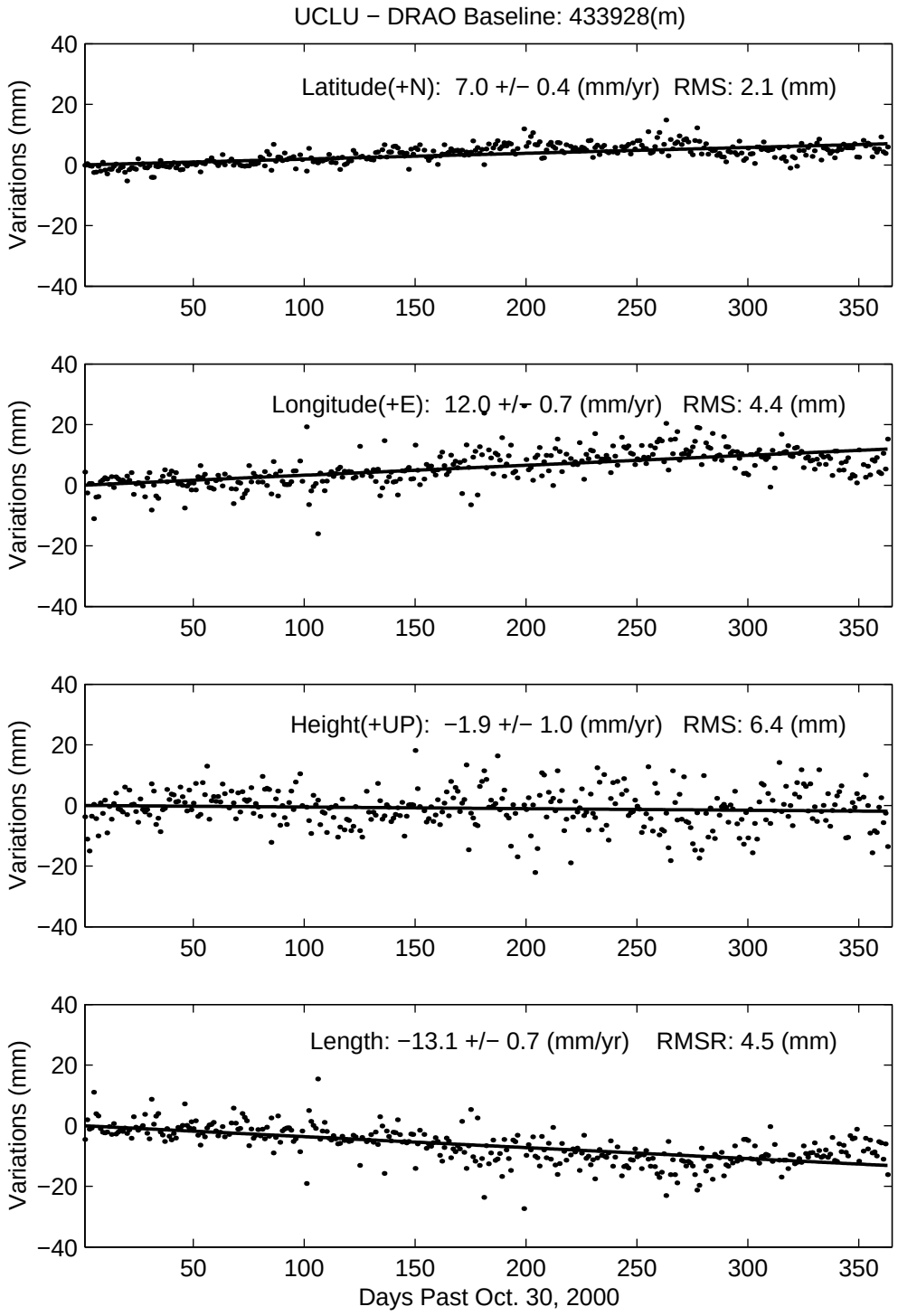

Figure 6.5 Time series of variations at UCLU with respect to DRAO in latitude (+N), longitude (+E) and height (+up) and of the baseline DAUL length

Chapter 7

Conclusions and Recommendations

This thesis focuses on the investigation of GPS data processing techniques applied in monitoring crustal deformation via analyzing the data from WCDA with the software DIPOP. The research conducted tests of error correction models, analysis of daily solutions, comparison of positioning results, computations of position time series and improvements of cycle slip detecting algorithms. This chapter gives conclusions of the research and recommendations for future studies.

7.1 Conclusions

In Chapter 4, the one-week daily solutions for 7 WCDA sites in reference to the station DRAO show that repeatabilities of height component and baseline length are both better than 1 cm. Except for the site NANO, the daily variations of the height component and baseline length are within a range of 1 cm. The relative precision along the baseline length is better than 0.01PPM, within a range of 0.004-0.008 PPM. The preliminary results indicate the solutions from DIPOP can reach a daily repeatability better than 1 cm in static relative positioning measurements for baselines spanning a few hundreds of km.

The comparison between the DIPOP solutions of the 5 WCDA sites and the IERS ITRF2000 solutions (at 1997.0 epoch in ITRF97) in Chapter 4 indicates an agreement better than 1.5 cm between the two sets of absolute Cartesian coordinate solutions for three coordinate components. The relative difference of baseline lengths shows a scale of 1 - 2 parts per 0.01 PPM. The results imply that the level of coordinate conformity between the two solutions from DIPOP and IERS is of the order of a few cm. And DIPOP is capable of providing a comparable accuracy to that of other GPS software suites in static relative positioning.

The error budget in Chapter 4 shows that the multipath interference, the tropospheric delay, and the offset from antenna phase center variations are main error sources affecting the precision and accuracy of the DIPOP solutions.

DIPOP's performance in extracting the crustal deformation signals was evaluated by an analysis of the position time series from three WCDA GPS baselines for a period of 52 weeks. It is shown in Chapter 6 that the crustal deformation signals of yearly mm level have been extracted from the time series. Especially, the sites ALBH and UCLU have displayed significant relative displacement with respect to the reference station DRAO. Their yearly horizontal displacements reach 10.9mm (σ: $\pm$0.62) and 13.9mm (σ: $\pm$0.82), respectively. However, comparing vertical components with horizontal components, it was found that the linear fittings of the former present a higher regression residual level than other components. The yearly varying trends in height components show uncertainties about 1.5 times larger than those in latitude and longitude components do. Improvement of the method for tropospheric zenith delay estimation in DIPOP may reduce the uncertainties of the vertical trend estimations.

An important part of the research was to improve the technique of detecting and fixing cycle slips in order to improve the efficiency of DIPOP. In this research, a method consisting of three subroutines to automatically detect the cycle slips was implemented in PREDD. The improvement enhances the automation level of detecting cycle slips and contributes to completeness of analyzing the time series. However, the events of falsely detecting cycle slips or missing cycle slips still happen. A further refinement of the method is needed.

7.2 Recommendations

The following is a list of recommendations for future studies based on this research:

- Although an elevation angle cut off of 15^o was used in all the data analysis, multipath still shows significant effects on the precision of DIPOP's solutions (see Chapter 4). Since the use of a higher elevation angle cutoff ($\geq 15^o$) may cause a high correlation between the tropospheric zenith delay and the height estimation, it is necessary to develop an efficient method to mitigate the effect of the multipath.
- The nature that tropospheric delay continuously varies with time has not been taken into account in the current version of DIPOP. It could be considered as a major reason causing the lower precision in the height component. A stochastic model characterized by an empirical variance which constrains the zenith delay changes by a time correlation is expected to be implemented for the estimation of residual tropospheric zenith delay in DIPOP. Such a model has been prototyped in an earlier version of DIPOP and needs to be reintroduced into the current version.

- In this research, the coordinates of satellites from the IGS precise ephemerides were held fixed as exact known parameters without corrections for the phase center offset of satellite antenna. As a result, a systematic error was caused. Since the phase center offset of a receiver antenna can change by many cm during the satellites' movement, the neglect of the phase center offset's variation may lead to baseline errors between mm and cm, and can even reach up to 10 cm for the height component. The variation of the phase center offset should be considered instead of simply using a constant of phase center offset in the high-precision GPS positioning with DIPOP.

- The analysis of the position time series for a period of 52 weeks shows that the annual crustal deformation rate at the three WCDA sites is very small. The long-term variations of the time series were not taken into account in the analysis. The data of WCDA over a longer time should be more useful for monitoring the variation of the crustal deformation in the WCDA area. In a future study of deformation time series, the correlation and spectral analysis of the time series should be carried out in order to get a more reasonable and realistic information of crustal deformation.

- The method of automatically detecting cycle slips largely enhances the productive efficiency of DIPOP, while avoiding the events of falsely detecting cycle slips or missing cycle slips is a major direction for refining the method.

- The current version of DIPOP can process data from different receiver antenna types. But when data from a new type of antenna are processed, modifications of a source code subroutine and compilation of the whole main program have to be done by users. So in the future a friendlier user interface should include a method of independently dealing with the new receiver antenna types from the main source program in DIPOP.

- In DIPOP, the satellite clock corrections from the IGS ephemerides are held as exact known parameters in data processing. If the clock corrections are very bad or absent at an epoch, they will be set to 999999.9999 at that epoch in the IGS ephemerides. Then a manual operation to remove the satellite at the epoch is needed. A program with the ability to automatically carry out the removal is expected in future refinement of DIPOP, especially in a case of large data set processing.
- Reduction of the correlation between the tropospheric parameters and height requires use of observations from low elevation angles. The current version of DIPOP has already included features such as de-weighting observations at low elevation angles to deal with this issue. This is not covered in this thesis. Further work on it will be particularly useful for improvements of the vertical component solutions.

References

Ammon, C.J. (2001). "An Introduction to Earthquakes." SLU EAS_A193 Class Notes, Last updated: 8/1/2001, Department of Geosciences, Saint Louis University, <http://eqseis.geosc.psu.edu/~cammon/HTML/Classes/IntroQuakes/Notes/notes_frame.html>

Argus, D.F. and M.B. Heflin (1995). "Plate Motion and Crustal Deformation Estimated with Geodetic Data from the Global Positioning System." *Geophysical Research Letter*, Vol. 22, No. 13, pp. 1973-1976.

Argus, D.F. and R.G. Gordon (1996). "Test of the Rigid-Plate Hypothesis and Bounds on Intraplate Deformation Using Geodetic data from Very Long Baseline Interferometry." Journal of Geophysical Research, Vol. 101, No. B6, pp. 13555-13572.

Baker, T.F., D.J. Curtis, and A.H. Dodson (1995). "Ocean Tide Loading and GPS." *GPS World,* Vol. 6, No.3, pp. 54-59.

Bisnath, S.B. (2000). "Efficient, Automated Cycle-Slip Correction of Dual-Frequency Kinematic GPS Data." *Proceeding of ION GPS-2000*, 19-22 September, Salt Lake City, Utah, pp. 145-153.

Bock, Y. (1991). "Continuous Monitoring of Crustal Deformation." *GPS World*, Vol. 2, No. 6, pp. 40-47.

Bock, Y. (1995).”Reference System.” *GPS for Geodesy*, Lecture Note of International School, Netherlands Geodetic Commission, Delft, The Netherlands, March 26-April 1, 1995.

Bock, Y., R.M. Nikolaidis, P.J. de Jonge, and M. Bevis (2000). “Instantaneous Geodetic Positioning at Medium Distances with the Global Positioning System.” *Journal of Geophysical Research*, Vol. 105, No. B12, pp. 28223-28253.

Boucher, C. and Z. Altamimi (1996). “International Terrestrial Reference Frame.” *GPS World*, Vol. 7, No.9, pp. 71-74.

Brunner, F.K. and W.M. Welsch (1993). “Effect of the Troposphere on GPS Measurement.” *GPS World*, Vol. 4, No.1, pp. 42-51.

Chen, X., R.B. Langley, and H. Dragert (1996). " Investigation of Annual Variations in the WCDA GPS Solutions." *Proceeding of ION GPS-96*, Kansas City, Missouri, U.S.A., 17-20 September 1996, pp. 1809-1818.

Chen, X.(1998). *Continuous GPS Monitoring of Crustal Deformation with the Western Canada Deformation Array: 1992–1995*. M.Sc.E. thesis, Department of Geodesy and Geomatics Engineering Technical Report No.195, University of New Brunswick, Fredericton, New Brunswick, Canada 158pp.

Collins, J.P. and R.B. Langley (1997). “Estimating the Residual Tropospheric Delay for Airborne Differential GPS Positioning” *Proceedings of ION GPS-97*, the 10th International Technical Meeting of the Satellite Division of the Institute of Navigation, Kansas City, MO, U.S.A., 16-19 September 1997; pp. 1197-1206.

Collins, J.P. and R.B. Langley (1998). “The Residual Tropospheric Propagation Delay: How Bad Can It Get?” *Proceeding of ION GPS-98,* 11th International Technical Meeting of the Satellite Division of the Institute of Navigation, Nashville, Tennessee, U.S.A., 15-18 September 1998, pp. 729-739.

Collins, J.P. (1999). "An Overview of GPS Inter-Frequency Carrier Phase Combinations." <http://gauss.gge.unb.ca/papers.pdf/L1L2combinations.collins.pdf >

Dragert, H., X. Chen, and J. Kouba (1995). "GPS Monitoring of Crustal Strain in Southwest British Columbia with the Western Canada Deformation Array." *Geomatica,* Vol. 49, No. 3, pp. 301-313.

Dragert, H., T.S. James, and A. Lambert (2000). "Ocean Loading Corrections for Continuous GPS: A Case Study at the Canadian Coastal Site Holberg." *Geophysical Research Letter*, Vol. 27, No. 14, pp. 2045-2048.

Dragert, H., K. Wong, and T.S. James (2001). "A Silent Slip Event on the Deeper Cascadia Subduction Interface." *Science*, Vol. 292, pp. 1525-1528.

Dragert, H., M. Schmidt, J. Henton, and Y. Lu (2001). "The Western Canada Deformation Array: Measuring Crustal Motion in Coastal British Columbia with Continuous GPS." *Geodynamics Program*, Last updated: 06/28/2001, <http://www.pgc.nrcan.gc.ca/geodyn/docs/wcda_bc/content.htm >.

Georgiadou, Y., F. van den Heuvel, P. Heroux, A. Kleusberg, A. Komjathy, R.B. Langley, C.J. Lewis, V.B. Mendes, R. Santerre, and A.D. van der Wal (1993). *GPS Data Processing with DIPOP 3.0,* Draft 1, Geodetic Research Laboratory, Department of Geodesy and Geomatics Engineering, University of New Brunswick, Fredericton, New Brunswick, Canada.

Guthrie, W., J. Filliben, and A. Heckert (2002). "Process Modeling." *NIST/SEMATECH e-Handbook of Statistical Methods*, Last updated: 10\28\2002, <http://www.itl.nist.gov/div898/handbook/toolaids/pff/index.htm>.

Hartinger, H. and F.K. Brunner (1999). "Variances of GPS Phase Observations: the SIGAMA-ε Model." *GPS Solution*, Vol. 2, No. 4, pp. 35-43.

Hay, C. and J. Wong (2000). "Enhancing GPS: Tropospheric Delay Prediction at the Master Control Station." *GPS World,* Vol. 11, No. 1, pp. 56-61.

Henton, J.A. (2000). *GPS Studies of Crustal Deformation in the Northern Cascadia Subduction Zone,* thesis for Doctor of Philosophy in the School of Earth and Ocean Sciences, University of Victoria.

Khazaradze, G., A. Qamer, and H. Dragert (1999). "Tectonic Deformation in Western Washington from Continuous GPS Measurement." *Geophysical Research Letter,* Vol. 26, No 20, pp. 3153-3158.

Kleusberg, A., Y. Georgiadou and H. Dragert (1988). "Establishment of crustal deformation networks using GPS: a case study." *CISM Journal ACSGC,* Vol. 42, No. 4, Winter 1988, pp. 341-351.

Kleusberg A., Y. Georgiadou, F. van den Heuvel, and P. Heroux (1989). *DIPOP version 2.1: Single and dual frequency GPS data preprocessing with DIPOP 2.1*, Geodetic Research Laboratory, Department of Geodesy and Geomatics Engineering, University of New Brunswick.

Lambeck K. (1988). *Geophysical Geodesy – the Slow Deformation of the Earth.* Oxford University Press, New York.

Lambert, A., S.D. Pagiatakis, A.P. Billyard, and H. Dragert (1998). "Improved Ocean Tide Loading Corrections for gravity and Displacement: Canada and Northern United States." *Journal of Geophysical Research*, Vol. 103, No. B12, pp. 30,231-302,44.

Langley, R.B. (1992). "Basic Geodesy for GPS." *GPS World,* Vol. 3, No. 2, pp. 44-49.

Langley, R.B. (1995). "Propagation of the GPS Signals." *GPS for Geodesy,* Lecture Note of International School, Netherlands Geodetic Commission, Delft, The Netherlands, March 26-April 1, 1995.

Langley, R.B. (1997). "The GPS Error Budget." *GPS World,* Vol. 8, No. 3, pp. 51-55.

Langley, R.B. (1997).”GPS Receiver System Noise.” *GPS World,* Vol. 8, No. 8, pp. 40-45.

Larson, K.M., J.T. Freymueller, and S. Philipsen (1997). “Global Plate Velocities from the Global Positioning System.” *Journal of Geophysical Research*, Vol. 102, No. B5, pp. 9961-9981.

Leick, A. (1995). G*PS Satellite Surveying.* Second edition, Jhon wiley & Sons, Inc, New York.

Mader, G. and F. Czopek (2002). “Calibrating Antenna Phase Centers.” *GPS World,* Vol. 13, No. 5, pp. 40-46.

Mendes, V.B. and R.B. Langley (1994). “A comprehensive Analysis of Mapping Functions Used in Modeling Tropospheric Propagation Delay in Space Geodetic Data.” KIS94, Proceedings of the International Symposium on Kinematic Systems in Geodesy, geomatics and Navigation, Banff, Alberta, 30 August – 2 September, The University of Calgary, Calgary, Alberta, Canada, pp. 87-98.

Mendes, V.B., J.P. Collins, and R.B. Langley (1995). “The effect of Tropospheric Propagation Delay Error in Airborne GPS Precision Positioning.” *Proceedings of ION GPS - 95,* 8th International Technical Meeting of the Satellite Division of the Institute of Navigation, 12-15 September, Palm Springs, CA, Vol. 2, pp. 1681-1689.

Mendes, V.B.**,** G. Prates, L. Santos, and R.B. Langley (2000). “An Evaluation of Models for the Determination of the Weighted Mean Temperature of the Atmosphere.” *Proceedings of the Institute of Navigation 2000 National Technical Meeting*, Anaheim, CA, U.S.A., 26-28 January 2000; pp. 433-438

Mendes, V.B. and R.B. Langley (2000). “An Analysis of High-accuracy Tropospheric Delay Mapping Functions.” *Phys. Chem. Earth (A*), Vol. 25, No. 12, pp. 809-812.

Mikhail, E.M. and F. Ackerman (1982). *Observations and Least Squares.* University Press of Amarica, NewYork.

McCarthy, D.D. (1996). *IERS Conventions (1996)*, IERS Technical Note 21, U.S. Naval Observatory.

Pagiatakis, S.D. (1992). “Program LOADSDP for the Calculation of Ocean Load Effects.” *Manuscripta Geodaetica,* Vol. 17, pp. 315-320.

Santerre, R., A. Kleusberg and G. Beutler (1985). "*DIPOP: Software documentation*." Canadian Geodetic Survey Research Contract No OST83-00353, Department of Geodesy and Geomatics Engineering Technical Memorandum No. 6, University of New Brunswick, Fredericton, Canada.

Santerre, R. (1987). *DIPOP version 2.1: Structure, Modifications and User Guide.* Interim Technical Memorandum, Geodetic Research Laboratory, Department of Geodesy and Geomatics Engineering, University of New Brunswick, Fredericton, New Brunswick, Canada.

Seeber, G. (1993). *Satellite Geodesy: Foundations, Methods & Applications*. Walter de Gruyter, Berlin New York.

Snedecor, G.W. and W.G. Cochran (1989), *Statistical Methods,* Eighth Edition, Iowa State University Press.

Shedlock, K.M. and L.C. Pakiser (1997). *Earthquakes*, Last modified 10/23/97, General Interest Publications of the U.S. Geological Survey, Denver, Colorado, US, <http://pubs.usgs.gov/gip/earthq1/>.

Tham, M. (1998). “Dealing with Measurement Noise.” Department of Chemical and Process Engineering, University of Newcastle, Tyne, UK, <http://lorien.ncl.ac.uk/ming/filter/filter.htm>.

Tiberius, C., N. Jonkman, and F. Kenselaar (1999). “The Stochastic of GPS Observables.” *GPS World,* Vol. 10, No. 2, pp. 49-54.

Tsuji, H., Y. Hatanaka, and S. Miyazaki (1996). "Tremors! Monitoring Crustal Deformation in Japan." *GPS World*, Vol. 7, No. 4, pp.18-29.

Van der Wal, A. (1995). *Evaluation of Strategies for Estimating Residual Neutral-atmosphere Propagation Delay in High Precision Global Positioning System Data Analysis.* M.Sc.E. thesis, Department of Geodesy and Geomatics Engineering Technical Report No. 177, University of New Brunswick, Fredericton, New Brunswick, Canada.

Vaníček, P., G. Beutler, A. Kleusberg, R.B. Langley, R. Santerre and D.E. Wells (1985). *DIPOP: Differential Positioning Package for the Global Positioning System,* Department of Geodesy and Geomatics Engineering Technical Report No.115, University of New Brunswick, Fredericton, New Brunswick, Canada.

Whar, J.M. (1981). "The Force Nutations of an Elliptical, Rotating, Elastic, and Oceanless Earth." *Geophys. J. Roy. Astron. Soc.*, Vol. 64, pp. 705-727

Whar, J.M. (1985). "Deformation Induced by Pole." *J. Geophys, Res.* Vol. 90, pp. 9363-9368.

Wells, D., N. Beck, D. Delikaraoglou, A. Kleusberg, E.J. Krakiwsky, G. Lachapelle, R.B. Langley, M. Nakiboglu, K.P. Schwarz, J.M. Tranquilla, and P. Vaníček (1986). *Guide to GPS Positioning*, Canadian GPS Associates, Fredericton, New Brunswick, Canada.

Wieser, A. and F.K. Brunner (2000). "An Extended Weight Model for GPS Phase Observations." *Earth, Planets and Space*, Vol. 52, No.10, pp. 777-782.

Wübbena, G., F. Menge, M. Schmitz, G. Seeber, and C. Völksen (1996). "A New Approach for Field Calibration of Absolute Antenna Phase Center Variations." *Proceedings International Technical Meeting*, ION GPS-96, Kansas City, Missouri, 1205-1214.

Appendix A

DIPOP References

PAPERS

Kleusberg, A., R.B. Langley, R. Santerre, P. Vaníček, D.E. Wells and G. Beutler (1985). "*Comparison of Survey Results from Different Types of GPS Receivers*." Proceedings of First International Symposium on Precise Positioning with the Global Positioning System, IUGG, IAG, U.S.DoD, U.S.DoC, Rockville, Md., 15-19 April 1985, National Geodetic Information Center, NOAA, Rockville, Md., Vol. II, pp. 579-592

Langley, R.B., D. Parrot, R. Santerre, P. Vaníček and D.E. Wells (1986). " *The Spring 1985 GPS High-Precision Baseline Test: Preliminary Analysis with DIPOP*." Proceedings of Fourth International Geodetic Symposium on Satellite Positioning, Austin, TX, 28 April-2 May 1986, pp.1073-1088.

Kleusberg, A., Y. Georgiadou, and H. Dragert (1988). "*Establishment of Crustal Deformation Networks Using GPS: A Case Study*." CISM Journal, Vol, 42, No. 4, pp. 341-351.

Chen, D. and R.B. Langley (1990). "*DIPOP-E: An Enhanced Version of the UNB GPS DIfferential POsitioning Program Package*." Proceedings of the Second International Symposium on Precise Positioning with the Global Positioning System, Ottawa, Ontario, 3-7 September 1990, pp.269-284.

Mendes, V.B. and R.B. Langley (1993). "*Application of the Global Positioning System to the Assessment of Crustal Deformation in the Charlevoix Seismic Zone*." Proceedings of ION GPS-93, the 6th International Technical Meeting of the Satellite Division of the Institute of Navigation, Salt Lake City, UT, 22-24 September 1993, Vol. II, pp. 1205-1219.

Santos, M.C., P. Vaníček and R.B. Langley (1995). "*Orbit Improvement and Generation of Ephemerides for the Global Positioning System Satellites: A Summary*." Revista Brasileira de Cartografia (Journal of the Brazilian Society of Cartography, Geodesy, Photogrammetry, and Remote Sensing), No. 46, October 1995, pp. 95-99.

Santos, M.C., P. Vaníček and R.B. Langley (1997). "*Effect of Mathematical Correlation in GPS Network Computation Using Carrier Phase Double Difference Observations*." Journal of Surveying Engineering, Vol. 123, No. 3, pp. 101-112.

REPORTS

Vaníček, P., G. Beulter, A. Kleusberg, R.B. Langley, R. Santerre and D.E. Wells (1985). "*DIPOP: Differential Positioning Program Package for the Global Positioning Systems*." Department of Surveying Engineering Technical Report No. 115, University of New Brunswick, Fredericton, N.B., August 1985.

TM-6, "*DIPOP: Software Documentation*."

Kleusberg, A. and L. Wanninger (1986). "*Analysis of the Juan de Fuca GPS Survey 1986.*" Department of Surveying Engineering Technical Report No. 127, University of New Brunswick, Fredericton, N.B., 1986.

Collins, J.P. and R.B. Langley (1997). "*Preliminary Investigation on the Use of the Global Positioning System for Structural Deformation Surveying*." Contract report

for the United States Army Corps of Engineers Topographic Engineering Center, No. DAAH04-96-C-0086 / TCN 97145, November.

Collins, J.P. and R.B. Langley (1999). "*Possible Weighting Schemes for GPS Carrier Phase Observations in the Presence of Multipath*." Contract report for the United States Army Corps of Engineers Topographic Engineering Center, No. DAAH04-96-C-0086 / TCN 98151, March.

THESES (Based in whole or in part, on DIPOP)

Denis Parrot. M.Sc.E. June 1989. *Short-Arc Orbit Improvemrnt for GPS Satellites*. Published as Department of Surveying Engineering Technical Report No. 143, University of New Brunswick, Fredericton, N.B., Canada.

Chen Ding-Sheng. M.Sc.E. May 1991. *A Long Arc Approach To GPS Satellite Orbit Improvement.* Published as Department of Surveying Engineering Technical Report No. 171, University of New Brunswick, Fredericton, N.B., Canada.

Anthony van der Wal. M.Sc.E. September 1995. *Evaluation of Strategies for Estimating Residual Neutral-atmosphere Propagation Delay in High Precision Global Positioning System Data Analysis.* Published as Department of Surveying Engineering Technical Report No. 177, University of New Brunswick, Fredericton, N.B., Canada.

Marcelo Santos. Ph.D. September 1995. *Real-time Orbit Improvement for GPS Satellites*. Published as Department of Surveying Engineering Technical Report No. 178, University of New Brunswick, Fredericton, N.B., Canada.

Vita

Full Name:	Chunlin Shen
Place and Date of Birth:	Yueyang, Hunan, P.R. China
	1964
Permanent Address:	36 Oldfield Street
	Ottawa, Ontario, Canada, K2G 6S8
Schools Attended:	Elementary School, Xiaogan, Hubei, P.R. China
	Middle & High School, Yueyang, Hunan, P.R. China
Universities Attended:	Tongji University,
	Shanghai, P.R. China
	University of New Brunswick,
	Fredericton, New Brunswick, Canada